Evaluation of Ground-Motion Modeling Techniques for Use in Global ShakeMap—A Critique of Instrumental Ground-Motion Prediction Equations, Peak Ground Motion to Macroseismic Intensity Conversions, and Macroseismic Intensity Predictions in Different Tectonic Settings

By Trevor I. Allen and David J. Wald

Open-File Report 2009–1047

U.S. Department of the Interior
U.S. Geological Survey

U.S. Department of the Interior
KEN SALAZAR, Secretary

U.S. Geological Survey
Suzette M. Kimball, Acting Director

U.S. Geological Survey, Reston, Virginia 2009

For product and ordering information:
World Wide Web: http://www.usgs.gov/pubprod
Telephone: 1-888-ASK-USGS

For more information on the USGS—the Federal source for science about the Earth,
its natural and living resources, natural hazards, and the environment:
World Wide Web: http://www.usgs.gov
Telephone: 1-888-ASK-USGS

Suggested citation:
Allen, T.I., and Wald, D.J., 2009, Evaluation of ground-motion modeling techniques for use in Global ShakeMap—A critique of instrumental ground-motion prediction equations, peak ground motion to macroseismic intensity conversions, and macroseismic intensity predictions in different tectonic settings: U.S. Geological Survey Open-File Report 2009–1047, 114 p.

Contents

Figures

Tables

Abbreviations

COSMOS	Consortium of Organizations for Strong-Motion Observation Systems
DYFI?	Did You Feel It?
ENA	Eastern North America
GMPE	Ground Motion Prediction Equation
GSM	Global ShakeMap
ISESD	Internet Site for European Strong-Motion Data
K-NET	Kyoshin Network
MMI	Modified Mercalli Intensity
M_W	Moment magnitude
NEHRP	National Earthquake Hazard Reduction Program
NGA	Next Generation Attenuation Program
PAGER	Prompt Assessment of Global Earthquakes for Response
PEER	Pacific Earthquake Engineering Research Center
PGA	Peak Ground Acceleration
PGM	Peak Ground Motion
PGM–MMI	Peak ground-motion-to-intensity conversion
PGV	Peak ground velocity
R	Generic distance metric
R_{epi}	Epicentral distance
R_{hyp}	Hypocentral distance
R_{rup}	Closest distance to rupture
SCR	Stable continental region

Evaluation of Ground-Motion Modeling Techniques for Use in Global ShakeMap—A Critique of Instrumental Ground-Motion Prediction Equations, Peak Ground Motion to Macroseismic Intensity Conversions, and Macroseismic Intensity Predictions in Different Tectonic Settings

By Trevor I. Allen[1] and David J. Wald[2]

Introduction

Several recent studies have sought to evaluate the applicability of predictive ground-motion techniques developed for a *host* region, and transfer them to a *target* region (for example, Scherbaum and others, 2004; Cotton and others, 2006; Douglas, 2007; Stafford and others, 2008; Douglas and Mohais, 2009). The necessity for this practice is often driven by the lack of knowledge regarding the source and attenuation characteristics of ground-motion in the *target* region where the model is to be applied. These studies are also important for weighting multiple Ground Motion Prediction Equations (GMPEs) in probabilistic seismic hazard analyses in order to capture the epistemic uncertainty (for example, Petersen and others, 2004; Bommer and others, 2005; Scherbaum and others, 2005; Bommer and Scherbaum, 2008; Petersen and others, 2008; Scherbaum and others, 2008). Regional differences in ground-motion attenuation have long been thought to add uncertainty in the prediction of ground motion (for example, Atkinson and Boore,

[1] National Earthquake Information Center, U.S. Geological Survey (present address, Risk and Impact Analysis Group, Geoscience Australia; trevor.allen@ga.gov.au).

[2] National Earthquake Information Center, U.S. Geological Survey (wald@usgs.gov).

2003). However, there is now a growing body of evidence to suggest that regional differences in ground-motion attenuation may not be as significant as previously thought (for example, Douglas, 2004, 2007) and that the key differences observed between regions may be a consequence of limitations in ground-motion datasets over incomplete magnitude and distance ranges (Bommer and others, 2007; Douglas, 2007). One extreme of GMPE regionalization is observed in the national Italian ShakeMap installation, which uses three GMPEs in six different geographic regions (Michelini and others, 2008) in a spatial area less than that of California. Undoubtedly, regional differences in attenuation can exist owing to differences in crustal structure and tectonic setting, and these often contribute to differences in ground-motion attenuation at larger source-receiver distances (approximately greater than 100 km). But do these differences outweigh the epistemic uncertainties associated with limitations in the magnitude and distance range of the local dataset used to develop region-specific GMPEs? And does this lead to the unnecessary contribution of aleatory uncertainties into the development of a regional ground-motion model?

The Pacific Earthquake Engineering Research (PEER) Center's Next Generation Attenuation (NGA) Project (Power and others, 2008) attempted to reduce epistemic uncertainties, and also to improve near-source ground-motion estimation, by gathering a comprehensive dataset of earthquake ground motions from California and other global earthquakes (Chiou and others, 2008). Additional studies have since seized upon the NGA dataset and have developed alternative GMPEs using these, and other supplementary data (for example, Graizer and Kalkan, 2008; G. Cua, written commun., 2008).

Although the foregoing discussion has concentrated on the prediction of instrumental ground-motion values, herein we examine the use of a variety of techniques for the prediction of several ground-motion metrics (peak ground acceleration and velocity, response spectral ordinates, and macroseismic intensity) and compare them against a global dataset of instrumental ground-motion recordings and intensity assignments. The primary goal of this study is to determine whether existing ground-motion prediction techniques are applicable for use in the U.S. Geological Survey's Global ShakeMap (GSM; Wald and others, 1999b; Wald and others, 2005) and Prompt Assessment of Global Earthquakes for Response (PAGER; Earle and others, 2008; Wald and others, 2008a) systems. Because it is not practical to configure regionally dependent ground-motion models for these real-time applications, we seek the most appropriate ground-motion predictive technique, or techniques, for each of the tectonic regimes considered: shallow active crust, subduction zone, and stable continental region. We hope that the analyses of instrumental ground-motion and macroseismic intensity included herein will promote the use of more robust ground-shaking prediction techniques in the first minutes-to-hours after any global earthquake in the absence of direct measurements or observations. These first-order assessments of ground-shaking are essential to decision support tools, such as PAGER, which provide rapid estimates of earthquake impact to emergency responders.

In evaluating ground-motion prediction techniques herein, we apply simple methods to examine the average residuals, binned by distance and magnitude, from observed and predicted ground-motion values. This is performed for each of the ground-motion metrics considered. More sophisticated methods that use information-theory to reduce the subjectivity among model selection have recently been published (Scherbaum and others, 2008). These methods quantitatively rank different GMPEs for instrumental ground motions using the California instrumental ground motions. Subsequent work using these methods that rank GMPEs based on observed intensities also offers promise for selecting instrumental ground-motion models for specific regions using historical macroseismic information (F. Scherbaum, written commun., 2009). However, these methods may suffer from magnitude and distance dependencies in converting peak ground motions to intensity, and vice versa. Consequently, in the evaluation of ground-motion prediction techniques outlined herein, we seek to evaluate many different components and metrics of ground-motion prediction techniques using simple analysis of residuals, assuming current ShakeMap methodologies.

Ground-Motion Datasets

In our analyses, we use strong ground-motion and macroseismic intensity datasets gathered to calibrate the Atlas of ShakeMaps (Allen and others, 2008, 2009b). Events included in the Atlas of ShakeMaps were chosen based on their magnitude and proximity to regions of significant population exposure. The data were subsequently characterized as either shallow-crust or subduction-zone datasets based on magnitude and hypocentral depth criteria outlined in Allen and others (2008). This was largely an automated process. However, some events were manually associated to either of the tectonic regimes if the automated association was inappropriate. The classification between active (both shallow crust and subduction zone) and stable crustal events was achieved using polygons of stable continents defined by Johnston and others (1994).

Instrumental Strong Motion

Three-component instrumental data for the ShakeMap Atlas were gathered from three key data sources: the Consortium of Organizations for Strong-Motion Observation Systems (COSMOS); the Internet Site for European Strong-Motion Data (ISESD, Ambraseys and others, 2004); and Kyoshin Network, Japan (K-NET). We deliberately avoided the use of the NGA dataset as this database provides the geometric mean (GM_{xy}) of response spectral ordinates (for example, Boore and others, 2006), while ShakeMap calls for peak values (or the larger of the two horizontal components). Consequently, for all our GMPE comparisons to recorded peak horizontal amplitudes, we follow the convention proposed by Beyer and Bommer (2006) for converting geometric mean to the larger of the two horizontal components (that is, larger PGA = 1.1 × GM_{xy} PGA).

Figure 1 indicates the magnitude-distance distribution of shallow-crust and subduction-zone data. Table 1 provides a summary of strong-motion data gathered for the Atlas of ShakeMaps (Allen and others, 2008). Individual earthquakes that compose the instrumental ground-motion database for active crustal, subduction-zone, and stable continents are indicated in Appendixes 1–3, respectively.

Table 1. Summary of the number of instrumental (peak horizontal component) data constraining earthquakes in the Atlas of ShakeMaps, categorized by tectonic environment, for peak ground acceleration (PGA), peak ground velocity (PGV) and spectral acceleration at 0.3, 1.0 and 3.0 seconds.

Tectonic setting	PGA	PGV	SA0.3	SA1.0	SA3.0
Active crust	10,168	8,524	8,468	8,479	8,423
Subduction zone	7,529	6,521	6,448	6,448	6,445
Stable continent	119	90	89	102	16
Total	17,816	15,135	15,005	15,029	14,884

Efforts were made to remove ground motions recorded on structures, such as dams or multi-level structures. However, we acknowledge that some structure-related recordings may have been included within the dataset owing to the assignment of an "unknown" structure type in our primary data sources. In this study, we assume that recordings on unknown structure types are free-field. In addition, we exclude all strong-motion data from aftershocks of the 1999 Chi-Chi, Taiwan, and 2004 Niigata, Japan, earthquakes for all active crust comparisons. Aftershock data from these events were not included in the global dataset because of concerns over spectral source scaling. For this reason, data from the Chi-Chi, Taiwan, aftershocks were not used in some of the NGA relations (for example, Boore and Atkinson, 2008; Campbell and Bozorgnia, 2008). Furthermore, because of the abundance of data gathered from aftershocks of these two events, we did not want to bias any of the ground-motion prediction comparisons by using these large regional datasets. For stable continental region (SCR) data, we include some weak-motion instrumental data to augment the strong-motion data for these earthquakes.

For each site, we assign topography-based shear-wave velocity (V_S^{30}) using the method of Wald and Allen (2007). This method uses the Shuttle Radar Topography Mission (SRTM, Balmer, 1999; Farr and Kobrick, 2000) digital elevation model to provide first-order estimates of V_S^{30} from the slope of topography for most global regions (Allen and Wald, 2007). Unfortunately, SRTM data are only available between latitudes of 60°N and 56°S. Consequently, for a few earthquakes in the catalog, we are unable to provide slope-based V_S^{30} estimates. For key earthquakes that are located outside these latitudinal bounds (for example, the 2002 M_W 7.9 Denali, Alaska, earthquake), we assign V_S^{30} values from the NGA dataset where these data are available. Topographically based V_S^{30} estimates are provided so that GMPE-specific site-correction factors can be applied during our comparisons.

To provide a reference frame for the amount of instrumental data collected in this study, the PEER NGA dataset contains more than 3,500 instrumental records from shallow crustal earthquakes (Chiou and others, 2008); Boore and Atkinson (2008) use approximately 1,600 of these records in development of their GMPE for California (Abrahamson and others, 2008). As is clearly seen in table 1, we use a much larger dataset to validate global GMPEs than is provided in the NGA database. It should be noted that great care was taken in the development of the NGA strong-motion dataset, which endeavored to include only high-quality records with comprehensive metadata. In contrast, we gather all available global data of variable quality. However, we make the assumption that the abundance of data used in these analyses will overwhelm any biases owing to poor data quality, or inaccuracies in digitization. This being acknowledged, it is important to note that the quality of the data presented herein is often superior to the data quality and quantity that we have to work with when generating ShakeMaps for real-time earthquake response.

Macroseismic Intensity

Many of the events in the Atlas of ShakeMaps were not captured by strong-motion instruments, but were nonetheless well documented with macroseismic observations. In our overall strategy for reproducing shaking levels for past events in the Atlas of ShakeMaps, documentation of observed shaking intensities from postdisaster surveys provides an important constraint.

For macroseismic intensity, the USGS uses Modified Mercalli Intensity (MMI) assignments consistent with the approach of Dewey and others (1995). Specifically, intensity XI and XII are no longer assigned, and intensity X is available but has not been applied for several decades. Where intensity assignments are made with Medvedev-Sponheuer-Karnik (MKS–64), European macroseismic (EMS–98), or other intensity scales, we assume equivalency, and herein we make no attempt to justify this assumption. Trifunac and Brady (1975) indicate the correlation between MMI and MKS intensity scales.

In addition to traditional intensity assignments conducted by experts (through field surveys, from engineering and other reports, or from postal questionnaires), we also use the "USGS Did You Feel It?" (DYFI?) system to augment the intensity dataset from recent earthquakes. The DYFI? system greatly facilitates and expedites collection of macroseismic data, allowing unprecedented numbers of direct shaking-intensity observations using online questionnaires (Wald and others, 2006; Atkinson and Wald, 2007). DYFI? data have also been shown to be consistent with USGS MMI assignments over the entire range of intensities (Dewey and others, 2002), with minor differences at the lowest intensities. Not only is DYFI? information valuable for areas that experience significant damage, it is also effective in constraining moderate ground motions at larger distances (or for smaller earthquakes) that are not damaging. Such data explicitly constrain the fact that ground motions were not damaging, whereas traditional macroseismic data-collection approaches often fail to collect or document such observations, focusing more on higher intensity data and events with such data. The DYFI? data are invaluable to constrain many recent atlas events, both in the United States (post-1999) and globally (post-2003), particularly for areas with few seismic instruments. These intensity observations can be treated as "stations" and added directly to the output ShakeMap intensity map as observational constraints on ground-shaking. In addition, converting these measurements to peak ground-motion amplitudes further calibrates contoured ground-motion ShakeMaps (Wald and others, 1999a). Reported DYFI? intensities from global earthquakes tend to be from observers in large towns or cities, providing critical ground-truth data where the population is concentrated (and thus where accurate loss estimates are most important).

The number of macroseismic intensity and DYFI? data available at the time of writing are summarized in table 2. Individual earthquakes that compose the macroseismic database for active crust, subduction zone, and stable continents are indicated in Appendixes 4–6, respectively.

Table 2. Summary of macroseismic intensity and DYFI? data constraining earthquakes in the Atlas of ShakeMaps, categorized by tectonic environment. MMI, Modified Mercalli Intensity; DYFI?, Did You Feel It?

Tectonic setting	MMI	DYFI?
Active crust	19,711	2,169
Subduction zone	3,210	1,073
Stable continent	13,950	1,188
Total	36,871	4,430

Earthquake Source Parameters and Distance Metrics

Hypocentral earthquake locations, magnitudes, and focal mechanism information for this study are drawn from the composite earthquake catalog, PAGER-CAT (Allen and others, 2009a). Finite fault information for calculating distance to rupture R_{rup} and distance to the surface projection of the fault (or Joyner-Boore distance) R_{JB} was extracted from constrained faults in the Atlas of ShakeMaps. Four distance metrics, epicentral distance R_{epi}, hypocentral distance R_{hyp}, R_{rup}, and R_{JB} were calculated using tools provided in the Matlab™ Mapping Toolbox (The MathWorks, 2006) and additional functions. Fault information within the atlas was derived from many data sources (see Appendix 1 and 2 in Allen and others, 2008). However, an important consolidated resource of finite-fault models was obtained from the online database provided by Martin Mai of the Swiss Seismological Service, Zurich (*http://www.seismo.ethz.ch/srcmod/*).

Instrumental Ground-Motion Predictions

Here we evaluate various instrumental ground-motion relationships against data gathered for the Atlas of ShakeMaps to determine which might be most applicable for GSM and PAGER applications. The standard GSM configuration presently prescribes the use of the Boore and others (1997) GMPE for shallow crustal earthquakes in all global active crustal regions, and Youngs and others (1997) for subduction-zone events. These GMPEs both produce reliable ShakeMaps in most regions. However, little quantitative work had previously been done to see how they perform against a global strong-motion dataset. Below, we test these, and other ground-motion prediction equations against the ShakeMap Atlas dataset.

ShakeMap sometimes requires ground-motion predictions at distances greater than those distances defined by some of the common GMPEs evaluated herein, particularly for large-magnitude earthquakes (approximately M_W 7.0 and greater). Consequently, we evaluate each of the GMPEs at distances that are of interest to Global ShakeMap. We are conscious that this usage will not necessarily be consistent with the usage specified by the authors of each of the GMPEs and that extrapolation of these models beyond the distance range specified may lead to unphysical ground-motion predictions owing to the functional forms of the equations. Where possible, we indicate the distance limitations of the GMPEs in the following comparisons.

Shallow Crustal Relations

Significant progress has been made in the development of shallow crustal GMPEs following the completion of the PEER NGA project. We chose to evaluate the three NGA models developed for the Western United States (Boore and Atkinson, 2008; Campbell and Bozorgnia, 2008; Chiou and Youngs, 2008) that were used in the U.S. National Seismic Hazard Maps (Petersen and others, 2008), in addition to the GMPE of Boore and others (1997) and two models developed for Europe and the Middle East by Ambraseys and others (2005) and Akkar and Bommer (2007a; 2007b). Table 3 shows a summary of these GMPEs listing their specific distance metrics and conditions of use.

Table 3. Summary of the candidate GMPEs for active crustal regions indicating their distance metrics and conditions of use. R_{rup}, distance to rupture; R_{JB}, Joyner-Boore distance; M_W, moment magnitude.

Reference	Magnitude range	Distance range (km)	Distance metric	PGV	Region
Boore and others (1997)	$5.2 < M_W \leq 7.7$	0 – 100	R_{JB}	No	Western US
Ambraseys and others (2005)	$M_W \geq 5.0$	0 – 100	R_{JB}	No	Europe and Middle East
Akkar and Bommer (2007a,b)	$5.0 \leq M_W \leq 7.6$	0 – 100	R_{JB}	Yes	Europe and Middle East
Boore and Atkinson (2008)	$5.0 \leq M_W \leq 8.0$	0 – 200	R_{JB}	Yes	Western United States
Campbell and Bozorgnia (2008)	$4.0 \leq M_W \leq 8.5$	0 – 200	R_{rup}	Yes	Western United States
Chiou and Youngs (2008)	$4.0 \leq M_W \leq 8.5$	0 – 200	R_{rup}	Yes	Western United States

Many of the modern ground-motion relations include complex terms for fault geometry (hanging wall/footwall) and basin terms. Because this information is scarcely available in the first minutes-to-hours when responding to significant global earthquakes, we do not include these terms in our comparisons. This may result in some misrepresentation of the aforementioned relations. However, we feel that this practice is justified given our requirements in predicting reliable first-order ground motions with limited knowledge in near real-time. We do, however, include terms that use the earthquake mechanism and depth to top of rupture where this information is available. We also apply site-correction factors as prescribed by the individual GMPEs using topographically based estimates of seismic site conditions (V_S^{30}).

Figures 2 and 3 illustrate the median residuals, binned at 10-km increments, for the shallow crustal GMPEs listed in table 3 for PGA and PGV, respectively. It is observed that most of the candidate GMPEs generally represent PGA well when compared against the global ground-motion dataset. However, some of the GMPEs tend to overestimate the aggregated global PGA at larger distances ($R > \sim150$ km) by up to one-half an order of magnitude in some instances. Although the prediction of ground shaking at these greater distances is scarcely of interest to well-engineered structures, it can still be critical in the overall ShakeMap calibration of near-source ground shaking. For example, if instrumental records or macroseismic intensity observations are only available at distant sites, these can be used to estimate an intraevent bias term for ground-motion prediction near the source.

Of the six candidate active crustal GMPEs, the Chiou and Youngs (2008) model generally performs the best, yielding consistently low PGA and PGV residuals to distances up to R_{rup} 350 km (figs. 2F and 3F). The other NGA models (Boore and Atkinson, 2008; Campbell and Bozorgnia, 2008) also perform well for the global dataset of ground motions. However, the Boore and Atkinson (2008) GMPE does appear to overestimate PGA at intermediate distances relative to the global dataset (fig. 2D), while Campbell and Bozorgnia (2008) tend to overestimate PGA at distances $R_{rup} > 150$ km (fig. 2E). Despite only being defined to a Joyner-Boore distance of 100 km, both Ambraseys and others (2005) and Akkar and Bommer (2007a,b) perform well against global PGA and PGV ground motions when extrapolated to larger distances. The observation that the Europe and Middle Eastern and NGA GMPEs all perform well against an independent dataset of global ground motions (including extensive ground-motion data from Japan) suggests that regionalization of ground-motion attenuation in shallow active tectonic crust may not be significant, at least for earthquakes of magnitude $M_W \geq 5.0$. This seems to be particularly apparent at shorter distance ranges (for example, $R <$ 100–150 km). We do expect that regional crustal structure will affect ground-motion attenuation at larger distances. However, this first-order assessment of GMPEs developed for different regions and evaluated against global data, suggests there is little difference between the physical characteristics of ground-motion attenuation from each of the regions where the models are derived.

Given four of our candidate active crustal GMPEs were developed specifically for the Western United States, our final comparisons in the present section indicate ground-motion residuals for each model using California data only (figs. 4 and 5). We include instrumental data recorded within latitude and longitude bounds of 32.5°N–42.0°N and 124.4°W–114.1°W. In addition to California strong-motion data, some Nevada strong-motion data are included in these comparisons; in particular, data from the 2008 M_W 6.0 Wells earthquake. The generally larger standard deviations in each distance bin when compared to the global dataset (figs. 2 and 3) point towards aleatory variabilities in the limited California dataset. However, the median residuals appear consistent with trends observed in the full global dataset. Each of the GMPEs developed through the NGA project perform well for PGA at distances less than 150 km (fig. 4). However, beyond 150 km, the Campbell and Bozorgnia (2008) model appears to overestimate PGA, as was observed with the full global dataset (fig. 2E).

For PGV, the Chiou and Youngs (2008) model provides the lowest median residuals for distances up to approximately R_{rup} 300 km for the California and Nevada dataset. Of the other active crustal models evaluated, the Europe and Middle Eastern and NGA GMPEs all perform well for the California PGV dataset (fig. 5).

The previous analysis has focused on the overall performance of the evaluated GMPEs. However, because the strong-motion data are not equally distributed across the magnitude range considered, we examine the ground-motion residuals in discrete magnitude bins for the Boore and Atkinson (2008) GMPE (fig. 6). In general, this model does appear to overestimate PGA at intermediate distances (approximately $50 \leq R_{JB} \leq 100$ km), particularly for earthquakes of magnitude $M_W < 6.0$. However, this apparent poor performance may also be due to aleatory variabilities in the dataset used. The transition of residuals with magnitude for the other candidate GMPEs for active crustal regions is illustrated in Appendixes 7 and 8 for PGA and PGV, respectively. From these appendixes, it can be observed that several of the other candidate GMPEs also overestimate PGA in the M_{W} 5.5–5.9 range.

Though not explicitly mentioned in the present discussion of active crustal GMPEs, we also illustrate the magnitude dependence of the Abrahamson and Silva (2008) and Idriss (2008) NGA GMPEs (Appendixes 9 and 10) in addition to an as yet unpublished GMPE for southern California by Cua and Heaton (G. Cua, written commun., 2008; Appendix 11).

Subduction-Zone Relations

We evaluate five subduction-zone GMPEs: Youngs and others (1997), Atkinson and Boore (2003), Kanno and others (2006), Zhao and others (2006), and Lin and Lee (2008). Table 4 shows a summary of these GMPEs, listing their specific distance metrics and conditions of use. Where mechanism and intraslab or interplate parameters are specified for a GMPE, we consider this information when calculating the ground-motion residuals for each model. The distinctions between intraslab and interplate events were largely determined from the logic provided in Allen and others (2008), which uses magnitude and focal depth as discriminates.

Table 4. Summary of the candidate GMPEs for subduction zones indicating their distance metrics and conditions of use. R_{rup}, distance to rupture; R_{hyp}, hypocentral distance; M_W, moment magnitude.

Reference	Magnitude range	Distance range (km)	Distance metric	PGV	Region
Youngs and others (1997)	$M_W \geq 5.0$	10 – 500	R_{rup}	No	Global
Atkinson and Boore (2003)	$4.5 \leq M_W \leq 8.3$	10 – 300	R_{rup}	No	Cascadia/ Global
Kanno and others (2006)	$5.5 \leq M_W \leq 8.2$	0 – 300	R_{rup}	Yes	Japan
Zhao and others (2006)	$4.9 \leq M_W \leq 8.3$	0 – 300	R_{rup}	No	Japan
Lin and Lee (2008)	$4.1 \leq M_W \leq 8.1$	30 – 500	R_{hyp}	No	Taiwan

Figure 7 indicates PGA residuals for the aforementioned equations. In general we find that the Youngs and others (1997), the Kanno and others (2006), and the Zhao and others (2006) GMPEs indicate low average residuals for the PGA values in our global dataset recoded at distances less than 400 km. The Atkinson and Boore (2003) ground-motion model, however, generally tends to underestimate PGA, by as much as half an order of magnitude in some distance ranges. This systematic underestimation of PGA by the Atkinson and Boore (2003) relation was also observed by Douglas and Mohais (2009) who evaluated various subduction-zone GMPEs for use in the Lesser Antilles region. In their manuscript, Atkinson and Boore (2003) identified that ground-motion amplitudes in Japan can differ from those observed in Cascadia by a factor of 2. Given that Atkinson and Boore (2003) primarily developed their subduction-zone GMPE for the Cascadia region and the bulk of our dataset are from Japanese subduction-zone earthquakes, this model may have physical basis. The limited instrumental data from Cascadia (see Appendix 2) did not allow us to fully test the utility of the Atkinson and Boore (2003) relations in this region. Consequently, this model is likely to still be of use for the northwest United States.

Unfortunately, only one of the subduction-zone GMPEs evaluated above explicitly provides coefficients for evaluating PGV (see table 4). For the other models, we must approximate PGV from other response spectral ordinates. Newmark and Hall (1982) proposed that in the absence of direct coefficients, PGV could be approximated using 1.0-second spectral acceleration. This approximation has become common in several hazard studies (for example, Pankow and Pechmann, 2004; Field and others, 2005) and is prescribed by standard HAZUS (Federal Emergency Management Agency, 1994) and ShakeMap (Wald and others, 2005) practice. However, Bommer and Alarcón (2006) argue, there has never been any direct proposal that 1.0-second spectral acceleration and PGV are proportional, and this practice has arisen from the use of the 1.0-second spectral ordinate historically being used to map hazard at periods longer than PGA. In their analysis, Bommer and Alarcón (2006) find that 0.5-second spectral acceleration provides a better proxy to PGV than spectral acceleration at 1.0 second. Consequently, we approximate PGV for those GMPEs that do not explicitly define PGV for both 1.0- and 0.5-second spectral accelerations, respectively.

Figure 8 shows median PGV residuals, binned in 10-km windows for each subduction-zone GMPE. For all but the Kanno and others (2006) GMPE, we approximate PGV from 1.0-second spectral acceleration using the approach of Newmark and Hall (1982). Of the five candidate GMPEs, we observe that the Youngs and others (1997), and the Kanno and others (2006) GMPEs provide the most consistent estimate of PGV against the global dataset. Though slightly underestimating PGV, the Zhao and others (2006) GMPE also performs relatively well assuming the Newmark and Hall (1982) approximation. Again, Atkinson and Boore (2003) appear to underestimate PGV at distances less than approximately R_{rup} 200 km relative to the global subduction-zone ground-motion dataset. The Youngs and others (1997) GMPE systematically overestimates PGV for distances of approximately $R_{rup} > 50$ km but generally performs relatively well.

Next, we plot PGV residuals based on 0.5-second spectral acceleration using the approach of Bommer and Alarcón (2006) (fig. 9). Using this approach, we see significantly improved performance from the Zhao and others (2006) GMPE for PGV, with low median residuals over the distance range considered. The Atkinson and Boore (2003) GMPE also appears to improve slightly using the Bommer and Alarcón (2006) approach, though still underestimating PGV at distances less than R_{rup} 200 km. There appears to be no obvious improvement for other candidate models from taking the Bommer and Alarcón (2006) approach in estimating PGV from spectral ordinates.

The transition of residuals with magnitude for the candidate subduction-zone GMPEs is illustrated in Appendixes 12 and 13 for PGA and PGV, respectively. From these figures, we observe that the most consistently performing GMPE over all magnitude ranges for both PGA and PGV is Zhao and others (2006).

To summarize our findings of this section, we observe the Youngs and others (1997), Kanno and others (2006), and Zhao and others (2006) GMPEs all tend to yield the low median residuals for PGA and PGV assuming the use of site-correction factors prescribed by the authors. Overall, the approach for evaluating PGV from response spectral acceleration at 0.5 second as proposed by Bommer and Alarcón (2006) appears to perform slightly better than the Newmark and Hall (1982) approach. However, the differences between the two methods for approximating PGV from spectral acceleration are relatively minor.

One concern in using the Kanno and others (2006) or Zhao and others (2006) GMPEs in GSM is that these models tend to predict significantly larger near-source ground motions than most of the other candidate GMPEs, particularly for large-magnitude earthquakes on soil sites (fig. 10). However, the available instrumental dataset for subduction-zone earthquakes was not sufficient for high-magnitude, near-source sites, so this concern could not be studied in detail.

Stable Continental Regions

Finally, we evaluate four instrumental GMPEs developed for stable continental regions (SCRs): Atkinson and Boore (1995), Toro and others (1997), Campbell (2003; 2004), and Atkinson and Boore (2006). Table 5 shows a summary of these GMPEs listing their specific distance metrics and conditions of use. Unlike the large datasets we had to assess active crustal and subduction-zone GMPEs in the previous analyses, we only have a very limited ground-motion dataset from moderate-to-large earthquakes in SCRs. Furthermore, because of the sparse number of strong-motion recordings in SCRs, particularly for larger earthquakes, none of the candidate GMPEs are based upon empirical analyses of SCR strong-motion data. Three of the candidate models (Atkinson and Boore, 1995; Toro and others, 1997; Atkinson and Boore, 2006) use stochastic simulations to scale ground-motion properties observed from small-to-moderate magnitude earthquakes to estimate ground motions for large earthquakes. The Campbell (2003) GMPE uses a hybrid approach to transfer GMPEs developed in active crustal areas to SCRs based on the different scaling characteristics of intraplate earthquakes.

Table 5. Summary of the candidate GMPEs for stable continental regions indicating their distance metrics and conditions of use. R_{rup}, distance to rupture; R_{hyp}, hypocentral distance; R_{JB}, Joyner-Boore distance; M_W, moment magnitude; ENA, Eastern North America.

Reference	Magnitude Range	Distance Range (km)	Distance Metric	PGV	Region
Atkinson and Boore (1995)	$4.0 \leq M_W \leq 7.25$	10 – 500	R_{hyp}	Yes	ENA
Toro and others (1997)	$4.5 \leq M_W \leq 8.0$	1 – 500	R_{JB}	No	ENA
Campbell (2003; 2004)	$5.0 \leq M_W \leq 8.0$	1 – 1000	R_{rup}	No	ENA
Atkinson and Boore (2006)	$4.0 \leq M_W \leq 8.0$	30 – 1000	R_{rup}	Yes	ENA

Since we do not possess abundant SCR ground-motion data, we do not provide plots indicating median residuals of PGA and PGV as in the above analyses. Rather, we plot individual ground-motion residuals for each GMPE, color-coded by earthquake magnitude (figs. 11 and 12). We use NEHRP site-class amplification factors (Borcherdt, 1994) and topographically based V_S^{30} estimates (Wald and Allen, 2007) to correct the observed ground-motion amplitudes to BC rock conditions when comparing these SCR GMPEs. Based on our limited collection of SCR ground-motion data, we observe that the Atkinson and Boore (2006) relation provides the lowest residuals for PGA, particularly in the near-source region (less than R_{rup} 150 km). However, this is a very subjective inference based on limited, highly variable, SCR data. The other stable continent GMPEs tend to overestimate PGA at near-source distances. The Campbell (2003) GMPE appears to predict PGA quite well at distances larger than approximately 150 km from the earthquake source. It should be noted that some of these stable continent ground-motion relations are not designed to predict ground motions for small-magnitude (M < 4.5-5.0) earthquakes (see table 5).

For PGV we observe that the hybrid GMPE of Campbell (2003) appears to provide the lowest residuals for our limited dataset over the distance range considered. The Atkinson and Boore (2006) model also appears to provide low residuals near the source but tends to slightly underestimate PGV at larger distances. The other GMPEs considered perform better for PGV than PGA but still tend to overestimate ground motions in the near-source region.

Based on analyses of macroseismic intensity data, Bakun and McGarr (2002) suggest that there are significant differences in attenuation characteristics among SCRs. Allen and Atkinson

(2007) also show there are differences in attenuation between eastern North America and southeastern Australia at hypocentral distances greater than 70 km. However, their studies suggest that there is little difference in the attenuation characteristics between the two SCRs at distances less than approximately 70 km based on the analysis of small-to-moderate-sized earthquakes. In selecting a reliable stable continental GMPE for Global ShakeMap and PAGER purposes, we are most concerned about predicting ground motions that are more likely to produce significant losses near the earthquake source. Consequently, this must be an important consideration in the choice of our preferred GMPE.

As an alternative approach, we test the six active crustal candidate GMPEs considered previously to evaluate whether any of these models could be used as a proxy for predicting ground motions for stable continental regions given the relative uncertainty in ground-motion prediction using SCR GMPEs for large earthquakes (that is, SCR GMPEs are derived from very little ground-motion data from large earthquakes). All active crustal GMPEs, except Boore and others (1997), appear to underestimate PGA for SCR ground motions at intermediate-to-large distances (fig. 13). This is to be expected given the commonly acknowledged phenomenon that attenuation of ground-shaking with distance is lower in stable continental regions (for example, Nuttli, 1973; Nuttli and Zollweg, 1974; Frankel and others, 1990; Bakun and McGarr, 2002; Atkinson and Wald, 2007). However, when we examine the PGV residuals (fig. 14), it appears that many of the active crustal GMPEs systematically overestimate ground shaking in the near-source region for these moderate-magnitude earthquakes. These active crustal GMPEs, however, generally tend to target ground-motion prediction for larger-magnitude earthquakes and may not be as well calibrated to the lower-magnitude SCR ground motions considered here. Recent research now suggests faster attenuation in the near-source region than previously thought in some SCRs (for example, Atkinson, 2004; Allen and others, 2007). Consequently, usage of these active crustal ground-motion models may be a valid alternative, at least at shorter source-receiver distances (approximately R_{rup} < 100 km) and longer periods of ground shaking.

Peak Ground-Motion-to-Intensity Relations

Equations that relate peak ground motions to macroseismic intensity observations are an important component in GSM and PAGER applications (Wald and others, 1999b). In generating a

ShakeMap, instrumental peak ground motions (PGMs) are first calculated over the spatial extent of the map by using a GMPE similar to the models previously discussed. Once the peak ground motions are estimated, they are then converted to macroseismic intensity to produce a map of shaking intensity. These maps of macroseismic intensity calculated in GSM are subsequently used in PAGER to estimate the number of people exposed to potentially fatal ground-shaking intensities.

We examine the use of four candidate equations for converting peak ground motions to macroseismic intensity: Wald and others (1999a), Atkinson and Sonley (2000), Atkinson and Kaka (2007), and Tselentis and Danciu (2008). Each of these equations relate Modified Mercalli Intensity (MMI) to both PGA and PGV, and the authors generally recommend the use of PGV as the most reliable predictor of MMI, particularly at higher intensities. The Wald and others (1999a) equation recommends a combination of PGV and PGA. These PGM–MMI relations are tested for both shallow active crust and subduction-zone regions. Given the uncertainty in selecting a preferred GMPE for stable continental regions, we do not test the PGM–MMI relations using the methods described herein. Table 6 provides a summary of the PGM–MMI relations evaluated with their conditions of use.

Table 6. Summary of the candidate peak ground-motion-(PGM) to-intensity relations indicating their conditions of use.

Reference	Magnitude range	Distance range (km)	Intensity range	Region
Wald and others (1999a)	$5.8 < M_W \leq 7.3$	–	4 – 9	California
Atkinson and Sonley (2000)	$4.9 < M_W \leq 7.4$	1 – 300	3 – 9	California
Atkinson and Kaka (2007)	$1.8 < M_W \leq 7.1$	4 – 788	1 – 9	North America
Tselentis and Danciu (2008)	$4.0 \leq M_W \leq 6.9$	1 – 124	4 – 8	Greece

Active Shallow Crust

In order to test the applicability of each of these conversion equations for active shallow crustal regions, we first estimate PGA and PGV using a GMPE for the magnitude and distance pairs equivalent to those of the macroseismic intensity observations. For shallow active crustal observations, we predict peak ground motions using the Chiou and Youngs (2008) GMPE. We also apply seismic site corrections prescribed by Chiou and Youngs (2008) based on V_S^{30} estimates from topographic slope (Wald and Allen, 2007) for each intensity observation. The Chiou and Youngs (2008) GMPE was chosen to predict the peak ground motions because it yielded robust ground-motion predictions relative to the global instrumental ground-motion database. Once we have estimated the peak ground motions, we then use these values to predict MMI at each intensity observation point using PGM–MMI conversions. The residual of the observed and predicted intensities are subsequently calculated for all global macroseismic intensity data. The median residuals, binned in 10-km windows, are plotted in figure 15. The use of PGA only, as implemented by Atkinson and Sonley (2000) and Atkinson and Kaka (2007) are generally observed to be a relatively poor predictors of MMI (figs. 15A and 15C). The Tselentis and Danciu (2008) PGA–MMI equation provides the best estimate of MMI from PGA predictions but still tends to underestimate MMI by approximately one-half an intensity unit (fig. 15E). We use R_{rup} as the distance metric since this is the metric used by the Chiou and Youngs (2008) prediction model.

The combination of the Chiou and Youngs (2008) PGV prediction and the Tselentis and Danciu (2008) intensity conversion equation, although systematically underestimating intensity, provides the best estimate of MMI from a purely predictive sense (fig. 15E). Although having slightly larger median residuals, the Atkinson and Kaka (2007) conversion yields lower median residuals than Tselentis and Danciu (2008) at near-source distances (approximately $R_{rup} < 20$ km; fig. 15D). It is possible that the good performance of the Atkinson and Kaka (2007) and Tselentis and Danciu (2008) equations for conversion of PGV–MMI is because they both include corrections for both distance and magnitude. It should be noted the median underestimate using these PGM–MMI equations is still almost one-half an intensity unit (median residual ≈ 0.3). The Atkinson and Sonley (2000) also use distance and magnitude as predictor variables, but this model does not appear to perform well against global intensity data, particularly at distances greater than R_{rup} 20 km (fig. 15B).

Next we test the Wald and others (1999a) PGM–MMI equation, which uses a combination of PGA and PGV to convert instrumental ground motions to intensity (fig. 16A). This relation specifies using PGA for low intensities and PGV at higher intensities, with a smooth transition between the two relations between MMI V and VII. Using this combined approach, the Wald and others (1999a) relations perform relatively well in the near-source region (approximately R_{rup} 10–20 km). However, these relations systematically underestimate MMI at larger distances, with a median MMI residual of 1.2 when used with Chiou and Youngs (2008) peak ground-motion predictions.

To examine the discrepancies between our predicted and observed intensities from the Wald and others (1999a) relations, we recalculate the residuals using the Boore and others (1997) GMPE to estimate peak ground motions. The combination of these relations has been the standard configuration for ShakeMap instrumental intensity prediction since GSM was first implemented in 2004 and is currently used to estimate PAGER global population exposures for shallow crustal earthquakes. We observe that the combination of these two relations results in a much improved mapping of observed-to-predicted intensities, with a median residual near zero over the distance range considered (fig. 16B). Consequently, the net result of the underestimation of MMI from the Wald and others (1999a) relations and the overestimation of ground-motion at larger distances from the Boore and others (1997) GMPE combines to provide relatively robust estimates of the overall shaking intensity.

Finally, because both the Wald and others (1999a) and Atkinson and Sonley (2000) PGM–MMI equations were based solely from regressions on California instrumental and macroseismic ground motions, we isolate all macroseismic intensities assigned in California and Nevada from our dataset to examine whether there are any regional dependencies that might cause ambiguity in the application of these conversion equations for global data. As in the previous examples, we use the Chiou and Youngs (2008) GMPE to predict peak ground motions at the intensity observation points using magnitude, distance to the rupture, earthquake mechanism (if known) and topographically derived V_S^{30} as predictor variables. Though we see some improvement in the median residuals, we observe the same general underestimation of intensity at increasing source-receiver distances (see fig. 17A for the example of Wald and others, 1999a). When using the Wald and others (1999a) relations in combination with the Boore and others (1997) GMPE for the California intensity data, we observe that the median residuals are again consistently low and have values near zero over a large distance range (fig. 17B). From figures 4 and 5, we know that the Boore and others (1997) GMPE generally tends to overestimate peak ground motions for the contemporary dataset of California and Nevada ground motions. However, the combination of the Boore and others (1997) GMPE and the Wald and others (1999a) PGM–MMI for the California intensity data suggests that both of these relations are faithful to their respective ground-motion datasets. The relatively poor performance of these relations in previous examples — which use much larger ground-motion datasets — suggests that they may suffer from aleatory uncertainties owing to the limited number of data used to derive them. This limited number of data is particularly apparent when we consider the relative abundance of ground-motion data used to derive modern ground-motion models (for example the NGA equations).

In summary, to obtain a reliable combination of both GMPE and PGM–MMI equations, we recommend using the Chiou and Youngs (2008) GMPE with either the Atkinson and Kaka (2007) or the Tselentis and Danciu (2008) PGM–MMI conversion equation. Since we obtain lower near-source residuals — where constraining ground-shaking is most important — our current preference would be to use the Atkinson and Kaka (2007) PGV conversion.

Subduction Zones

We repeat the process above to examine the use of PGM–MMI conversion equations for subduction zones (fig. 18). In this case, we use the Youngs and others (1997) GMPE to predict ground motions for the magnitude, distance, and site condition combinations equivalent to those of the macroseismic intensity observation points from subduction-zone events. We observe the Atkinson and Kaka (2007) PGV conversion equation to provide the most reliable estimates of MMI from instrumental ground-motion predictions (fig. 18D), under the assumption that the Youngs and others (1997) GMPE provides reliable PGA and PGV values over all distance and magnitude ranges. Consequently, the combination of the Youngs and others (1997) GMPE with the Atkinson and Kaka (2007) PGM–MMI conversion results in median MMI residuals near zero, though there are larger variabilities among each the median residuals than observed for the shallow active crustal data (fig. 17).

Of particular interest, the Wald and others (1999a) PGM–MMI conversion equations appear to perform very well when compared to intensity observations from subduction-zone earthquakes. It is unclear why the Wald and others (1999a) conversions perform better for subduction-zone events relative to the shallow crustal events compared previously (fig. 17A); however, it may be due to the overall larger magnitude events included in the subduction-zone intensity dataset (see Appendix 5) The combination of the Youngs and others (1997) GMPE and Wald and others (1999a) conversion is currently the default configuration for the prediction of instrumental intensity for subduction-zone events in GSM.

Macroseismic Intensity Prediction Equations

Although not presently used in ShakeMap applications, we considered the use of several macroseismic prediction equations for estimating the spatial variation of shaking intensity. As previously discussed, current ShakeMap practice is to first estimate instrumental peak ground-motion (both PGA and PGV) and convert these values to intensity to provide a macroseismic representation of the observed shaking. In this process, not only do we have to consider the uncertainty of the GMPE, but also the uncertainty in the conversion of instrumental to macroseismic ground motions. The Wald and others (1999a) PGM–MMI relation specifies a standard deviation of approximately one MMI unit, while the Atkinson and Kaka (2007) equation specifies a standard deviation of 0.8 MMI unit. Consequently, we examine whether using an MMI prediction equation to directly predict macroseismic intensity would lead to a reduction in uncertainty from the combination of a GMPE and PGM–MMI equation. To solve this problem, we evaluate eight macroseismic intensity prediction equations from various tectonic settings (table 7): Bakun and Wentworth (1997), Bakun and others (2003), Bakun (2006), Bakun and Scotti (2006), Atkinson and Wald (2007) for both California and Eastern United States; Pasolini and others (2008), and Sørensen and others (2009). The main criterion in selecting these models is that they are scaled to moment magnitude rather than the epicentral intensity I_0. Each of these equations is subsequently tested against observed macroseismic intensities from global shallow crustal, subduction-zone, and stable tectonic regions. In performing these comparisons, we do not consider the magnitude or distance criteria specified by the authors of a particular macroseismic intensity prediction model. In contrast, we include earthquake data of magnitude and distance ranges that are of interest to Global ShakeMap operations. Furthermore, we note that some of the prediction equations tested model use different intensity scales (for example, EMS or MCS). However, as mentioned previously, we do not consider differences among the various intensity scales and assume equivalence between them. We also only consider macroseismic observations recorded at distances less than 400 km.

Table 7. Summary of the candidate macroseismic intensity prediction equations indicating their conditions of use and host tectonic setting. R_{rup}, distance to rupture; R_{epi}, epicentral distance; R_{JB}, Joyner-Boore distance; M_W, moment magnitude; MMI, Modified Mercalli Intensity; MCS, Mercalli-Cancani-Sieberg Intensity; MSK, Medvedev-Sponheuer-Karnik Intensity; EMS-98, European Macroseismic Scale; ENA, Eastern North America.

Reference	Magnitude range	Distance range (km)	Intensity range	Distance metric	Intensity type	Region
Bakun and Wentworth (1997)	$4.4 \leq M_W \leq 6.9$	< 500	3 – 9	R_{epi}	MMI	California
Bakun and others (2003)	$3.7 \leq M_W \leq 7.3$	< 1200	3 – 7	R_{epi}	MMI	ENA
Bakun (2006)	$4.6 \leq M_W \leq 7.3$	< 500	3 – 8	R_{epi}	MMI	Basin and Range
Bakun and Scotti (2006)	$4.9 \leq M_W \leq 6.0$	< 150	3 – 7	R_{epi}	MSK	Southern France
Atkinson and Wald (2007)	$2.3 \leq M_W \leq 7.8$	2 – 500	2.0 – 10†	R_{rup}	MMI	California
Atkinson and Wald (2007)	$2.0 \leq M_W \leq 7.8$	6 – 1000	2.0 – 11+†	R_{rup}	MMI	ENA
Pasolini and others (2008)	$4.4 \leq M_W \leq 7.4$	1 – 200	4 – 11	R_{epi}	MCS	Italy
Sørensen and others (2009)	$5.9 \leq M_W \leq 7.4$	0 – 335	5 – 10	R_{JB}	EMS-98	Marmara Sea, Turkey

† Estimated from figure 4 of Atkinson and Wald (2007).

Active Shallow Crust

Figure 19 indicates median residuals, binned with distance for each of the candidate MMI intensity prediction models. Over 21,000 macroseismic intensity observations from active crustal regions around the world were used to evaluate the models. Of the candidate models, we observe that the Bakun and Wentworth (1997) prediction model, developed for California earthquakes, yields the lowest average residuals over the distance range examined (fig. 19A). However, this model tends to overestimate intensity at small epicentral distances (R_{epi} < 20 km) because it does not saturate at near-source distances. The Bakun and Wentworth (1997) model also appears to slightly underestimate MMI at distances larger than approximately R_{epi} 70 km. The Bakun (2006) and Bakun and Scotti (2006) intensity prediction models appear to perform relatively well over the distance range considered. However, both of the aforementioned prediction equations overestimate intensity at distances less than approximately R_{epi} 80–100 km.

The Atkinson and Wald (2007) prediction model, which is largely based on DYFI? data from the Western United States, appears to systematically underestimate observed intensities by one-half to a full-intensity unit for much of the distance range considered. Other relations examined herein do not appear to be applicable for use in GSM for active tectonic regions based on the comparison against our global macroseismic intensity dataset.

Subduction Zones

In our literature survey, we did not find any modern macroseismic intensity prediction equations for subduction zones that were specifically scaled to moment magnitude M_W. Consequently, we test the same set of macroseismic intensity prediction equations as in table 7. A relatively modest number of over 3,600 macroseismic intensity observations from global subduction-zone earthquakes were used in this analysis (fig. 20). Of the eight candidate intensity-prediction equations, we observe that the Bakun and Scotti (2006) model developed for southern France provides the lowest median residuals for subduction-zone earthquakes (fig. 20D). This raises some questions as to the physical meaning of this result, given that we could argue that the southern France region could not be considered indicative of an active subduction zone, particularly given that the calibration events are from moderate-magnitude shallow crustal earthquakes.

The Bakun and Wentworth (1997) model overestimates intensity at epicentral distances less than approximately 40 km. However, at larger epicentral distances the Bakun and Wentworth (1997) prediction model yields consistently low median residuals. It is interesting to note that the Bakun and Wentworth relation provides low residuals at distant sites (approximately R_{epi} > 40 km) for both active crustal (fig. 19A) and subduction-zone (fig. 20A) earthquakes. This suggests that average global attenuation properties in the crust surrounding shallow active tectonic and subduction zones are similar at intermediate epicentral distances from the earthquake source. It is likely that at distances greater than approximately 50 km, high-frequency surface waves (*Lg*) dominate observed ground motions (for example, Herrmann and Kijko, 1983), and these are the seismic waves that are perceptible to humans (for example, Trifunac and Brady, 1975; Frankel, 1994) and those that dominate macroseismic earthquake effects. The observation that the Bakun and Wentworth (1997) prediction model overestimates subduction-zone intensity data at shorter epicentral distances may be a consequence of more emergent ground motions at longer periods than typically observed from shallow active crustal earthquakes.

Stable Continent

Some 13,300 macroseismic observations from stable continental regions around the world were used to evaluate the candidate macroseismic intensity prediction equations (fig. 21). Of the candidate models, the Bakun (2006) prediction model for the Basin and Range (fig. 21C) provides the lowest median residuals for near-source (approximately $R_{epi} < 50$ km) intensity observations in stable continental regions. However, this model does not perform very well beyond this distance range, underestimating ground shaking for combined stable continent observations.

The Bakun and others (2003) model for eastern North America, which has consistently overestimated intensity in previous comparisons for active crust and subduction zones (figs. 19B and 20B, respectively), performs better in the present evaluation (fig. 21B), as should be expected. This model performs very well at epicentral distances greater than approximately 200 km, where it predicts higher intensities than many of the other models, commensurate with the observation that ground-motion energy attenuates slower in stable continental regions. However, the Bakun and others (2003) model systematically overestimates macroseismic intensity at distances less than 200 km. Furthermore, at near-source distances, this model overestimates median intensity by over 2 intensity units.

Of significant interest is that the observed residuals for the Bakun and Wentworth (1997), Bakun (2006), and Sørensen and others (2009) models, in particular, behave similarly in both the active crustal (fig. 19) and stable continent (fig. 21) comparisons for epicentral distances less than 50–60 km. This suggests that near-source attenuation of macroseismic intensities may be similar in both tectonic regimes. Although differences in high-frequency source energy between active and stable tectonic earthquakes are expected (for example, Atkinson, 1996), attenuation of lower-frequency energy ($f \approx 2$–4 Hz) may not be too different. This is significant in that these are the frequencies perceptible to humans (Trifunac and Brady, 1975; Frankel, 1994) and also are among the range of frequencies most likely to cause the most serious damage to common residential structures. If differences in the attenuation of intensity observations between active crust and stable continental regions are deemed to be insignificant at near-source distances, then active crustal data could be used to supplement stable continent intensities for prediction models in the absence of large-magnitude earthquake data. Indeed, Hanks and Johnston (1992) suggested that body-wave attenuation between the Eastern and Western United States is comparable out to distances of approximately 150 km based on their analysis of the spatial area enclosed by damaging MM intensities (MMI VI to VII). The augmentation of near-source active crustal data to SCR datasets may also have implications for development of instrumental SCR GMPEs. However, in addition to limitations at larger distances, it is likely that there will be some limitations in the frequency range of the supplemental active crustal data owing to the contribution of higher frequency energy, and consequently higher stress drops, commonly observed from SCR earthquakes (for example, Atkinson, 1993, 1996; Negishi and others, 2002).

Discussion and Application for Global ShakeMap

Though not exhaustive, this overview provides a comprehensive analysis of GMPEs and macroseismic intensity prediction techniques in different tectonic regimes. The primary purpose for this study was to evaluate these techniques with a view to improving current practices in ground-motion prediction for the Global ShakeMap and PAGER systems for near real-time earthquake response. In this study, we evaluate several commonly used GMPEs for active tectonic crust, subduction zones, and stable continental regions. We also evaluate peak ground-motion-to-intensity (PGM–MMI) conversion equations, which are an important component of estimating shaking intensity in ShakeMap from instrumental ground-motion predictions. Finally, we evaluate several macroseismic intensity prediction equations against a large dataset gathered for the Atlas of ShakeMaps (Allen and others, 2008, 2009b).

Of the active crustal GMPEs, the Chiou and Youngs (2008) model appears to provide the lowest median residuals against the global ground-motion dataset for PGA and PGV over the magnitude and distance range considered for GSM usage. For instrumental ground-motion predictions in active crustal regions, we recommend the use of this GMPE, using the site-correction factors as prescribed by Chiou and Youngs (2008). Other active crustal GMPEs also perform well for active crustal data and should be viewed as valid alternatives (figs. 2–5, and Appendixes 7–11). Of interest to the authors was that there appeared to be little difference between GMPEs developed for the Western United States and those developed for Europe and the Middle East, particularly given the significant quantities of Japanese strong-motion data used in the comparisons. We acknowledge that global data were used in the development NGA relations, and this may explain some of these similarities. However, the primary objective in the development of the NGA models was to predict ground motions in the Western United States. This raises the fundamental question as to whether many of the historically observed regional differences in ground-motion attenuation can be more likely attributed to aleatory variabilities in the sparse, regionally specific datasets. We do expect that regional crustal structure will affect ground-motion attenuation distances larger than approximately 100 km. However, as a first-order assessment against global shallow crustal ground-motion data, median ground-motion residuals do not appear to be regionally dependent.

Of the GMPEs for subduction zones, we observe that the Youngs and others (1997), Kanno and others (2006), and Zhao and others (2006) equations all provide the median residuals over the distance range examined, for both PGA and PGV. The Youngs and others (1997) and Zhao and others (2006) GMPEs do not explicitly provide coefficients for PGV. However, the use of 0.5-second or 1.0-second spectral acceleration using conversion factors of Bommer and Alarcón (2006) and Newmark and Hall (1982), respectively, appears to provide a sufficient approximation to PGV. The Atkinson and Boore (2003) GMPE appears to systematically underestimate ground motion by up to one-half an order of magnitude at near-source distances. This underestimation was also identified by Douglas and Mohais (2009) in the Lesser Antilles region. Atkinson and Boore (2003) suggested that ground-motion amplitudes in Japan can differ from those observed in Cascadia by a factor of 2. Given that Atkinson and Boore (2003) primarily developed their subduction-zone GMPE for the Cascadia region and the bulk of our dataset are from Japanese subduction-zone earthquakes, this model may still have applicability in the United States (for example, Applied Technology Council, 2006). However, this was not explicitly studies herein.

Given the sparse ground-motion dataset for stable continental regions, no single GMPE emerged as a preferred model (figs. 11 and 12). The Campbell (2003) GMPE generally provides the lowest ground-motion residuals over the examined distance range, while the Atkinson and Boore (2006) model yields the most reliable estimates of ground motion near the earthquake source. However, we reiterate that these observations are based on subjective analysis on a limited instrumental ground-motion dataset.

We also evaluate the active crustal GMPEs against the SCR dataset. We observe that some of the active crustal models provide reasonable estimates of PGA and PGV at near-source distances (R_{rup} < 100 km). However, the active tectonic models invariably underestimate instrumental ground motion beyond these near-source distances (figs. 13 and 14). This is consistent with many studies that find lower ground-motion attenuation in SCRs (for example, Nuttli, 1973).

Peak ground-motion-to-intensity conversions are an important component in ShakeMap applications. Current ShakeMap practice is to use these conversions to estimate “instrumental intensity” to describe earthquake shaking distribution. We evaluated the use of four PGM-to-intensity conversion equations: Wald and others (1999a), Atkinson and Sonley (2000), Atkinson and Kaka (2007), and Tselentis and Danciu (2008). In active crustal regions, we find that the Atkinson and Kaka (2007) and Tselentis and Danciu (2008) models both provide robust estimates of MMI based on the use of the Chiou and Youngs (2008) GMPE as the predictor of PGV (fig. 15). However, both of these PGM–MMI relations still result in a net underestimation of MMI. For subduction-zone regions, the combination of the Youngs and others (1997) GMPE and the Atkinson and Kaka (2007) PGV–MMI conversion generally yields low residuals over the magnitude and distance range considered (fig. 18D).

In our analyses, we also evaluate the current GMPE and PGM–MMI configuration for active crust used in GSM: the Boore and others (1997) GMPE and the Wald and others (1999a) PGM–MMI equation. We observe that the combination of these two relations results in a much improved mapping of observed to predicted intensities, with a median residual near zero (fig. 16B and 17B). Consequently, the net result of the underestimation of MMI from the Wald and others (1999a) relations and the overestimation of ground motion at larger distances from the Boore and others (1997) GMPE provides a reasonable estimate of the overall shaking intensity. Our analysis suggests that both the Boore and others (1997) GMPE and Wald and others 1999a PGM–MMI conversions are faithful to their respective ground-motion datasets and that they may suffer from aleatory uncertainties owing to the limited number of earthquakes used to derive them, compared to the relative abundance of contemporary ground-motion datasets.

We evaluated eight macroseismic intensity-prediction equations to see whether these were able to reproduce shaking estimates in active tectonic, subduction-zone, and stable continental tectonic regimes. Motivation for evaluating this approach is that current ShakeMap practice requires us not only to consider the uncertainty of the GMPE, but also the uncertainty in the conversion of instrumental predictions to macroseismic ground motions (Wald and others, 2008b). Consequently, an equation where macroseismic intensity could be directly predicted may be more desirable since it could reduce this combined uncertainty. In general we find that none of the macroseismic intensity equations are necessarily desirable against the global macroseismic dataset for any of the tectonic regimes considered. However, some important trends in the data residuals between the tectonic regimes were identified. First, it appears that attenuation of macroseismic intensity data between active-crust and subduction zones at epicentral distances greater than approximately 50 km appear quite similar (figs. 19 and 20). This may be because intensities are being assigned based on the felt effects of high-frequency surface waves (*Lg*), which dominate observed ground motions at distances larger than 50 km. Furthermore, these are the seismic waves propagating at frequencies that are perceptible to humans (Trifunac and Brady, 1975; Frankel, 1994) and the waves that dominate macroseismic earthquake effects to residential dwellings. Second, we note that macroseismic attenuation between active crust and stable continental regions does not appear to be significantly different at distances less than approximately 50–60 km (figs. 19 and 21). If differences in the attenuation of macroseismic intensity between active crust and stable continental regions are deemed to be insignificant at near-source distances, then active-crustal data could be used to supplement stable continent intensities for prediction models in the absence of large-magnitude SCR earthquake data. The augmentation of near-source active-crustal data to SCR datasets may also have implications for development of empirical SCR GMPEs.

We acknowledge that, unlike the NGA project which took great care in gathering a high-quality strong-motion dataset (Chiou and others, 2008), we have not been as careful in our data acquisition and quality assessment. However, we make the assumption that the abundance of data used in these analyses will overwhelm any minor biases owing to poor data quality or inaccuracies in digitization. This being said, it is important to note that the quality of the data presented herein is commonly superior to the data quality and quantity that we have to work with when generating ShakeMaps for real-time earthquake response.

Finally, some authors have suggested that low-period filtering effects at periods greater than 4 seconds can have a significant effect on PGV values derived from integration of strong-motion accelerograms (for example, Akkar and Bommer, 2006; Bommer and Alarcón, 2006). This is how many of our PGV values were processed, particularly those from the ISESD. Although very important for large critical infrastructure such as power stations, transport networks, or large dams, high PGV values at long periods often are not perceptible to humans and cause little to no damage to low-rise residential structures. At present, we accept that the PGV values in our database may have some problems for larger magnitude earthquakes, and this should also be a consideration in the selection of appropriate ground-motion modeling techniques.

Herein, we have provided a comprehensive, though not exhaustive, review of ground-motion modeling techniques that could be used in Global ShakeMap and PAGER applications. Although current ground-motion modeling techniques may presently be adequate, they are not necessarily ideal for our requirements on a global scale. Consequently, we suggest some changes to the default ground-motion prediction configurations in GSM. There is also some scope for developing improved GMPEs for stable continental regions, in addition to the development of improved macroseismic intensity prediction techniques.

Acknowledgments

Discussion of preliminary results with Frank Scherbaum, Bruce Worden, Art Frankel, Mark Petersen, Paul Earle, and Kuo-Wan Lin were very valuable throughout this study. John Douglas is thanked for providing information and advice on the use of the European Strong-Motion dataset and directing the authors towards several key studies referenced in this report. Steve Harmsen and Art Frankel are thanked for their reviews which improved this manuscript. Alicia Hotovec and Kristin Marano are thanked for helping to maintain the Atlas of ShakeMaps and for spending many hours digitizing macroseismic intensity data used in this study. Funding for this research was provided, in part, by a grant from U.S. Agency for International Development (USAID).

References Cited

Abrahamson, N., Atkinson, G., Boore, D., Bozorgnia, Y., Campbell, K., Chiou, B., Idriss, I.M., Silva, W., and Youngs, R., 2008, Comparisons of the NGA ground-motion relations: Earthquake Spectra, v. 24, no. 1, p. 45–66.

Abrahamson, N., and Silva, W., 2008, Summary of the Abrahamson & Silva NGA ground-motion relations: Earthquake Spectra, v. 24, no. 1, p. 67–97.

Akkar, S., and Bommer, J.J., 2006, Influence of long-period filter cut-off on elastic spectral displacements: Earthquake Engineering and Structural Dynamics, v. 35, p. 1145–1165.

Akkar, S., and Bommer, J.J., 2007a, Empirical prediction equations for peak ground velocity derived from strong-motion records from Europe and the Middle East: Bulletin of the Seismological Society of America, v. 97, no. 2, p. 511–530.

Akkar, S., and Bommer, J.J., 2007b, Prediction of elastic displacement response spectra in Europe and the Middle East: Earthquake Engineering and Structural Dynamics, v. 36, p. 1275–1301.

Allen, T.I., and Atkinson, G.M., 2007, Comparison of earthquake source spectra and attenuation in eastern North America and southeastern Australia: Bulletin of the Seismological Society of America, v. 97, no. 4, p. 1350–1354.

Allen, T.I., Cummins, P.R., Dhu, T., and Schneider, J.F., 2007, Attenuation of ground-motion spectral amplitudes in southeastern Australia: Bulletin of the Seismological Society of America, v. 97, no. 4, p. 1279–1292.

Allen, T.I., Marano, K.D., Earle, P.S., and Wald, D.J., 2009a, PAGER-CAT: A composite earthquake catalog for calibrating global fatality models: Seismological Research Letters, v. 80, no. 1, p. 57–62.

Allen, T.I., and Wald, D.J., 2007, Topographic slope as a proxy for seismic site-conditions (V_S^{30}) and amplification around the globe: U.S. Geological Survey Open-File Report 2007–1357, 69 p.

Allen, T.I., Wald, D.J., Earle, P.S., Marano, K.D., Hotovec, A.J., Lin, K., and Hearne, M., 2009b, An atlas of ShakeMaps and population exposure catalog for earthquake loss modeling: Bulletin of Earthquake Engineering, p. DOI: 10.1007/s10518-10009-19120-y.

Allen, T.I., Wald, D.J., Hotovec, A.J., Lin, K., Earle, P.S., and Marano, K.D., 2008, An atlas of ShakeMaps for selected global earthquakes: U.S. Geological Survey Open-File Report 2008–1236, 47 p.

Ambraseys, N.N., Douglas, J., Sarma, S.K., and Smit, P.M., 2005, Equations for the estimation of strong ground motions from shallow crustal earthquakes using data from Europe and the Middle East: Horizontal peak ground acceleration and spectral acceleration: Bulletin of Earthquake Engineering, v. 3, p. 1–53.

Ambraseys, N.N., Smit, P., Douglas, J., Margaris, B., Sigbjornsson, R., Olafsson, S., Suhadolc, P., and Costa, G., 2004, Internet site for European strong-motion data: Bollettino di Geofisica Teorica Applicata, v. 45, no. 3, p. 113–129.

Applied Technology Council, 2006, Third ATC-35/USGS national earthquake ground-motion mapping workshop: Applied Technology Council, San Mateo, California, p. 308.

Atkinson, G.M., 1993, Earthquake source spectra in eastern North America: Bulletin of the Seismological Society of America, v. 83, no. 6, p. 1778–1798.

Atkinson, G.M., 1996, The high-frequency shape of the source spectrum for earthquakes in eastern and western Canada: Bulletin of the Seismological Society of America, v. 86, no. 1A, p. 106–112.

Atkinson, G.M., 2004, Empirical attenuation of ground-motion spectral amplitudes in southeastern Canada and the northeastern United States: Bulletin of the Seismological Society of America, v. 94, no. 3, p. 1079–1095.

Atkinson, G.M., and Boore, D.M., 1995, Ground-motion relations for eastern North America: Bulletin of the Seismological Society of America, v. 85, no. 1, p. 17–30.

Atkinson, G.M., and Boore, D.M., 2003, Empirical ground-motion relations for subduction-zone earthquakes and their application to Cascadia and other regions: Bulletin of the Seismological Society of America, v. 93, no. 4, p. 1703–1729.

Atkinson, G.M., and Boore, D.M., 2006, Earthquake ground-motion predictions for eastern North America: Bulletin of the Seismological Society of America, v. 96, p. 2181–2205.

Atkinson, G.M., and Kaka, S.I., 2007, Relationships between felt intensity and instrumental ground motion: Bulletin of the Seismological Society of America, v. 97, no. 2, p. 497–510.

Atkinson, G.M., and Sonley, E., 2000, Relationships between Modified Mercalli Intensity and response spectra: Bulletin of the Seismological Society of America, v. 90, p. 537–544.

Atkinson, G.M., and Wald, D.J., 2007, "Did You Feel It?" intensity data—A surprisingly good measure of earthquake ground motion: Seismological Research Letters, v. 78, no. 3, p. 362–368.

Bakun, W.H., 2006, MMI attenuation and historical earthquakes in the Basin and Range Province of western North America: Bulletin of the Seismological Society of America, v. 96, no. 6, p. 2206–2220.

Bakun, W.H., Johnston, A.C., and Hopper, M.G., 2003, Estimating locations and magnitudes of earthquakes in eastern North America from Modified Mercalli Intensities: Bulletin of the Seismological Society of America, v. 93, no. 1, p. 190–202.

Bakun, W.H., and McGarr, A., 2002, Differences in attenuation among the stable continental regions: Geophysical Research Letters, v. 29, no. 23, p. 2121, doi:2110.1029/2002GL015457.

Bakun, W.H., and Scotti, O., 2006, Regional intensity attenuation models for France and the estimation of magnitude and location of historical earthquakes: Geophysical Journal International, v. 164, p. 596–610.

Bakun, W.H., and Wentworth, C.M., 1997, Estimating earthquake location and magnitude from seismic intensity data: Bulletin of the Seismological Society of America, v. 87, no. 6, p. 1502–1521.

Balmer, R., 1999, The SRTM mission—A world-wide 30 m resolution DEM from SAR interferometry in 11 days, *in* Fritsch, D., and Spiller, R., eds., Proceedings of the 47th Photogrammetric Week ’99: Heidelberg, Germany, Wichmann Verlag, p. 145–154.

Beyer, K., and Bommer, J.J., 2006, Relationships between median values and between aleatory variabilities for different definitions of the horizontal component of motion: Bulletin of the Seismological Society of America, v. 96, no. 4A, p. 1512–1522.

Bommer, J.J., and Alarcón, J.E., 2006, The prediction and use of peak ground velocity: Journal of Earthquake Engineering, v. 10, no. 1, p. 1–31.

Bommer, J.J., and Scherbaum, F., 2008, The use and misuse of logic-trees in probabilistic seismic hazard analysis: Earthquake Spectra, v. 24, no. 4, p. 997–1009.

Bommer, J.J., Scherbaum, F., Bungum, H., Cotton, F., Sabetta, F., and Abrahamson, N.A., 2005, On the use of logic trees for ground-motion prediction equations in seismic-hazard analysis: Bulletin of the Seismological Society of America, v. 95, no. 2, p. 377–389.

Bommer, J.J., Stafford, P.J., Alarcón, J.E., and Akkar, S., 2007, The influence of magnitude range on empirical ground-motion prediction: Bulletin of the Seismological Society of America, v. 97, no. 6, p. 2152–2170.

Boore, D.M., and Atkinson, G.M., 2008, Ground-motion prediction equations for the average horizontal component of PGA, PGV, and 5%-damped PSA at spectral periods between 0.01 s and 10.0 s: Earthquake Spectra, v. 24, no. 1, p. 99–138.

Boore, D.M., Joyner, W.B., and Fumal, T.E., 1997, Equations for estimating horizontal response spectra and peak acceleration from Western North American earthquakes: A summary of recent work: Seismological Research Letters, v. 68, no. 1, p. 128–153.

Boore, D.M., Watson-Lamprey, J., and Abrahamson, N.A., 2006, Orientation-independent measures of ground motion: Bulletin of the Seismological Society of America, v. 96, no. 4A, p. 1502–1511.

Borcherdt, R.D., 1994, Estimates of site-dependent response spectra for design (methodology and justification): Earthquake Spectra, v. 10, no. 4, p. 617–653.

Campbell, K.W., 2003, Prediction of strong ground motion using the hybrid empirical method and its use in the development of ground-motion (attenuation) relations in eastern North America: Bulletin of the Seismological Society of America, v. 93, no. 3, p. 1012–1033.

Campbell, K.W., 2004, Erratum to: Prediction of strong ground motion using the hybrid empirical method and its use in the development of ground-motion (attenuation) relations in eastern North America: Bulletin of the Seismological Society of America, v. 94, no. 6, p. 2418.

Campbell, K.W., and Bozorgnia, Y., 2008, NGA ground motion model for the geometric mean horizontal component of PGA, PGV, PGD and 5% damped linear elastic response spectra for periods ranging from 0.01 to 10 s: Earthquake Spectra, v. 24, no. 1, p. 139–171.

Chiou, B., Darragh, R., Gregor, N., and Silva, W., 2008, NGA project strong-motion database: Earthquake Spectra, v. 24, no. 1, p. 23–44.

Chiou, B.S.-J., and Youngs, R.R., 2008, An NGA model for the average horizontal component of peak ground motion and response spectra: Earthquake Spectra, v. 24, no. 1, p. 173–215.

Cotton, F., Scherbaum, F., Bommer, J.J., and Bungum, H., 2006, Criteria for selecting and adjusting ground-motion models for specific target regions—Application to Central Europe and rock sites: Journal of Seismology, v. 10, no. 2, p. 137–156.

Dewey, J.W., Hopper, M.G., Wald, D.J., Quitoriano, V., and Adams, E.R., 2002, Intensity distribution and isoseismal maps for the Nisqually, Washington, earthquake of 28 February 2001: U.S. Geological Survey Open-File Report 02–0346, 57 p.

Dewey, J.W., Reagor, B.G., Dengler, L., and Moley, K., 1995, Intensity distribution and isoseismal maps for the Northridge, California, earthquake of January 17, 1994: U.S. Geological Survey Open-File Report, v. 95–92, p. 35.

Douglas, J., 2004, An investigation of analysis of variance as a tool for exploring regional differences in strong ground motions: Journal of Seismology, v. 8, p. 485–496.

Douglas, J., 2007, On the regional dependence of earthquake response spectra: ISET Journal of Earthquake Technology, v. 44, no. 1, Paper No. 477, p. 471–499.

Douglas, J., and Mohais, R., 2009, Comparing predicted and observed ground motions from subduction earthquakes in the Lesser Antilles: Journal of Seismology, p. DOI 10.1007/s10950-10008-19150-y.

Earle, P.S., Wald, D.J., Allen, T.I., Jaiswal, K.S., Porter, K.A., and Hearne, M.G., 2008, Rapid exposure and loss estimates for the May 12, 2008 M_W 7.9 Wenchuan earthquake provided by the U.S. Geological Survey's PAGER system, in 14th World Conference of Earthquake Engineering, Beijing, China, Paper S31-039.

Farr, T.G., and Kobrick, M., 2000, Shuttle Radar Topography Mission produces a wealth of data: EOS Transactions, v. 81, p. 583–585.

Federal Emergency Management Agency, 1994, NEHRP recommended provisions for the development of seismic regulations for new buildings: FEMA, v. Part 1—Provisions, 290 p.

Field, E.H., Seligson, H.A., Gupta, N., Gupta, V., Jordan, T.H., and Campbell, K.W., 2005, Loss estimates for a Puente Hills blind-thrust earthquake in Los Angeles, California: Earthquake Spectra, v. 21, no. 2, p. 329–338.

Frankel, A., 1994, Implications of felt area-magnitude relations for earthquake scaling and the average frequency of perceptible ground motion: Bulletin of the Seismological Society of America, v. 84, no. 2, p. 462–465.

Frankel, A., McGarr, A., Bicknell, J., Mori, J., Seeber, L., and Cranswick, E., 1990, Attenuation of high-frequency shear waves in the crust—Measurements from New York State, South Africa, and southern California: Journal of Geophysical Research, v. 95, no. B11, p. 17441–17457.

Graizer, V., and Kalkan, E., 2008, A novel approach to strong ground motion attenuation modeling: 14th World Conference of Earthquake Engineering, Beijing, China, Paper 02–0022.

Hanks, T.C., and Johnston, A.C., 1992, Common features of the excitation and propagation of strong ground motion for North American earthquakes: Bulletin of the Seismological Society of America, v. 82, no. 1, p. 1–23.

Herrmann, R.B., and Kijko, A., 1983, Modeling some empirical vertical component *Lg* relations: Bulletin of the Seismological Society of America, v. 73, no. 1, p. 157–171.

Idriss, I.M., 2008, An NGA empirical model for estimating the horizontal spectral values generated by shallow crustal earthquakes: Earthquake Spectra, v. 24, no. 1, p. 217–242.

Johnston, A.C., Coppersmith, K.J., Kanter, L.R., and Cornell, C.A., 1994, The earthquakes of stable continental regions, Volume 1—Assessment of large earthquake potential: Electric Power Research Institute, Palo Alto, California, TR-102261-V1.

Kanno, T., Narita, A., Morikawa, N., Fujiwara, H., and Fukushima, Y., 2006, A new attenuation relation for strong ground motion in Japan based on recorded data: Bulletin of the Seismological Society of America, v. 96, no. 3, p. 879–897.

Lin, P.-S., and Lee, C.-T., 2008, Ground-motion attenuation relationships for subduction-zone earthquakes in northeastern Taiwan: Bulletin of the Seismological Society of America, v. 98, no. 1, p. 220–240.

Michelini, A., Faenza, L., Lauciani, V., and Malagnini, L., 2008, ShakeMap implementation in Italy: Seismological Research Letters, v. 79, no. 5, p. 688–697.

Negishi, H., Mori, J., Sato, T., Singh, R., Kumar, S., and Hirata, N., 2002, Size and orientation of the fault plane for the 2001 Gujarat, India earthquake (Mw7.7) from aftershock observations—A high stress drop event: Geophysical Research Letters, v. 29, no. 20, p. 1949, doi:1910.1029/2002GL015280.

Newmark, N.M., and Hall, W.J., 1982, Earthquake spectra and design: Berkeley, Calif., Earthquake Engineering Research Institute, 103 p.

Nuttli, O.W., 1973, Seismic wave attenuation and magnitude relations for Eastern North America: Journal of Geophysical Research, v. 78, no. 5, p. 876–885.

Nuttli, O.W., and Zollweg, J.E., 1974, The relation between felt area and magnitude for central United States earthquakes: Bulletin of the Seismological Society of America, v. 64, no. 1, p. 73–85.

Pankow, K.L., and Pechmann, J.C., 2004, The SEA99 ground-motion predictive relations for extensional tectonic regimes—Revisions and a new peak ground velocity relation: Bulletin of the Seismological Society of America, v. 94, no. 1, p. 341–348.

Pasolini, C., Albarello, D., Gasperini, P., D'Amico, V., and Lolli, B., 2008, The attenuation of seismic intensity in Italy, part II—Modeling and validation: Bulletin of the Seismological Society of America, v. 98, no. 2, p. 692–708.

Petersen, M.D., Dewey, J., Hartzell, S., Mueller, C., Harmsen, S., Frankel, A.D., and Rukstales, K., 2004, Probabilistic seismic hazard analysis for Sumatra, Indonesia and across the southern Malaysian Peninsula: Tectonophysics, v. 390, p. 141– 158.

Petersen, M.D., Frankel, A.D., Harmsen, S.C., Mueller, C.S., Haller, K.M., Wheeler, R.L., Wesson, R.L., Zeng, Y., Boyd, O.S., Perkins, D.M., Luco, N., Field, E.H., Wills, C.J., and Rukstales, K.S., 2008, Documentation for the 2008 update of the United States National Seismic Hazard Maps: U.S. Geological Survey Open-File Report 2008–1128, 128 p.

Power, M., Chiou, B., Abrahamson, N., Bozorgnia, Y., Shantz, T., and Roblee, C., 2008, An overview of the NGA project: Earthquake Spectra, v. 24, no. 1, p. 3–21.

Scherbaum, F., Bommer, J.J., Bungum, H., Cotton, F., and Abrahamson, N.A., 2005, Composite ground-motion models and logic trees—Methodology, sensitivities, and uncertainties: Bulletin of the Seismological Society of America, v. 95, no. 5, p. 1575–1593.

Scherbaum, F., Cotton, F., and Smit, P., 2004, On the use of response spectral-reference data for the selection and ranking of ground-motion models for seismic-hazard analysis in regions of moderate seismicity—The case of rock motion: Bulletin of the Seismological Society of America, v. 94, no. 6, p. 2164–2185.

Scherbaum, F., Delavaud, E., and Riggelsen, C., 2008, Model selection in seismic hazard analysis: an information-theoretic perspective: Eos Transactions, AGU, v. 89, no. 53, p. Fall Meeting Supplement, Abstract S13C-1809.

Sørensen, M.B., Stromeyer, D., and Grünthal, G., 2009, Attenuation of macroseismic intensity—A new relation for the Marmara Sea region, northwest Turkey: Bulletin of the Seismological Society of America, v. 99, no. 2A, p. 538–553.

Stafford, P.J., Strasser, F.O., and Bommer, J.J., 2008, An evaluation of the applicability of the NGA models to ground-motion prediction in the Euro-Mediterranean region: Bulletin of Earthquake Engineering, v. 6, p. 149–177.

The MathWorks, 2006, Mapping Toolbox user's guide (Version 2.4 ed.): Natick, Mass., The MathWorks.

Toro, G.R., Abrahamson, N.A., and Schneider, J.F., 1997, Model of strong ground motions from earthquakes in central and eastern North America—Best estimates and uncertainties: Seismological Research Letters, v. 68, no. 1, p. 41–57.

Trifunac, M.D., and Brady, A.G., 1975, On the correlation od seismic intensity scales with the peaks of recorded strong ground motion: Bulletin of the Seismological Society of America, v. 65, no. 1, p. 139–162.

Tselentis, G.-A., and Danciu, L., 2008, Empirical relationships between Modified Mercalli Intensity and engineering ground-motion parameters in Greece: Bulletin of the Seismological Society of America, v. 98, no. 4, p. 1863–1875.

Wald, D.J., and Allen, T.I., 2007, Topographic slope as a proxy for seismic site conditions and amplification: Bulletin of the Seismological Society of America, v. 97, no. 5, p. 1379–1395.

Wald, D.J., Earle, P.S., Allen, T.I., Jaiswal, K., Porter, K., and Hearne, M., 2008a, Development of the U.S. Geological Survey's PAGER system (Prompt Assessment of Global Earthquakes for Response), in 14th World Conference of Earthquake Engineering, Beijing, China, Paper 10-0008.

Wald, D.J., Lin, K., and Quitoriano, V., 2008b, Quantifying and qualifying ShakeMap uncertainty: U.S. Geological Survey Open-File Report 2008–1238, 27 p.

Wald, D.J., Quitoriano, V., and Dewey, J.W., 2006, USGS "Did you feel it?" community internet intensity maps: macroseismic data collection via the internet, First European Conference on Earthquake Engineering and Seismology: Geneva, Switzerland, 10 p.

Wald, D.J., Quitoriano, V., Heaton, T.H., and Kanamori, H., 1999a, Relationship between peak ground acceleration, peak ground velocity, and Modified Mercalli Intensity in California: Earthquake Spectra, v. 15, no. 3, p. 557–564.

Wald, D.J., Quitoriano, V., Heaton, T.H., Kanamori, H., Scrivner, C.W., and Worden, B.C., 1999b, TriNet "ShakeMaps": Rapid generation of peak ground-motion and intensity maps for earthquakes in southern California: Earthquake Spectra, v. 15, no. 3, p. 537–556.

Wald, D.J., Worden, B.C., Quitoriano, V., and Pankow, K.L., 2005, ShakeMap manual: technical manual, user's guide, and software guide: U.S. Geological Survey, 132 p.

Youngs, R.R., Chiou, S.-J., Silva, W.J., and Humphrey, J.R., 1997, Strong ground motion attenuation relationships for subduction zone earthquakes: Seismological Research Letters, v. 68, no. 1, p. 58–73.

Zhao, J.X., Zhang, J., Asano, A., Ohno, Y., Oouchi, T., Takahashi, T., Ogawa, H., Irikura, K., Thio, H.K., Somerville, P.G., Fukushima, Y., and Fukushima, Y., 2006, Attenuation relations of strong ground motion in Japan using site classification based on predominant period: Bulletin of the Seismological Society of America, v. 96, no. 3, p. 898–913.

Figures

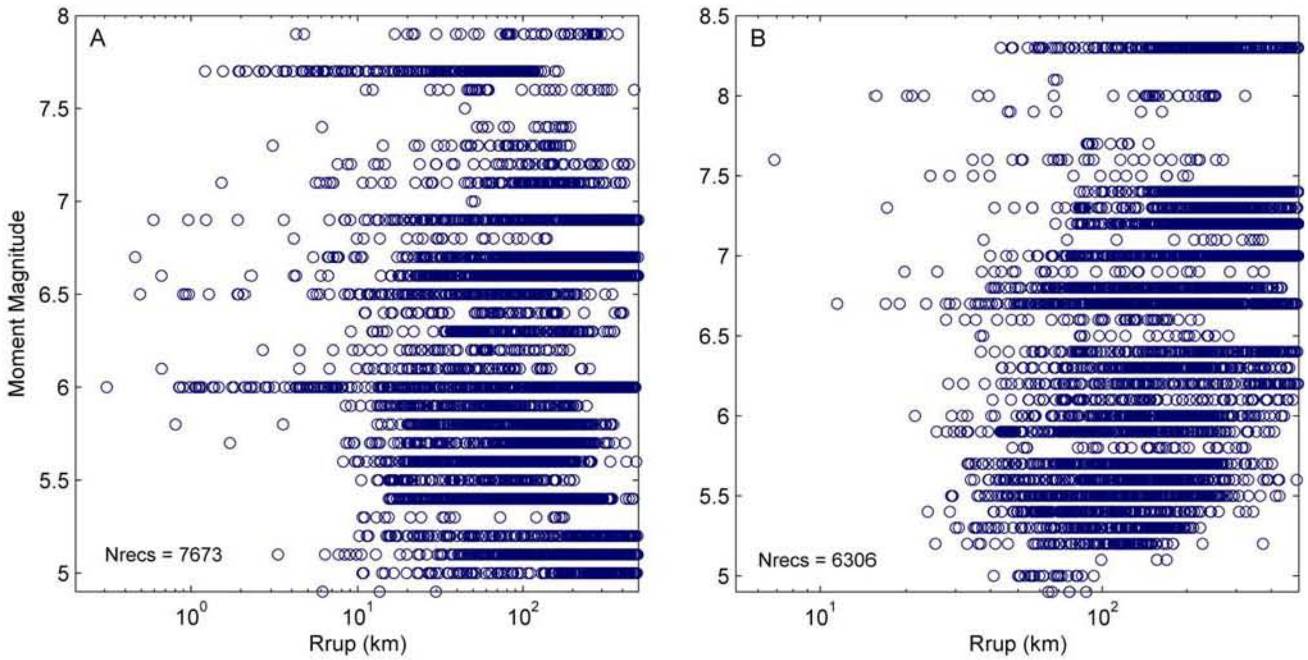

Figure 1. Magnitude-distance distribution of global PGA dataset gathered for the Atlas of ShakeMaps for (A) active crustal regions and (B) subduction zones. Only data recorded at distances R_{rup} 500 kilometers and less are indicated.

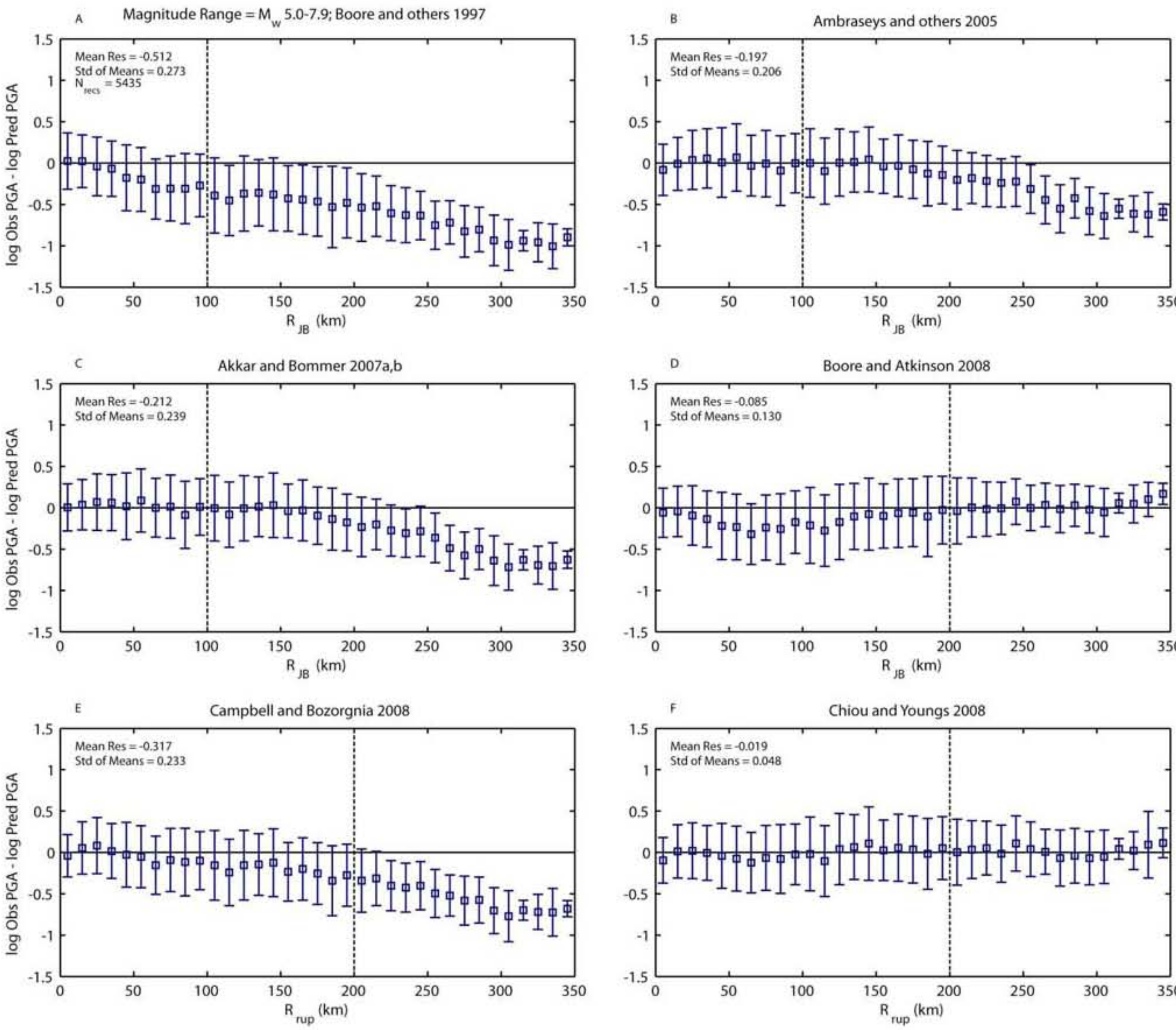

Figure 2. Residuals for the active crustal GMPEs against the global PGA dataset. Residuals are binned in 10-kilometer windows and the median residual is plotted. The standard deviation of the residuals is indicated. Vertical dashed lines indicate the maximum distance of usage as recommend by each of the authors.

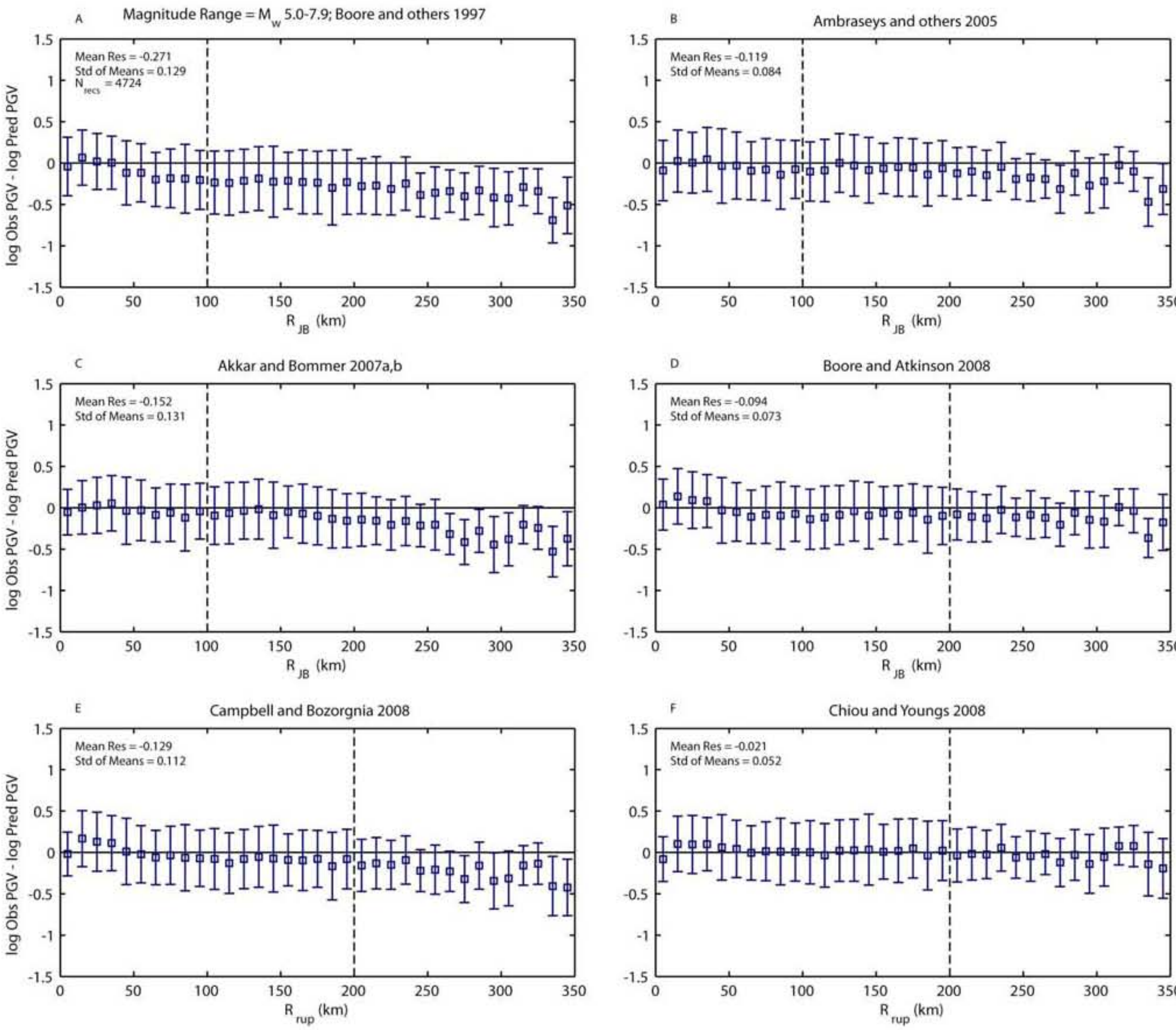

Figure 3. Residuals for the active crustal GMPEs against the global PGV dataset. Residuals are binned in 10-kilometer windows and the median residual is plotted. The standard deviation of the residuals is indicated. Vertical dashed lines indicate the maximum distance of usage as recommend by each of the authors.

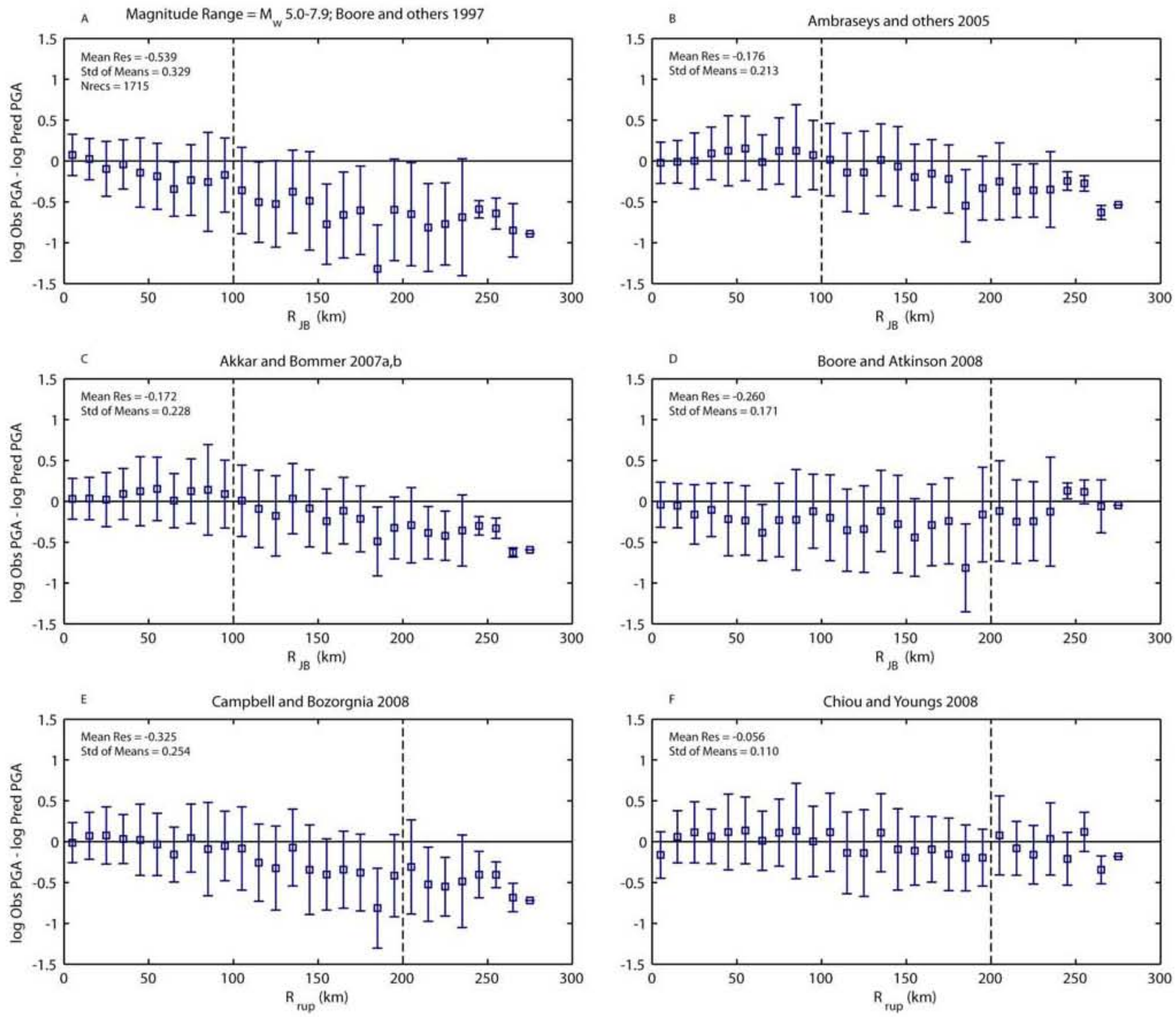

Figure 4. Residuals for the active crustal GMPEs against the California and Nevada PGA dataset. Residuals are binned in 10-kilometer windows and the median residual is plotted. The standard deviation of the residuals is indicated. Vertical dashed lines indicate the maximum distance of usage as recommend by each of the authors.

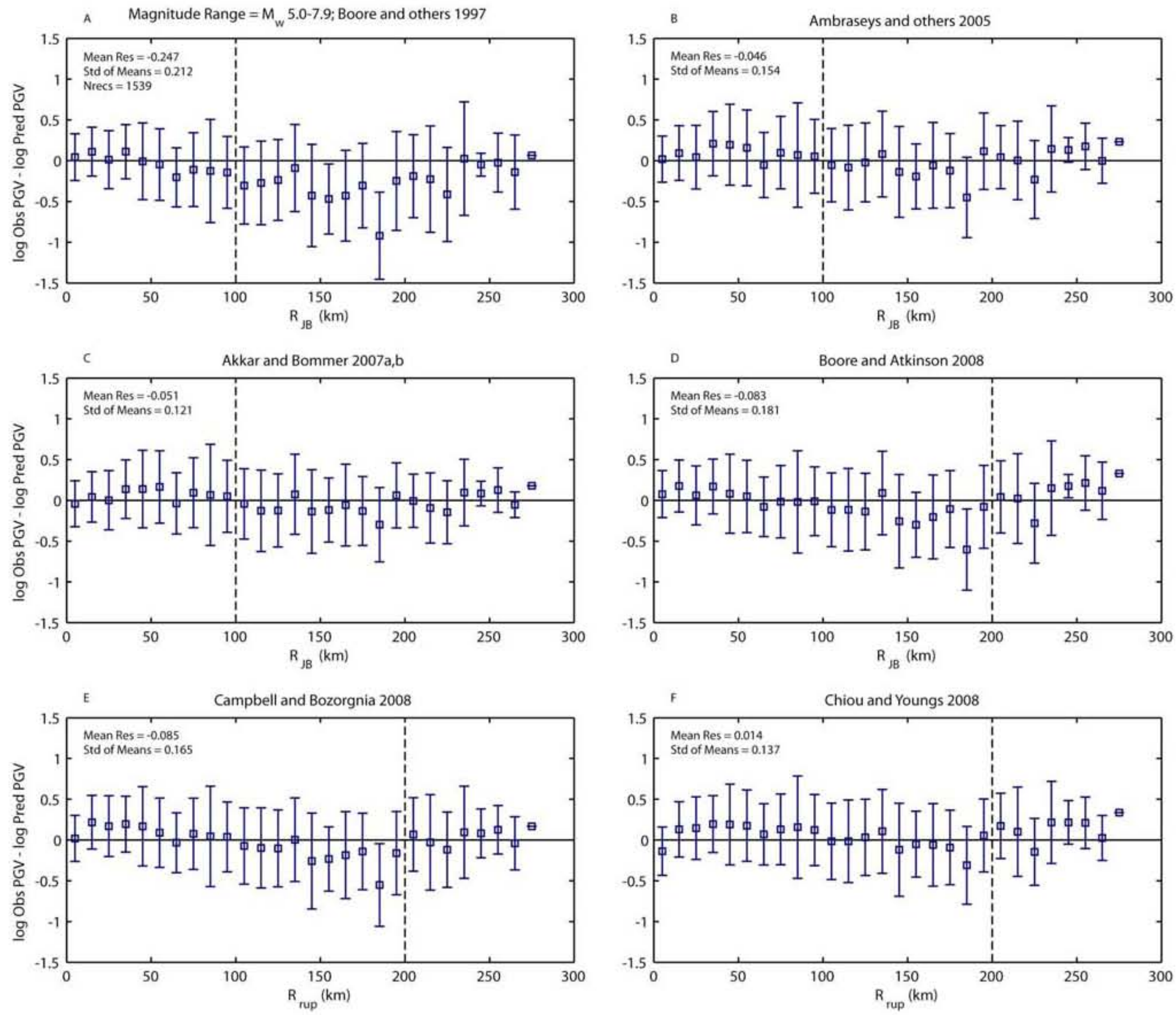

Figure 5. Residuals for the active crustal GMPEs against the California and Nevada PGV dataset. Residuals are binned in 10-kilometer windows and the median residual is plotted. The standard deviation of the residuals is indicated. Vertical dashed lines indicate the maximum distance of usage as recommend by each of the authors.

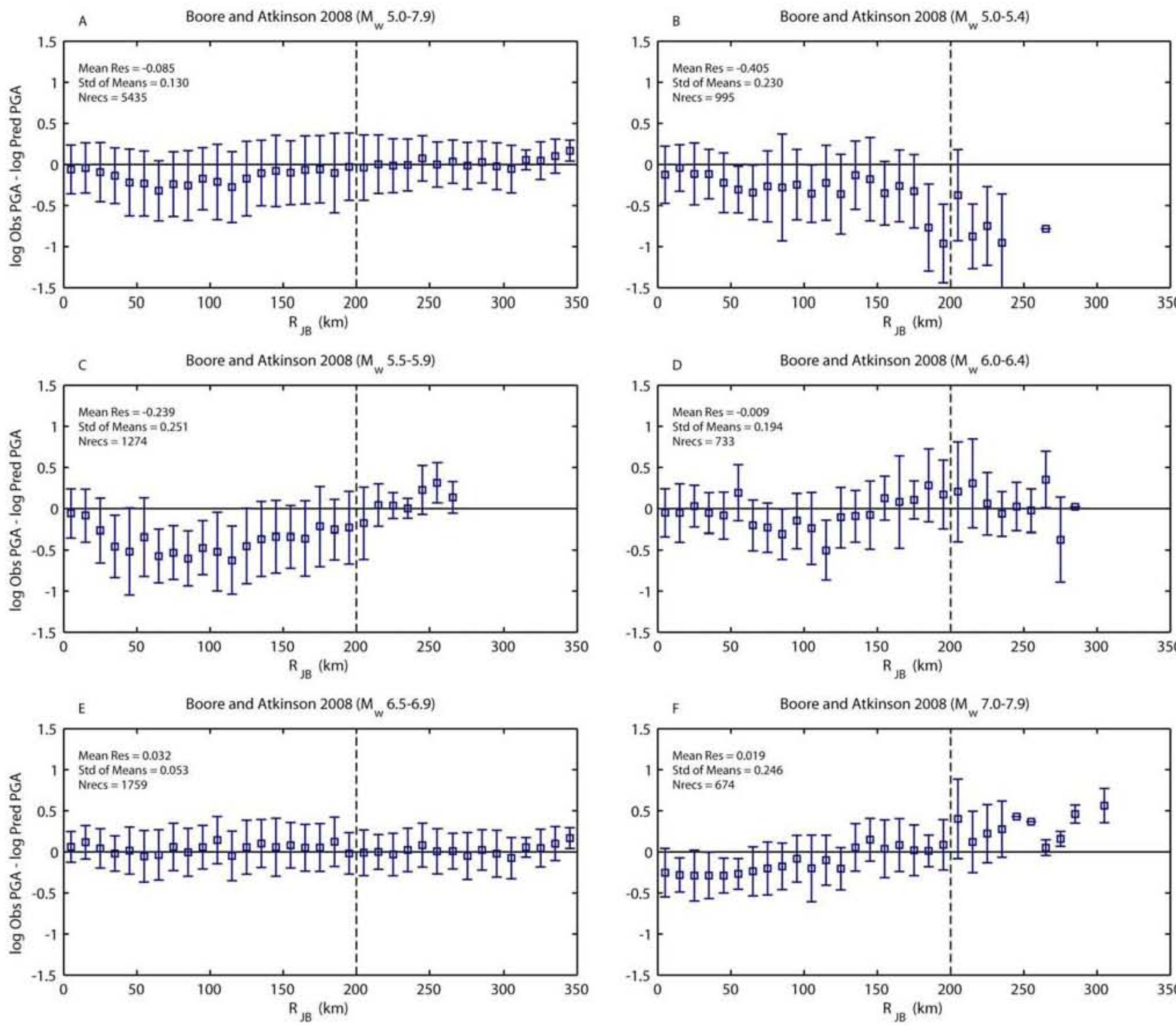

Figure 6. Residuals for the Boore and Atkinson (2008) active crustal GMPE against the global PGA dataset. Each subplot indicates the discrete magnitude window, and residuals are binned in 10-kilometer windows and the median residual is plotted. The standard deviation of the residuals is indicated. Vertical dashed lines indicate the maximum distance of usage as recommend by Boore and Atkinson (2008).

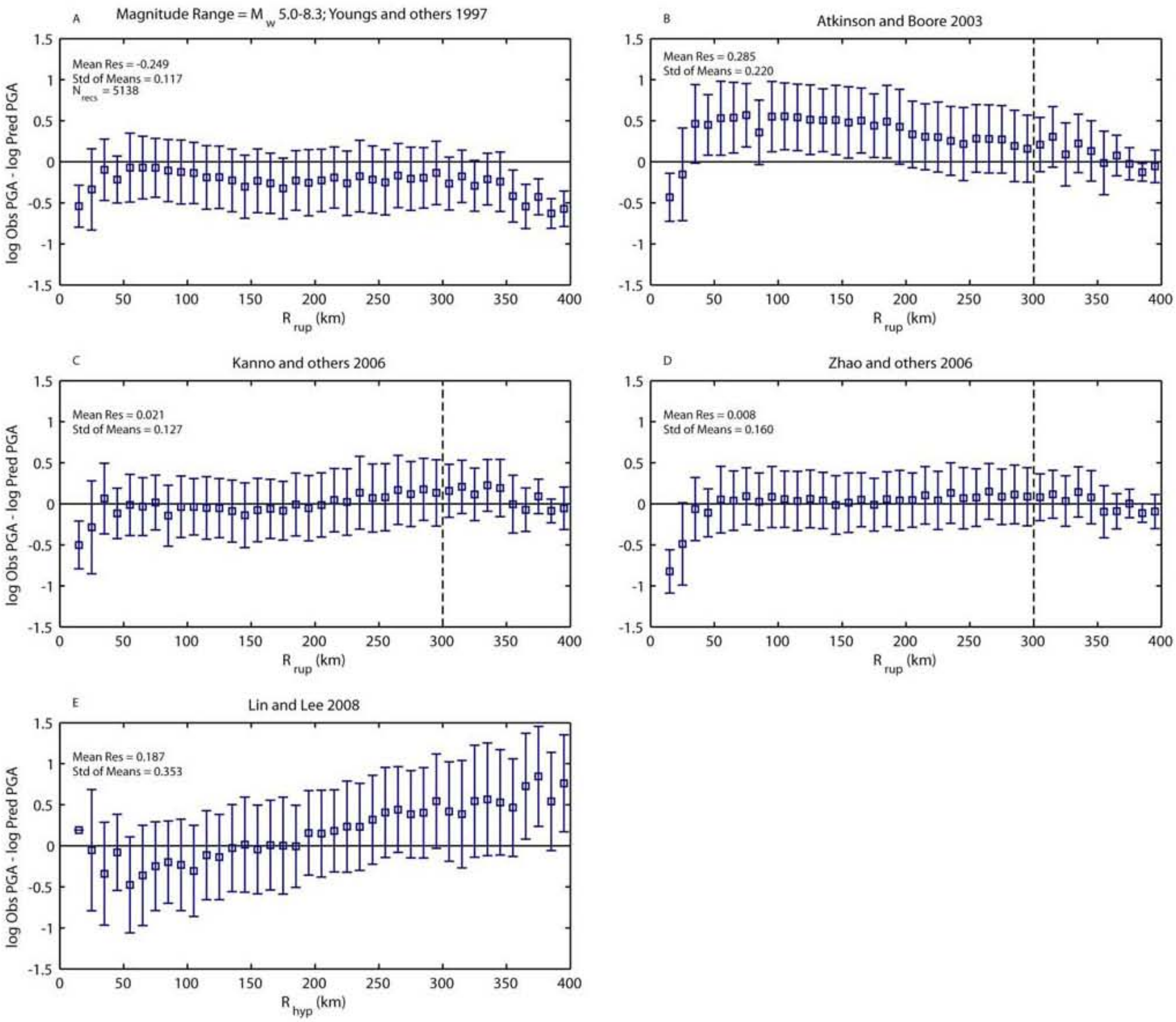

Figure 7. Residuals for the subduction-zone GMPEs against the global PGA dataset. Residuals are binned in 10-kilometer windows and the median residual is plotted. The standard deviation of the residuals is indicated.

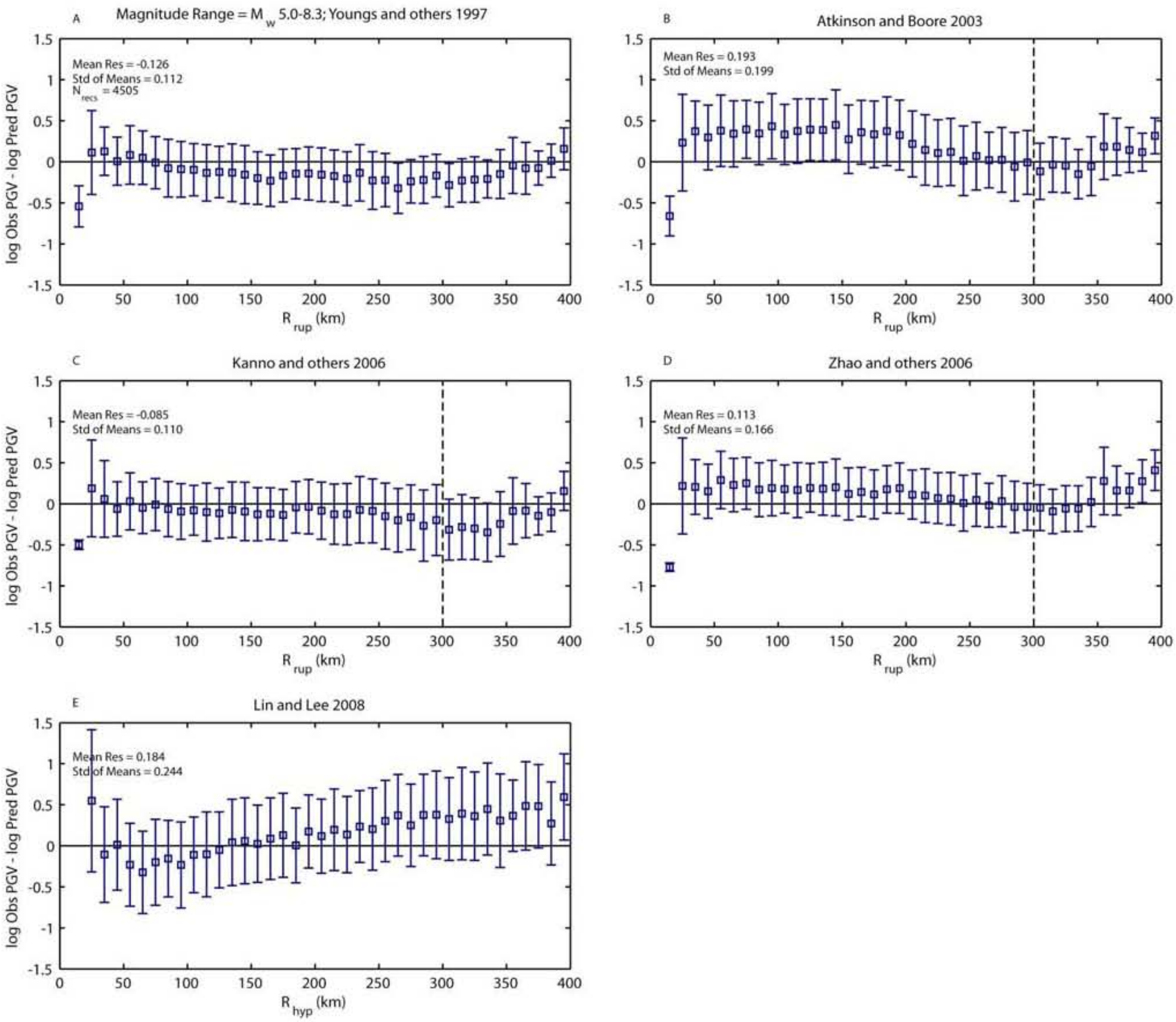

Figure 8. Residuals for the subduction-zone GMPEs against the global PGV dataset. For all GMPEs but the Kanno and others (2006), PGV is approximated from 1.0-second spectral acceleration as prescribed by Newmark and Hall (1982). Residuals are binned in 10-kilometer windows and the median residual is plotted. The standard deviation of the residuals is indicated. Vertical dashed lines indicate the maximum distance of usage as recommend by each of the authors.

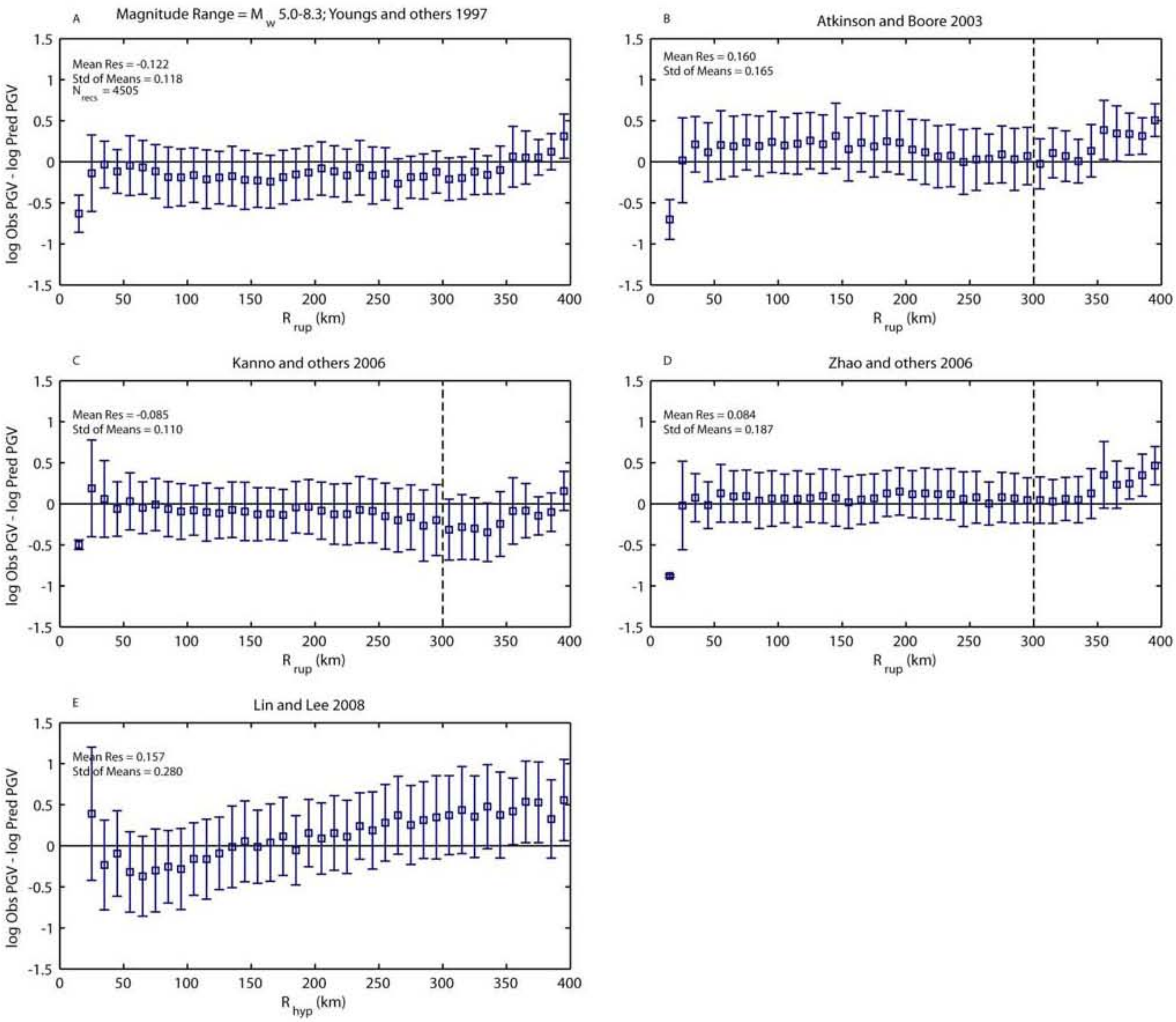

Figure 9. Residuals for the subduction-zone GMPEs against the global PGV dataset. For all GMPEs but the Kanno and others (2006), PGV is approximated from 0.5-second spectral acceleration as prescribed by Bommer and Alarcón (2006). Residuals are binned in 10-kilometer windows and the median residual is plotted. The standard deviation of the residuals is indicated. Where indicated, vertical dashed lines indicate the maximum distance of usage as recommend by each of the authors.

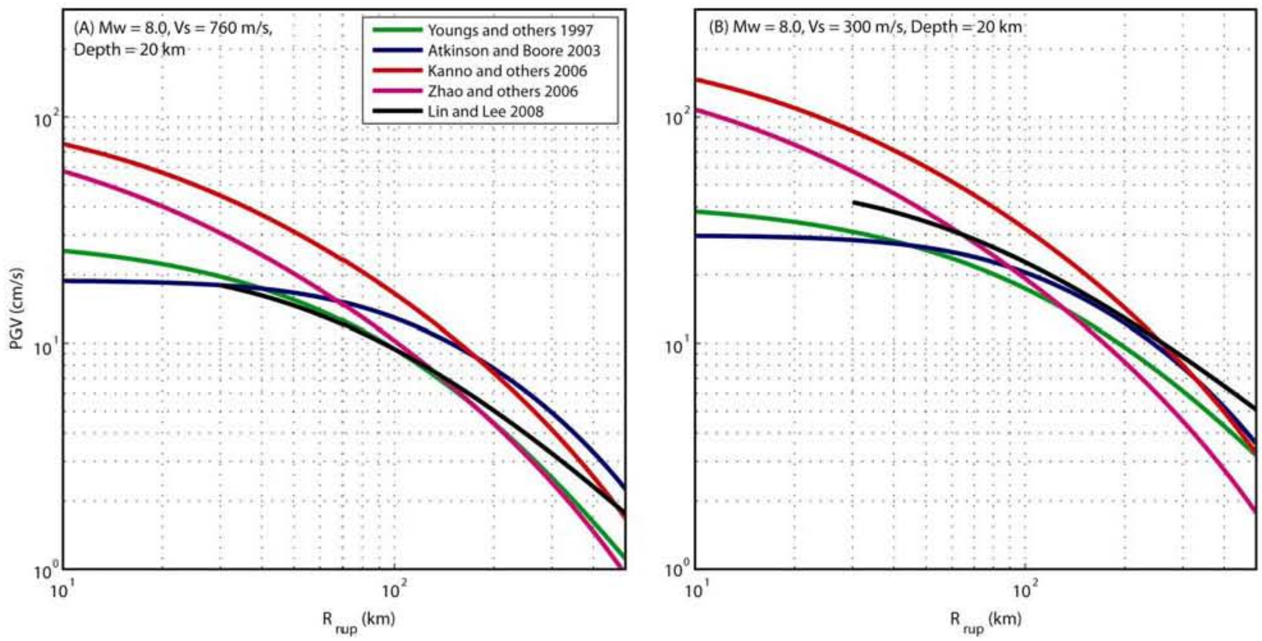

Figure 10. Amplitude-distance comparisons for the candidate subduction-zone GMPEs for an earthquake of magnitude M_W 8.0 and focal depth of 20 kilometers, on (A) rock and (B) soil, respectively.

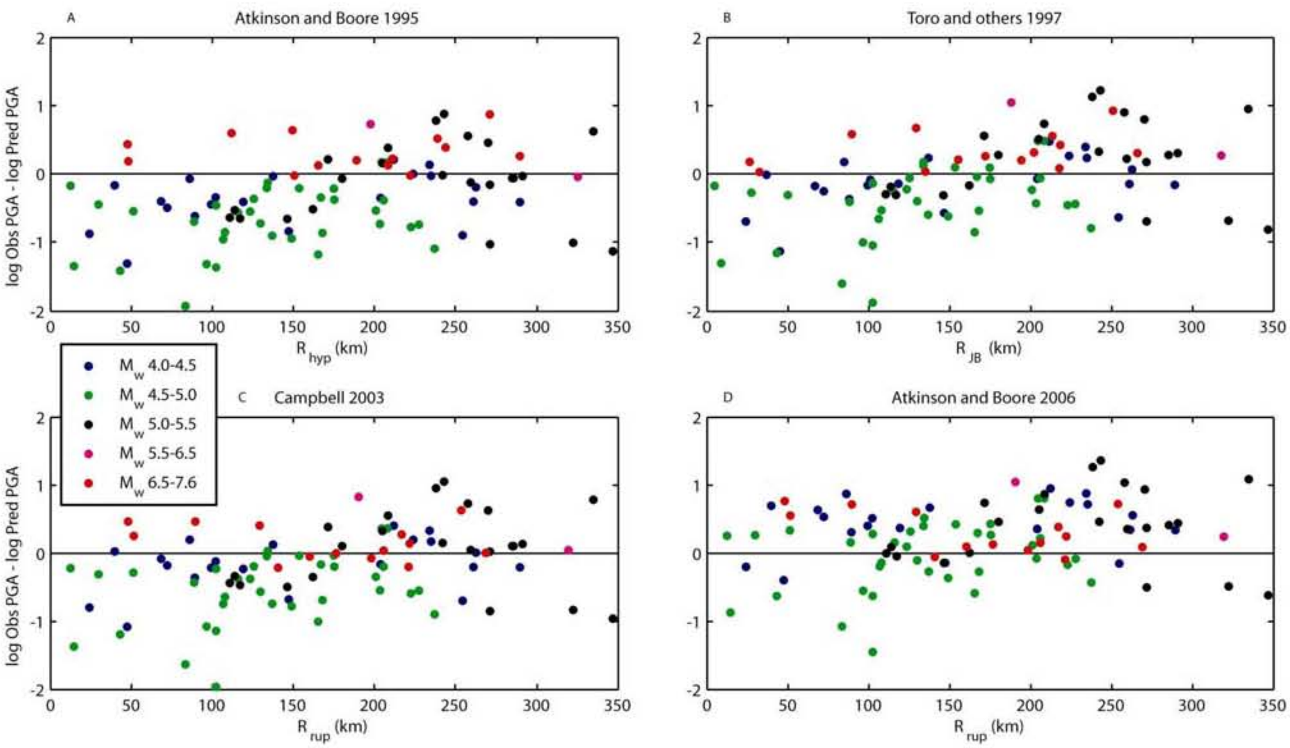

Figure 11. Residuals for the stable continent GMPEs against the global PGA dataset. Individual data residuals are plotted, color-coded by earthquake magnitude. The Atkinson and Boore (2006) GMPE for BC site classes is computed for a stress parameter of 140 bar.

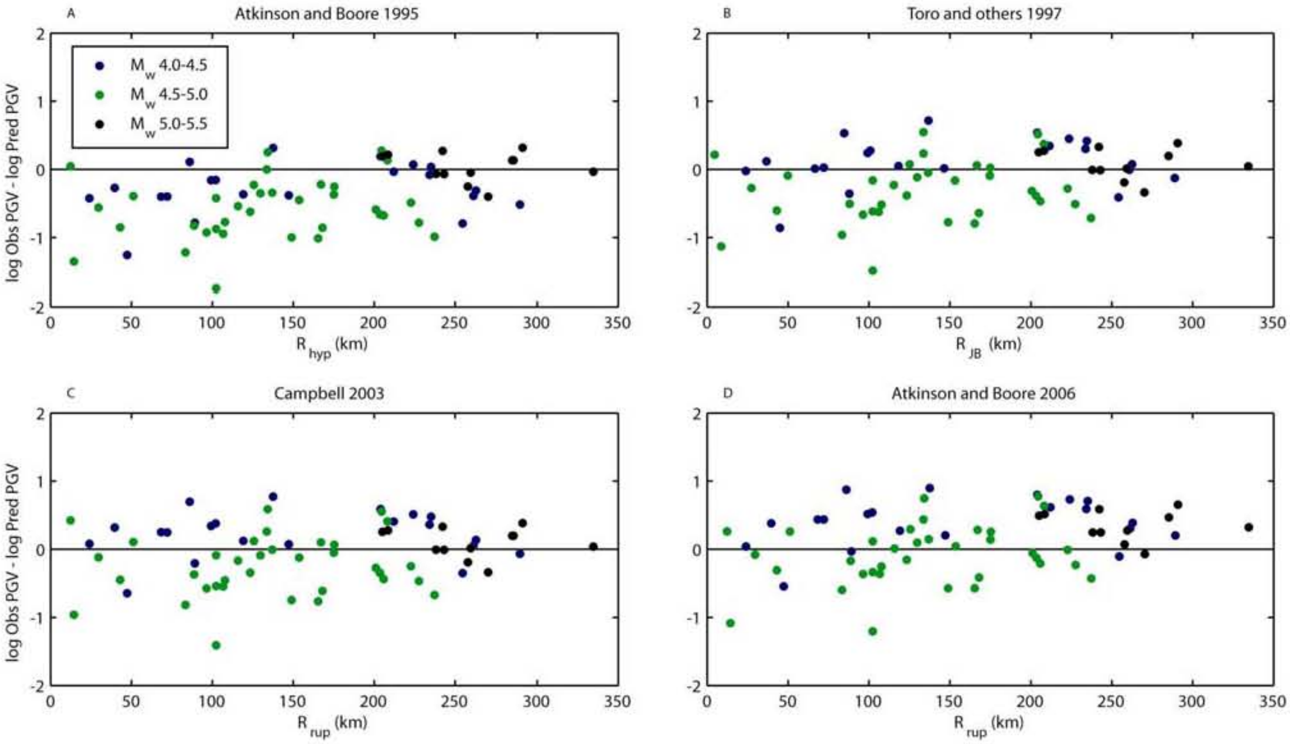

Figure 12. Residuals for the stable continent GMPEs against the global PGV dataset. Individual data residuals are plotted, color-coded by earthquake magnitude. The Atkinson and Boore (2006) GMPE is computed for a stress parameter of 140 bar.

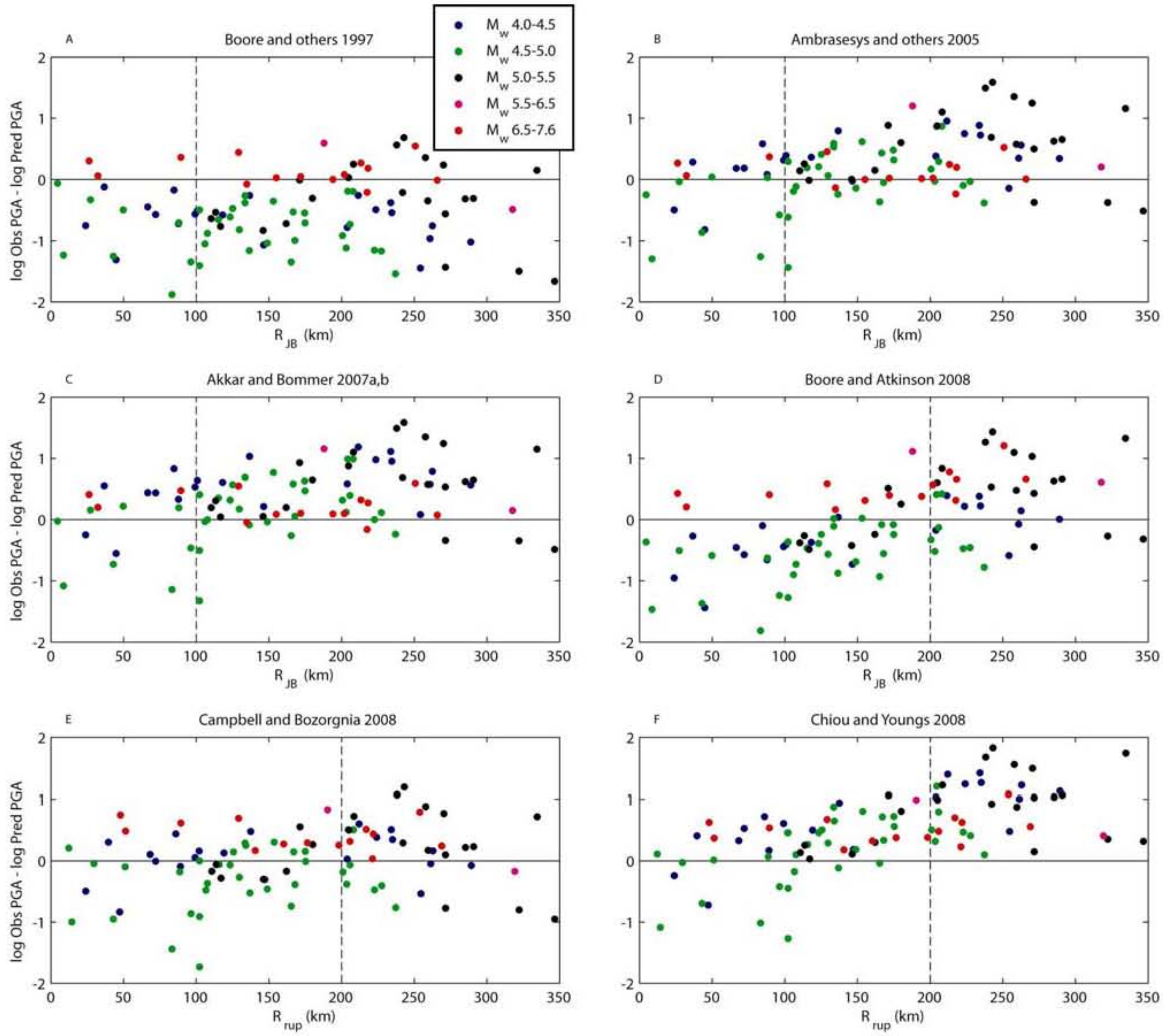

Figure 13. Residuals for the active crustal GMPEs against the global stable continental region PGA dataset. Individual data residuals are plotted, color-coded by earthquake magnitude. Vertical dashed lines indicate the maximum distance of usage as recommend by each of the authors.

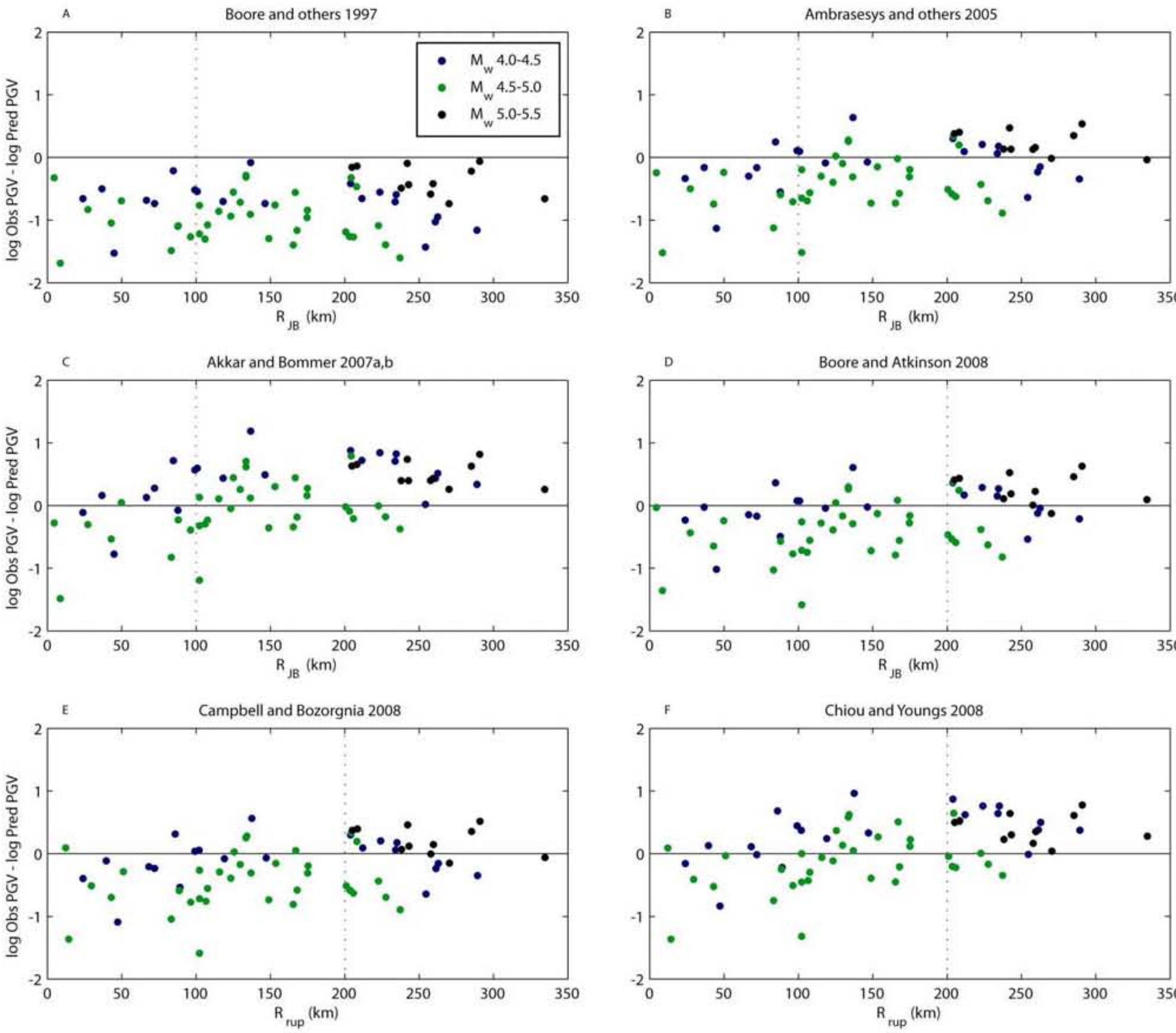

Figure 14. Residuals for the active crustal GMPEs against the global stable continental region PGV dataset. Individual data residuals are plotted, color-coded by earthquake magnitude. Vertical dashed lines indicate the maximum distance of usage as recommend by each of the authors.

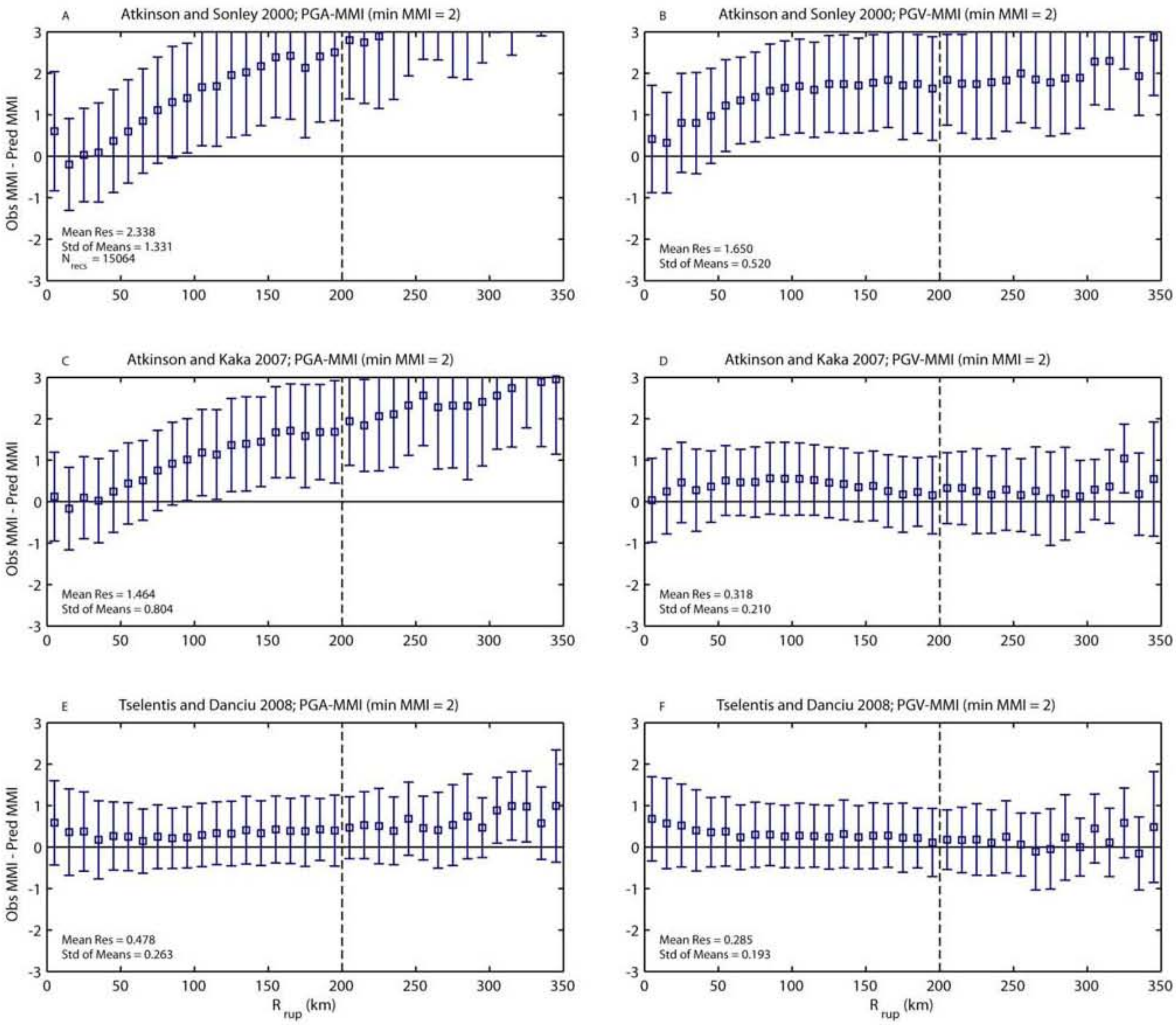

Figure 15. Residuals for the peak ground-motion-to-intensity conversions for active crustal regions. Peak ground-motion (PGA and PGV) is first calculated using the Chiou and Youngs (2008) GMPE at magnitude and distance pairs consistent with the macroseismic intensity observations. Earthquake mechanism and topographically-based V_S30 values at each intensity observation point is also considered in evaluating the peak ground-motion. Predicted instrumental ground motions, calculated using the aforementioned GMPE, are converted to intensity using the candidate PGM–MMI conversion equations. The intensity residual is subsequently calculated. Residuals are binned in 10-kilometer windows and the median residual is plotted. The standard deviation of the residuals is indicated. Vertical dashed lines indicate the maximum distance of usage as recommend for the Chiou and Youngs (2008) GMPE.

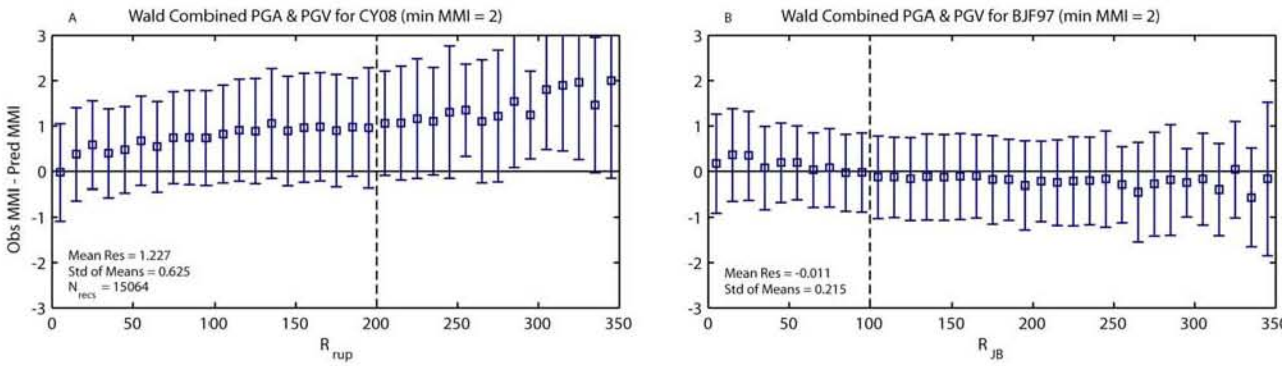

Figure 16. Residuals for the peak ground-motion-to-intensity conversions for global active crustal regions using the Wald and others (1999a) relations. (A) Indicates the median intensity residuals using the Chiou and Youngs (2008) GMPE as the predictor of peak ground motions. (B) Indicates the median intensity residuals using the Boore and others (1997) GMPE as the predictor of peak ground motions. Predicted instrumental ground motions are calculated using the aforementioned GMPEs and converted to intensity. The intensity residual is subsequently calculated. Residuals are binned in 10-kilometer windows and the median residual is plotted. The standard deviation of the residuals is indicated and vertical dashed lines indicate the maximum distance of usage of the GMPEs.

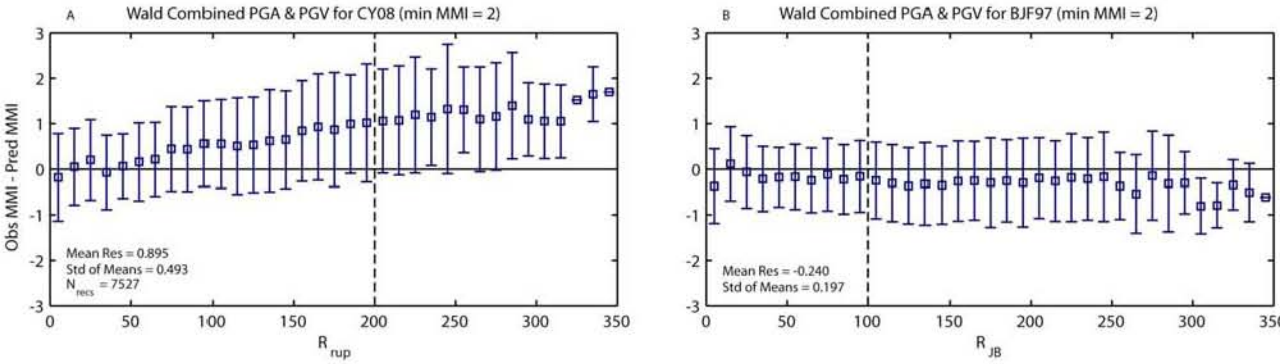

Figure 17. Residuals for the peak ground-motion-to-intensity conversions for California and Nevada using the Wald and others (1999a) relations. (A) Indicates the median intensity residuals using the Chiou and Youngs (2008) GMPE as the predictor of peak ground motions. (B) Indicates the median intensity residuals using the Boore and others (1997) GMPE as the predictor of peak ground motions. Predicted instrumental ground motions are calculated using the aforementioned GMPEs and converted to intensity. The intensity residual is subsequently calculated. Residuals are binned in 10-kilometer windows and the median residual is plotted. The standard deviation of the residuals is indicated and vertical dashed lines indicate the maximum distance of usage of the GMPEs.

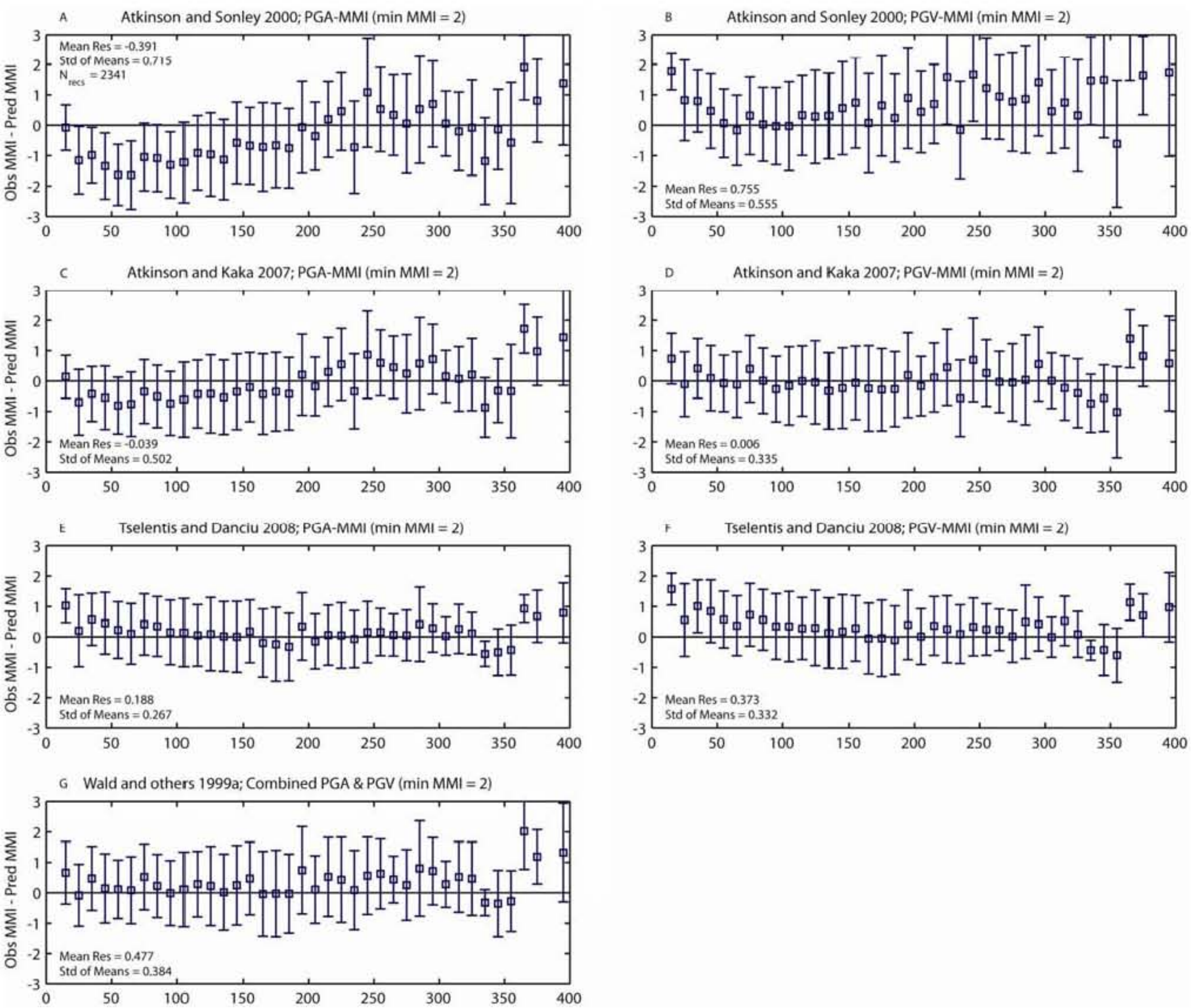

Figure 18. Residuals for the peak ground-motion-to-intensity conversions for global subduction zones. Peak ground motion is first calculated using the Youngs and others (1997) GMPE at magnitude and distance pairs of macroseismic intensity observations. Predicted instrumental ground motions are calculated using the aforementioned GMPE and converted to intensity. The intensity residual is subsequently calculated. Residuals are binned in 10-kilometer windows and the median residual is plotted. The standard deviation of the residuals is indicated.

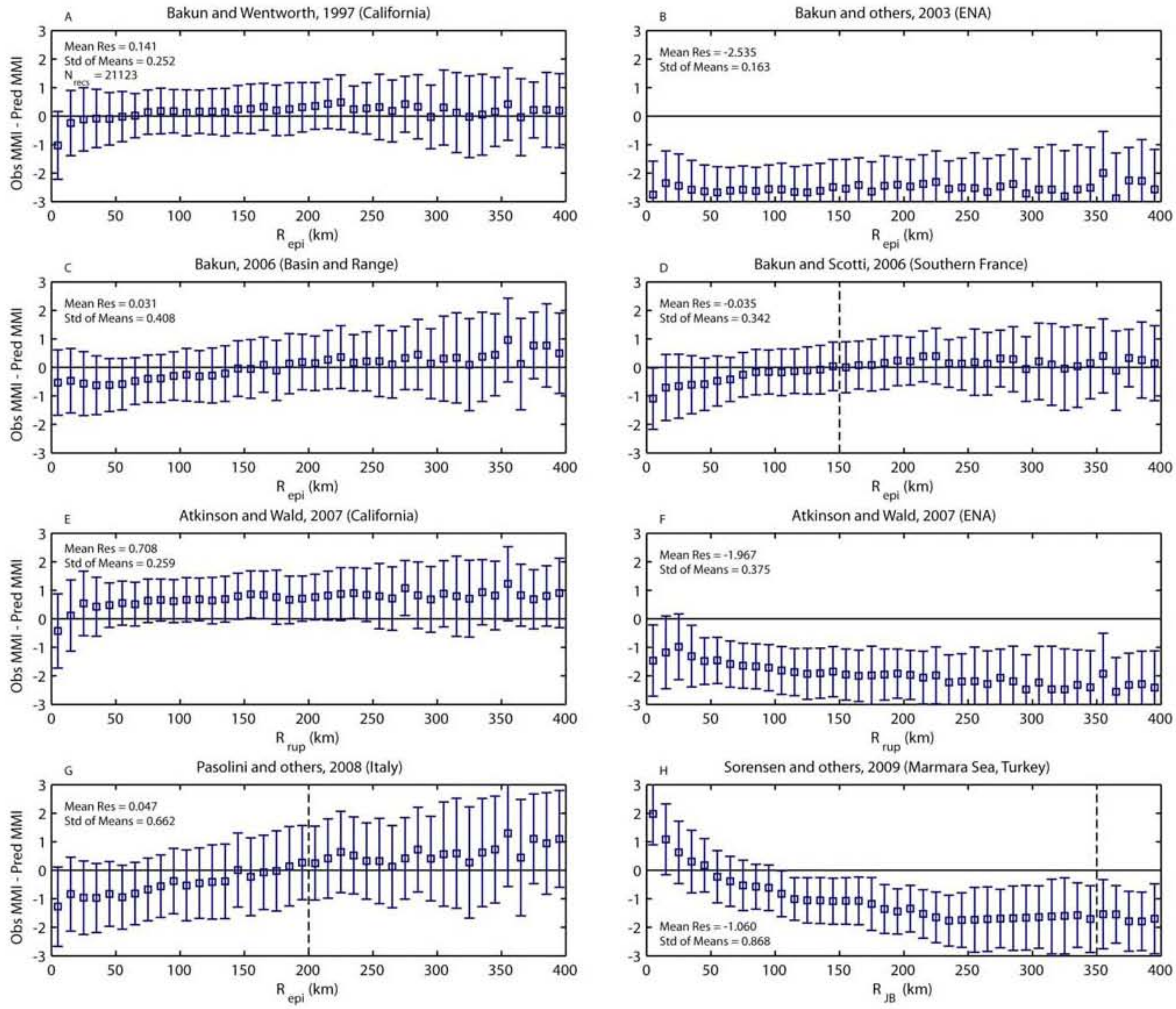

Figure 19. Residuals for macroseismic intensity prediction equations against global active crust intensity data. Residuals are binned in 10-kilometer windows and the median residual is plotted. The standard deviation of the residuals is indicated. Vertical dashed lines indicate the maximum distance of usage as recommend by each of the authors.

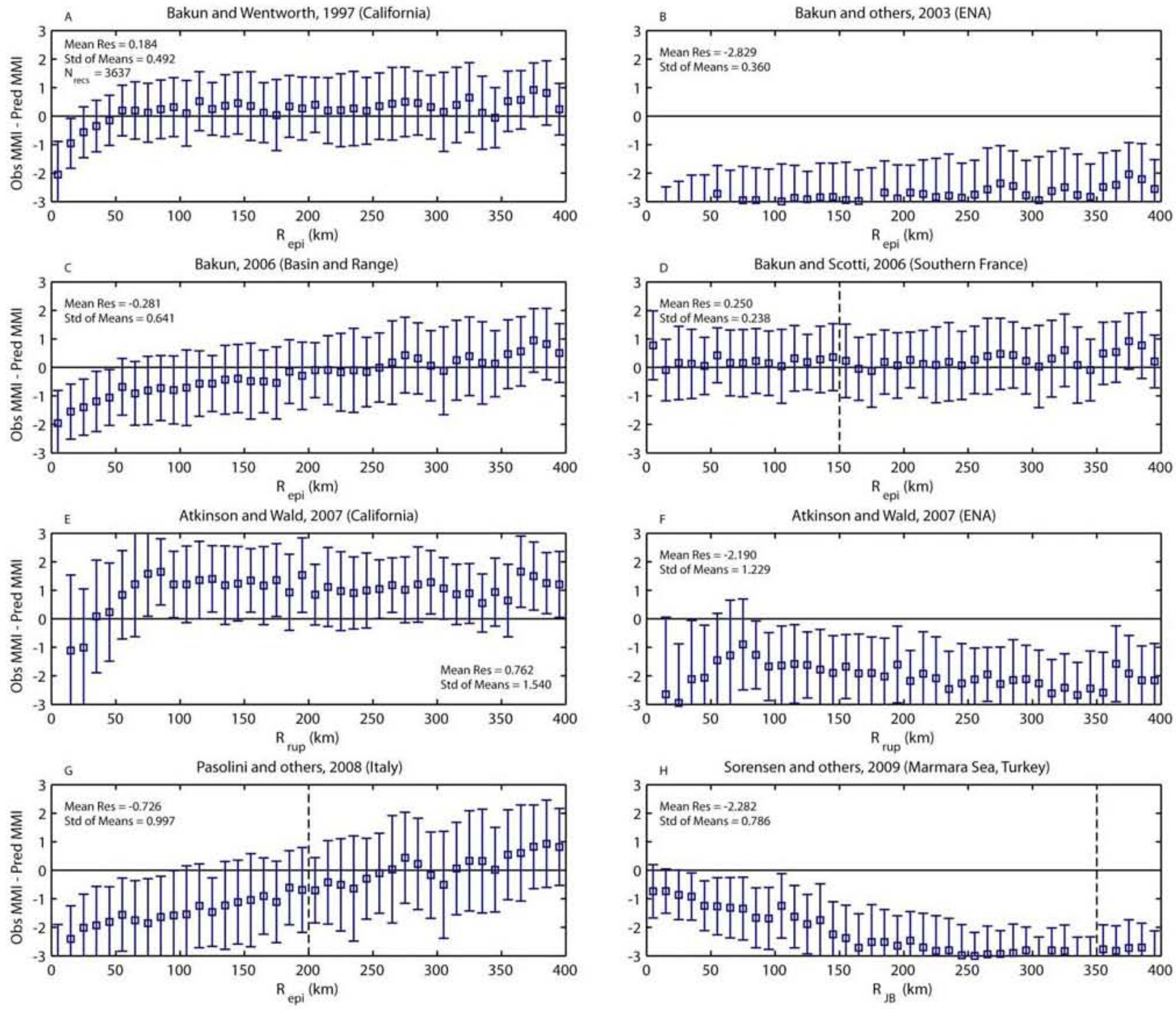

Figure 20. Residuals for macroseismic intensity prediction equations against global subduction-zone intensity data. Residuals are binned in 10-kilometer windows and the median residual is plotted. The standard deviation of the residuals is indicated. Vertical dashed lines indicate the maximum distance of usage as recommend by each of the authors.

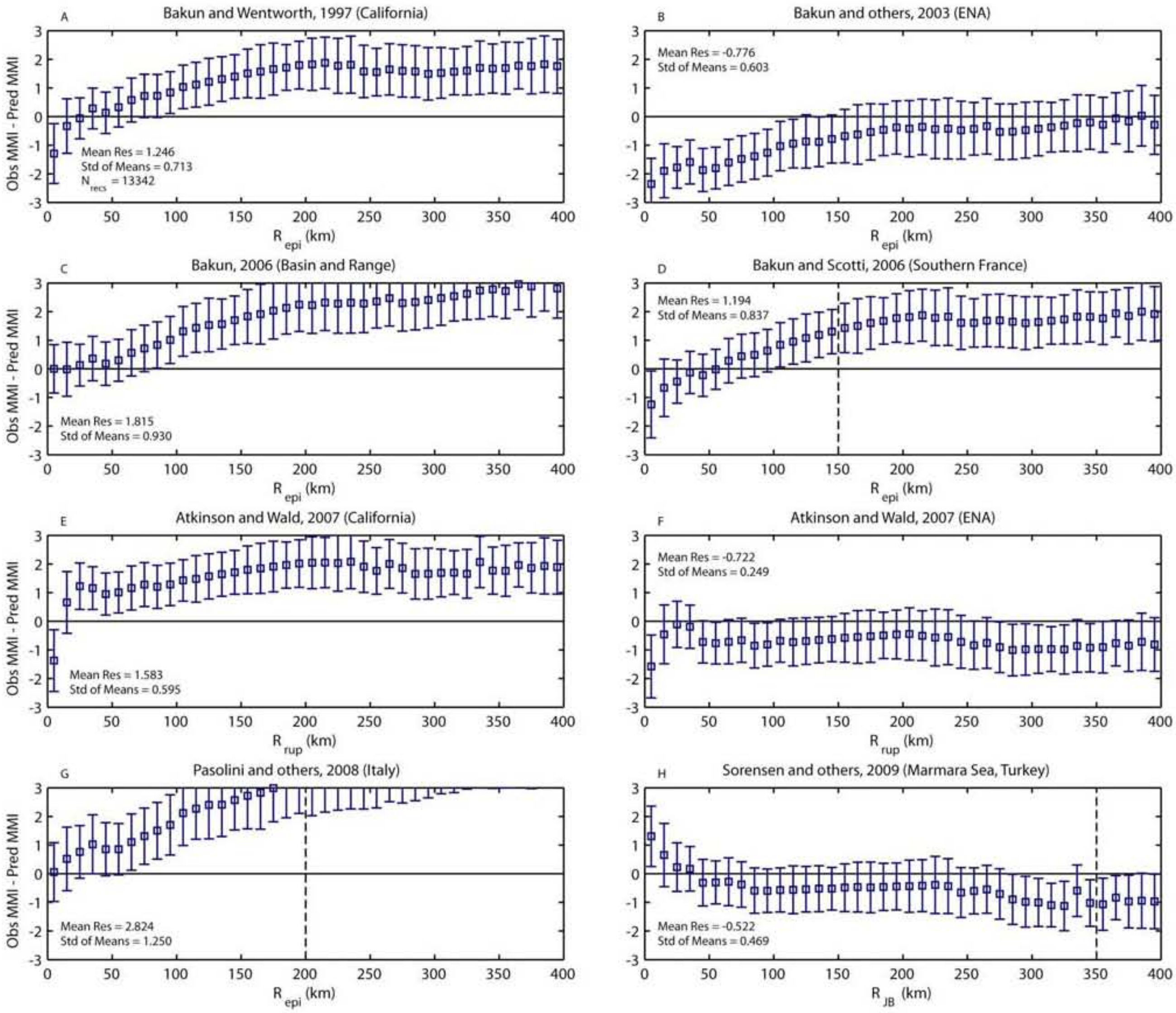

Figure 21. Residuals for macroseismic intensity prediction equations against global stable continental region intensity data. Residuals are binned in 10-kilometer windows and the median residual is plotted. The standard deviation of the residuals is indicated. Vertical dashed lines indicate the maximum distance of usage as recommend by each of the authors.

Appendix 1 – Active Crustal Instrumental Data

Individual earthquakes that comprise the active crustal instrumental ground-motion database.

Event ID	Event name	Mag	Latitude	Longitude	No. recs	Max PGA (%g)	R_{rup} range (km)
196606280426	Parkfield, California	6.1	35.875	-120.487	4	48.94	0.7-14.2
196804090229	Borrego Mountain, California	6.6	33.157	-116.194	1	1.26	220
196805231724	Inangahua, New Zealand	7.2	-41.76	171.96	15	58	9.1-300.8
197009121430	Lytle Creek, California	5.4	34.27	-117.54	1	2.04	76.7
197102091400	San Fernando, California	6.6	34.4	-118.391	111	124.92	4.2-305
197212230629	Managua, Nicaragua	6.2	12.146	-86.269	1	39	4.4
197311231336	Azores, Portugal	5.2	38.486	-28.329	1	27.45	22
197508012020	Oroville, California	5.8	39.503	-121.392	1	9.24	13.9
197605062000	Friuli, Italy	6.5	46.262	13.3	13	35.71	22.9-187.6
197605112244	Friuli, Italy (Aftershock)	5.2	46.3	12.992	4	30.61	11.4-20
197605170258	Gazli, Uzbekistan	6.7	40.373	63.428	1	72.14	5.4
197606171428	Friuli, Italy (Aftershock)	5.2	46.155	12.917	1	5.43	26.8
197607271942	Tangshan, China	7.6	39.59	118.185	6	17.25	139.6-363.2
197608190112	Denizli, Turkey	5.0	37.743	29.015	1	34.59	16.5
197609111631	Friuli, Italy (Foreshock)	5.5	46.339	13.181	7	19.69	13.4-32.7
197609111635	Friuli, Italy (Foreshock)	5.4	46.32	13.205	8	23.16	18.7-183.4
197609150315	Friuli, Italy	6.0	46.314	13.206	9	50.61	13.6-182.7
197609150921	Friuli, Italy (Aftershock)	5.9	46.354	13.087	14	42.24	17.6-182.7
197611241222	Muradiye, Turkey	7.0	39.082	44.031	1	9.76	51.1

Event ID	Event name	Mag	Latitude	Longitude	No. recs	Max PGA (%g)	R_{rup} range (km)
197704061336	Chahar Mahal Bakhtiari, Iran	6.0	31.961	50.649	1	90.92	18.6
197806202003	Thessaloniki, Greece	6.2	40.76	23.303	4	14.59	11.9-125.3
197807042223	Volvi, Greece	4.6	40.718	23.112	1	11.43	19.3
197808132254	Santa Barbara, California	5.8	34.373	-119.652	3	36.83	19.9-25
197809161535	Tabas, Iran	7.3	33.242	57.382	9	110.2	3.1-183.7
197902282127	St. Elias, Alaska	7.5	60.661	-141.652	1	6.41	44.6
197904150619	Montenegro, Serbia	6.9	42.001	19.154	20	45.41	15.8-302.8
197904151443	Montenegro, Serbia (Aftershock)	5.8	42.289	18.716	5	9.96	28.3-51.6
197904231301	Dead Sea, Israel	5.1	31.191	35.529	3	1.99	46.2-82.1
197905241723	Montenegro, Serbia (Aftershock)	6.2	42.239	18.827	9	27.55	10.1-116
197908061705	Coyote Lake, California	5.7	37.069	-121.6	2	11.34	13.3-32.4
197909192135	Valnerina, Italy	5.8	42.773	13.01	7	20.51	16.2-50.9
197910152316	Imperial Valley, California	6.5	32.814	-115.648	38	77.36	0.5-49.8
198001011642	Terceira Island, Portugal	6.9	38.726	-27.751	1	5.67	80.3
198001241900	Livermore, California	5.8	37.712	-121.728	4	7.79	27.8-37.6
198001270233	Livermore, California	5.8	37.737	-121.74	5	25.04	15.4-35
198002200234	Cosenza, Italy	4.8	39.291	16.152	1	16.73	11.7
198002251047	Anza, California	5.6	33.517	-116.55	3	12.68	8.2-24.1
198005182002	Kopaonik, Serbia	5.9	43.259	20.908	2	3.74	80.8-85
198005271450	Mammoth Lakes, California	5.9	37.417	-118.797	1	10.06	18.6
198006090328	Victoria, Mexico	6.3	32.268	-114.908	6	87.3	18.8-67.9
198007090211	Volos, Greece	6.6	39.257	23.008	1	4.47	67.5
198011081027	Trinidad, California	7.3	41.111	-124.299	1	14.7	71.6
198011231834	Irpinia, Italy	6.9	40.788	15.31	21	32.35	8.3-127.9

Event ID	Event name	Mag	Latitude	Longitude	No. recs	Max PGA (%g)	R_{rup} range (km)
198102141727	Baiano, Italy	4.9	40.995	14.614	2	2.93	13.6-29.8
198102242053	Corinth, Greece	6.6	38.159	22.976	2	31.02	30.4-35.4
198102250235	Corinth, Greece (Aftershock)	6.3	38.097	23.17	1	12.04	28.7
198107230005	Urmiya, Iran	5.8	37.082	45.197	1	4.9	55.3
198108130258	Banja Luka, Bosnia and Herzegovina	5.7	44.827	17.361	4	44.29	20.1-22.3
198301171241	Kefallinia Island, Greece	6.9	38.014	20.324	2	6.54	96.3-116.2
198305022342	Coalinga, California	6.3	36.218	-120.305	46	60.22	15-66.1
198307051201	Biga, Turkey	6.1	40.309	27.254	5	5.1	41-90.8
198307090740	Coalinga, California (Aftershock)	5.1	36.173	-120.372	7	41.91	3.3-12.9
198307220239	Coalinga, California	5.7	36.195	-120.338	7	116.91	8.5-16.6
198308061543	Magion Oros Peninsula, Greece	6.6	40.107	24.762	3	10.92	71.9-116.7
198310300412	Horasan-Narman, Turkey	6.6	40.327	42.176	2	16.12	22.4-77.8
198404242115	Morgan Hill, California	6.2	37.303	-121.707	9	31.2	2.7-63.2
198405071749	Lazio Abruzzo, Italy	5.9	41.738	13.889	15	14.69	26.1-74.2
198405111041	Lazio Abruzzo, Italy (Aftershock)	5.5	41.755	13.901	9	21.53	13.1-58.3
198406241329	Godley River, New Zealand	6.1	-43.598	170.667	1	4.11	101
198604260735	Dharmsala, India	5.5	32.118	76.397	9	24.8	10.5-37.9
198605050335	Golbasi, Turkey	6.0	37.999	37.781	1	5.49	26.9
198605200525	Hualien, Taiwan	6.2	24.146	121.643	36	21.5	56.7-61.2
198606061039	Golbasi, Turkey	5.8	38.007	37.91	2	3.15	40.9-56.8
198607080920	North Palm Springs, California	6.0	33.969	-116.779	11	94.05	12.1-57.7
198607201429	Chalfant Valley, California (Foreshock)	5.8	37.502	-118.443	4	27.27	20.7-31.1
198607211442	Chalfant Valley, California	6.2	37.494	-118.436	6	44.47	9.3-48.9
198607211451	Chalfant Valley, California (Aftershock)	5.7	37.496	-118.365	3	15.98	17.6-22.6

Event ID	Event name	Mag	Latitude	Longitude	No. recs	Max PGA (%g)	R_{rup} range (km)
198607310722	Chalfant Valley, California (Aftershock)	5.5	37.456	-118.401	2	18.33	18.4-27.4
198609131724	Kalamata, Greece	5.9	37.072	22.176	3	29.69	23.1-95.6
198702272334	Kefallinia Island, Greece	5.7	38.439	20.393	3	3.42	36.1-67.9
198703020142	Edgecumbe, New Zealand	6.5	-38.015	176.921	2	3.66	63.4-123.6
198703020150	Edgecumbe, New Zealand (Aftershock)	5.8	-37.939	176.994	1	2.34	55.6
198705022043	Reggio nell'Emilia, Italy	5.2	44.809	10.68	2	7.74	16-24.1
198705251131	Mt. Vatnafjoll, Iceland	6.0	63.782	-19.685	7	6.1	37-84.4
198710011442	Whittier Narrows, California	5.9	34.061	-118.135	24	25.28	14.8-84
198710041059	Whittier Narrows, California (Aftershock)	5.2	34.02	-118.137	3	13.88	21.5-26.4
198711240154	Elmore Ranch, California	6.0	33.257	-115.756	1	7.84	18
198711241315	Superstition Hills, California	6.5	33.07	-115.952	4	44.66	12.7-25.1
198810161234	Kyllini, Greece	5.9	37.877	20.986	6	15.61	20.7-79.1
198812070741	Spitak, Armenia	6.7	40.919	44.118	2	18.37	32.3-67.8
198812070745	Spitak, Armenia (Aftershock)	5.9	40.942	44.222	1	14.8	34.2
198910180004	Loma Prieta, California	6.9	37.11	-121.764	34	120.11	8.4-116.7
198910291909	Chenoua, Algeria	5.9	36.706	2.441	3	28.88	25.2-52.1
199002100327	Lake Tennyson, New Zealand	6.0	-42.322	172.865	3	4.87	58.2-196.1
199002282343	Upland, California	5.7	34.136	-117.746	1	20.71	9.5
199005050721	Potenza, Italy	5.8	40.665	15.851	3	9.63	26.3-33
199005130423	Weber, New Zealand	6.4	-40.292	176.157	20	25.51	23.4-162.3
199006202100	Manjil, Iran	7.4	37.001	49.216	17	60.2	6.1-193.7
199012130024	Sicily, Italy	5.8	37.286	15.402	7	25.31	37.7-132.6
199012210657	Griva, Greece	6.1	40.977	22.346	6	10.07	33.9-83
199101281800	Hawks Crag, New Zealand	5.8	-41.97	171.769	10	22.55	26.2-261.9

Event ID	Event name	Mag	Latitude	Longitude	No. recs	Max PGA (%g)	R_{rup} range (km)
199102151048	Hawks Crag, New Zealand	5.4	-42.104	171.669	5	17.92	24.4-107.9
199104290912	Racha, Georgia	7.0	42.426	43.667	6	1.52	107.8-166.6
199105032019	Racha, Georgia (Aftershock)	5.6	42.68	43.245	4	50.92	19.4-31.1
199105261226	Basilicata, Italy	5.2	40.712	15.801	1	3.2	26.4
199106150059	Racha, Georgia (Aftershock)	6.2	42.406	44.011	8	11.23	40.2-175.2
199106281443	Sierra Madre, California	5.6	34.237	-118.011	20	46.04	9.4-43.3
199108171929	Honeydew, California	6.1	40.25	-124.117	5	49.87	20.5-39.1
199110192123	Uttarkashi, India	6.8	30.73	78.775	13	31.02	4.1-138.5
199203020905	Weber, New Zealand	5.5	-40.365	176.366	11	8.27	20-158.4
199203131718	Erzincan, Turkey	6.6	39.727	39.651	3	51.33	2.3-62.1
199203151616	Pulumur, Turkey	5.9	39.519	39.963	2	11.53	29.2-48.8
199204230450	Joshua Tree, California	6.2	33.873	-116.548	1	17.17	7.1
199206281157	Landers, California	7.3	34.19	-116.52	44	81.43	0.1-192.6
199206281505	Big Bear, California	6.5	34.289	-116.816	26	54.51	17.4-150.4
199211061908	Izmir, Turkey	6.0	38.046	27.007	5	8.17	32.7-299.4
199211182110	Tithorea, Greece	5.9	38.325	22.509	4	3.79	41.2-72.1
199303261158	Pyrgos, Greece	5.4	37.613	21.526	2	43.47	18-30
199307141231	Patras, Greece	5.6	38.212	21.826	10	34.08	20.1-71.6
199308100946	Ormond, New Zealand	6.4	-38.496	177.795	24	25.14	31.1-404.2
199401171230	Northridge, California	6.7	34.164	-118.563	71	99.88	6.7-359.8
199406180325	Arthurs Pass, New Zealand	6.7	-43.109	171.645	17	43.71	17.4-341.4
199406191343	Arthurs Pass, New Zealand (Aftershock)	5.9	-43.173	171.628	1	1.72	157.7
199406200909	Firuzabad, Iran	5.9	29.053	52.671	9	106.12	12-96.4
199409011515	Eureka, California	7.0	40.381	-125.778	2	7.19	121.4-150.8

Event ID	Event name	Mag	Latitude	Longitude	No. recs	Max PGA (%g)	R_{rup} range (km)
199409011612	Bitola, Macedonia	5.6	41.169	21.241	2	8.11	49-81.7
199409121223	Lake Tahoe, Nevada	5.9	38.859	-119.711	1	11.36	14
199501162046	Kobe, Japan	6.9	34.58	135.025	23	82.1	0.6-160.4
199505130847	Kozani-Grevena, Greece	6.6	40.151	21.713	10	20.82	22.7-138.1
199510011557	Dinar, Turkey	6.4	38.077	30.143	7	31.939	1.1-253.5
199511220415	Gulf of Akaba, Saudi Arabia	7.2	28.762	34.808	7	9.12	50.3-410.5
199511231807	Gulf of Akaba, Saudi Arabia (Aftershock)	5.7	29.246	34.831	1	4.26	39.3
199511240618	Cass, New Zealand	6.1	-42.986	171.839	11	14.49	17.7-228.3
199608101812	Honshu, Japan	5.9	38.998	140.549	82	47.31	13.1-243.2
199610091310	Cyprus	6.8	34.562	32.143	1	0.61	436.3
199702041037	Garmkhan, Iran	6.5	37.724	57.305	10	11.21	31.6-234.6
199702281257	Ardebil, Iran	6.1	38.108	48.069	19	56.02	11.7-147.8
199703260422	Sur, Lebanon	5.6	33.403	35.4	1	3.17	31.7
199703260831	Kagoshima, Japan	6.1	31.973	130.393	26	74.18	6.7-83
199704052346	Northwest China	5.9	39.525	76.83	2	27.38	17.2-58.4
199704060436	Northwest China	6.0	39.498	76.945	2	14.39	26.2-54.3
199704110534	Northwest China	6.1	39.536	76.892	2	30.03	24.3-55.2
199704151819	Northwest China	5.8	39.581	76.925	2	23.92	26.4-49.9
199705100757	Ardakul, Iran	7.2	33.848	59.81	26	19.88	38.4-437.1
199705130538	Kagoshimaen-Hoku-Seibu, Japan	6.0	31.943	130.277	23	92.04	5.9-76.8
199705231814	Sarria Becerrea, Spain	4.9	42.816	-7.156	1	14.9	6.1
199706250950	Yamaguchi, Japan	5.8	34.432	131.586	174	42.95	0.8-343
199706270439	Azores, Portugal	5.9	38.264	-26.72	3	4.88	55.2-144.2
199709260033	Umbria-Marche, Italy (Foreshock)	5.7	43.046	12.838	19	53.88	1.7-119.7

Event ID	Event name	Mag	Latitude	Longitude	No. recs	Max PGA (%g)	R_{rup} range (km)
199709260940	Umbria-Marche, Italy	6.0	43.078	12.781	26	52.45	1.3-126.3
199710030855	Umbria-Marche, Italy (Aftershock)	5.3	43.078	12.792	11	28.47	10.7-72.8
199710062324	Umbria-Marche, Italy (Aftershock)	5.5	43.037	12.803	19	52.24	15.6-92.1
199710141523	Umbria-Marche, Italy (Aftershock)	5.9	42.931	12.877	19	33.67	8.5-108.4
199803141940	Golbaf, Iran	6.6	30.126	57.585	5	4.16	56.6-117
199804121055	Bovec, Slovenia	5.6	46.271	13.653	13	4.05	24.8-149
199805030209	Honshu, Japan	5.5	34.929	139.118	78	12.96	16.6-203.6
199807090519	Faial Island, Portugal	6.1	38.621	-28.566	5	42.04	14.6-253.1
199808121410	San Juan Bautista, California	5.2	36.677	-121.525	2	9.66	14.9-27
199809030758	Iwate, Japan	5.8	39.791	140.741	66	10.58	13.9-216.8
199809292214	Brijezde, Serbia	5.5	44.203	20.094	1	0.44	237.5
199903281905	Chamoli, India	6.5	30.48	79.4	11	36	9-149.2
199905062300	Karebas, Iran	6.2	29.519	51.907	19	36.33	29.3-191.1
199908170001	Kocaeli, Turkey	7.6	40.773	30.003	33	36.12	11.2-344.5
199908310810	Kocaeli, Turkey (Aftershock)	5.1	40.767	29.912	17	19.59	10.5-164.6
199909071156	Athens, Greece	6.0	38.119	23.598	9	32.65	4.5-18.4
199909131155	Kocaeli, Turkey (Aftershock)	5.8	40.736	30.089	57	60.82	13.1-352.9
199909201747	Chi-Chi, Taiwan	7.7	23.819	120.877	407	101.03	1.2-163.3
199909290013	Kocaeli, Turkey (Aftershock)	5.2	40.736	29.35	3	9.34	47.6-152.4
199910160946	Hector Mine, California	7.1	34.517	-116.45	106	32.52	22.3-385
199910161257	Hector Mine, California (Aftershock)	5.7	34.267	-116.234	81	7.78	50.1-413.6
199910311509	Pol-e-Abgineh, Iran	5.2	29.372	51.848	6	9.36	19.8-103.4
199911082137	Salehabad, Iran	5.5	35.697	61.225	3	29.69	15.4-87.8
199911111441	Sapanca-Adapazari, Turkey	5.6	40.74	30.247	25	10.11	32.7-192.9

Event ID	Event name	Mag	Latitude	Longitude	No. recs	Max PGA (%g)	R_{rup} range (km)
199911121657	Duzce, Turkey	7.1	40.803	31.219	54	104.08	1.5-409.5
199911121717	Duzce, Turkey (Aftershock)	5.5	40.785	31.142	2	0.36	149.7-207.2
200006060241	Duzce, Turkey (Aftershock)	6.0	40.737	33.005	1	0.43	156.7
200006062116	Sea of Japan	5.9	36.81	135.5	22	14.16	107.1-258.6
200006171540	South Iceland	6.5	63.904	-20.475	25	62.65	11.5-152
200006171542	South Iceland (Aftershock)	6.5	63.71	-20.427	15	24.59	17.7-86.9
200006210051	South Iceland (Aftershock)	6.4	63.876	-20.748	24	83.88	11-158.7
200007070015	Duzce, Turkey (Aftershock)	4.2	40.857	29.344	1	0.54	152.2
200008231341	Hendek-Akyazi, Turkey	5.3	40.778	30.772	8	2.3	38.6-177.4
200009030836	Yountville, California	5.0	38.379	-122.413	27	50.83	14.1-97.1
200010060430	Tottori, Japan	6.7	35.38	133.174	301	83.19	6.6-443.5
200012061711	Turkmenistan	7.0	39.532	54.801	11	3.23	212-398.4
200012151644	Golcayir, Turkey	6.0	38.451	31.265	1	0.12	118
200102030304	Bhuj, India (Aftershock)	5.3	23.628	70.451	1	2.31	93.8
200106101311	Chios, Greece	5.6	38.525	25.625	3	0.38	192-283.6
200106251328	Meydan, Turkey	5.4	37.18	36.21	5	1.4	48.1-226.8
200110080339	Guerrero, Mexico	5.8	17.084	-100.008	15	8.2	20.6-216
200111101709	Guerrero, Mexico	5.4	16.197	-98.147	2	0.54	101-132
200112082336	Gulf of California, Mexico	5.7	32.048	-114.9	2	1.35	76.1-111.8
200202030711	Ishakli, Turkey	6.5	38.527	31.227	7	11.33	65.1-346.8
200202030926	Ishakli, Turkey (Aftershock)	5.8	38.668	30.919	5	5.17	35.7-234.9
200202201127	Polkowice, Poland	5.0	51.517	16.004	1	0.82	22.9
200206220258	Changureh-Avaj, Iran	6.5	35.597	49.02	62	50.84	17.5-214
200209252228	Masjed-E-Soleyman, Iran	5.6	32.076	49.328	3	6.21	26-62.6

Event ID	Event name	Mag	Latitude	Longitude	No. recs	Max PGA (%g)	R_{rup} range (km)
200210231127	Nenana Mountain, Alaska	6.6	63.53	-148.15	36	3.03	126.1-285.4
200211032212	Denali, Alaska	7.9	63.541	-147.731	24	35.8	4.2-277.9
200301270526	Pulumur, Turkey	6.0	39.503	39.851	3	1.11	57.4-109.6
200304100040	Seferihisar, Turkey	5.7	38.229	26.932	9	7.81	38.9-311.1
200305010027	Bingol, Turkey	6.3	38.97	40.458	4	51.53	9.1-117
200305211844	Boumerdes, Algeria	6.8	36.88	3.694	13	58	13.6-139.2
200307251513	Honshu, Japan	5.4	38.495	141.037	130	27.94	16.2-334.8
200307252213	Miyagi-Hokubu, Japan	6.0	38.485	141.036	199	35.62	3.9-380.5
200312221915	San Simeon, California	6.6	35.629	-121.075	46	46.84	4.1-273.4
200312260156	Bam, Iran	6.6	28.95	58.268	24	79.33	0.7-284.4
200405281238	Kojur-Firoozabad, Iran	6.3	36.257	51.565	100	85.82	33.1-356.9
200407180422	Rotorua, New Zealand	5.4	-38.013	176.432	8	6.22	25.7-124.5
200409281715	Parkfield, California	6.0	35.761	-120.307	397	131.24	0.1-442.4
200410230856	Niigata, Japan	6.6	37.23	138.801	327	174.87	6.6-358.8
200412140556	Hokkaido, Japan	5.7	44.133	141.805	70	114.95	11.9-181
200502220225	Dahuiyeh, Iran	6.4	30.691	56.794	18	28.6	14.4-234.5
200503200153	Fukuoka, Japan	6.6	33.802	130.209	258	36.27	23-449.5
200506150250	Coast of Northern California	7.2	41.229	-125.977	8	1.39	156.6-174.7
200507260408	Dillon, Montana	5.6	45.397	-112.574	7	12.76	23.5-337.6
200508210229	Honshu, Japan	4.8	37.292	138.615	6	19.22	21-46.2
200509020127	Obsidian Butte, California	5.2	33.16	-115.637	185	16.97	10.2-446.3
200604201750	Honshu, Japan	5.6	34.858	139.207	143	31.78	25.2-216.2
200703250041	Noto Peninsula, Japan	6.7	37.22	136.69	371	86.55	0.5-448.9
200704150319	Western Honshu, Japan	5.1	34.79	136.41	197	72.95	18-275.5

Event ID	Event name	Mag	Latitude	Longitude	No. recs	Max PGA (%g)	R_{rup} range (km)
200707160113	Honshu, Japan	6.6	37.56	138.61	389	68.02	23.8-447.4
200710310304	Milpitas, California	5.6	37.432	-121.776	228	41.36	9.7-423.7
200802090712	Baja California, Mexico	5.1	32.419	-115.292	159	13.18	36.8-445.3
200802120432	Baja California, Mexico (Aftershock)	5.0	32.459	-115.314	166	12.44	29.7-447.4
200802211416	Wells, Nevada	6.0	41.153	-114.867	80	2.75	36.9-281.2
200805120628	Wenchuan, China	7.9	30.986	103.364	32	97.66	4.7-374.8
200805291546	Olfus, Iceland	6.3	64.003	-21.012	8	66.43	12.3-41.7
200806132343	Iwate, Japan	6.9	39.03	140.88	319	75.42	13-446.1
200807291842	Chino Hills, California	5.4	33.953	-117.761	485	43.86	15.4-438.4

Appendix 2 – Subduction Zone Instrumental Data

Individual earthquakes that comprise the subduction zone instrumental ground-motion database.

Event ID	Event name	Mag	Latitude	Longitude	No. recs	Max PGA (%g)	R_{rup} range (km)
196504291528	Puget Sound, Washington	6.5	47.317	-122.333	1	19.831	84
197005312023	Peru	7.9	-9.248	-78.841	1	9.97	262.3
197311041552	Ionian, Greece	5.4	38.843	20.61	1	52.55	23.9
197401050833	Peru	6.6	-12.351	-76.307	2	15.94	125.1-125.6
197410031421	Lima, Peru	8.1	-12.254	-77.524	2	21.14	67.2-68.9
197411091259	Lima, Peru (Aftershock)	7.2	-12.525	-77.632	2	11.92	82.4-89.6
197605041356	Milford Sound, New Zealand	6.5	-44.726	167.664	3	9.21	37.6-120.9
197701180541	Cape Campbell, New Zealand	6.1	-41.748	174.384	31	27.66	59.6-85.9
197703041921	Vrancea, Romania	7.5	45.776	26.702	2	20.2	114.8-410.7
197712091553	Izmir, Turkey	4.6	38.362	27.216	1	20408	23.4
197803111920	Calabria, Italy	5.2	38.046	15.99	2	7.78	25.5-36.9
198007090235	Volos, Greece (Aftershock)	6.3	39.231	22.626	1	3.33	62.1
198010051532	Hastings, New Zealand	5.6	-39.616	176.668	1	12.04	43.3
198011080754	El Asnam, Algeria (Aftershock)	5.2	36.149	1.374	1	9.65	33
198101290451	Taiwan	5.9	24.503	121.924	27	16.03	46-48
198103101516	Preveza, Greece	5.4	39.382	20.813	2	14.29	60.5-71.9
198209021558	Hawkes Bay, New Zealand	5.4	-39.75	176.753	2	9.46	41.2-43.8
198303232351	Kefallinia Island, Greece (Aftershock)	6.2	38.221	20.361	3	23.47	28.3-77.8
198309211920	Taiwan	6.4	24.156	122.181	35	4.01	79-83.9
198311091629	Parma, Italy	5.0	44.664	10.291	1	3.35	41

Event ID	Event name	Mag	Latitude	Longitude	No. recs	Max PGA (%g)	R_{rup} range (km)
198503032247	Valparaiso, Chile	7.9	-33.132	-71.708	7	29.75	46.1-163.1
198503032338	Valparaiso, Chile (Aftershock)	7.0	-32.83	-71.211	1	4.05	49
198504301814	Anchialos, Greece	5.6	39.235	22.843	2	3.11	34-59.4
198506121722	Taiwan	5.9	24.624	122.118	35	15.15	43.3-46.5
198508310603	Preveza, Greece	4.5	39.086	20.653	2	8.73	44.9-50.7
198509191317	Michoacan, Mexico	8.0	18.42	-102.38	25	16.9	15.6-322.6
198509210137	Zihuatanejo, Mexico	7.5	17.831	-101.623	13	63.87	24.4-201.6
198510291502	Michoacan, Mexico	5.9	18.128	-102.599	1	4.06	32.9
198604300707	Michoacan, Mexico	6.9	18.371	-103	4	9.96	48-375.5
198608302128	Vrancea, Romania	7.2	45.524	26.269	10	30.31	138.2-250.5
198609151141	Kalamata, Greece (Aftershock)	4.8	37.048	22.213	3	33.47	45-56.3
198611142120	Taiwan	7.3	23.974	121.727	36	17.11	80.5-86.9
198801090102	Tirana, Albania	5.9	41.21	19.757	2	41.22	27.9-29.6
198802061450	India-Bangladesh Border	5.8	24.682	91.524	18	11.43	81.8-203.1
198806032327	Te Anau, New Zealand	6.7	-45.039	167.587	2	10.52	86.5-148.6
198808060036	India-Burma Border	7.2	25.105	95.126	33	34.39	192.5-400.6
198904251429	Guerrero, Mexico	6.9	16.779	-99.275	18	35.3	19.7-205.8
198905310554	Doubtful Sound, New Zealand	6.4	-45.302	167.071	2	9.64	57.2-130.4
198911300858	Gisborne, New Zealand	5.6	-38.881	178.231	4	7.17	45.2-45.2
199002190534	Weber, New Zealand	6.2	-40.368	176.2	21	29.9	31.9-159.9
199004032202	Imotski-Grude, Croatia	5.6	43.393	17.375	1	15.41	44.4
199005301040	Vrancea, Romania	7.0	45.861	26.64	12	16.73	89.3-222.4
199005310735	Guerrero, Mexico	5.9	17.247	-100.686	17	40.04	25.7-201.9
199006160216	Filippias, Greece	5.5	39.238	20.647	5	3.46	42.3-74.2

Event ID	Event name	Mag	Latitude	Longitude	No. recs	Max PGA (%g)	R_{rup} range (km)
199008151554	Weber, New Zealand	5.1	-40.403	176.363	3	1.52	99-169.2
199101281258	Hawks Crag, New Zealand	5.7	-41.968	171.774	7	20.77	33.1-262.2
199104010734	Coast of Guerrero, Mexico	5.8	16.179	-98.27	4	1.37	92.4-299.3
199104222156	Valle de la Estrella, Costa Rica	7.6	9.673	-83.072	13	26.17	6.9-115.8
199201230424	Kefallinia Island, Greece	5.6	38.372	20.525	3	22.65	47.2-83.9
199204251806	Petrolia, California	7.2	40.337	-124.088	7	104.02	7.6-37.2
199204260741	Petrolia, California (Aftershock)	6.5	40.508	-124.307	4	59.92	26.2-60.7
199204261118	Petrolia, California (Aftershock)	6.6	40.421	-124.416	4	49.34	26.8-64.2
199205161757	Tokomaru, New Zealand	5.7	-38.349	178.197	2	2.58	45.5-46.3
199206211743	New Zealand	6.2	-37.823	177.022	6	4.57	43.7-134.6
199303311018	Guerrero, Mexico	5.5	17.286	-100.964	8	16.8	29-176.1
199304110659	Tikokino, New Zealand	5.7	-39.72	176.482	10	18.06	37.6-217.4
199305150309	Guerrero, Mexico	6.0	16.747	-98.375	7	6.3	93.2-237.8
199305150312	Guerrero, Mexico	6.0	16.725	-98.325	8	6.87	99.8-243
199308100051	Secretary Island, New Zealand	6.9	-45.217	167.004	5	8.03	49-284.6
199310240752	Guerrero, Mexico	6.6	16.753	-98.758	16	37.31	35.4-220.6
199412151120	Te Kuha, New Zealand	6.3	-37.549	177.586	7	8.64	44-227.2
199502052251	East Cape, New Zealand	7.1	-37.824	178.879	15	4.03	120.8-480.3
199509141404	Copala, Mexico	7.3	16.849	-98.608	10	10.23	17.1-217.2
199602250308	Oaxaca, Mexico	7.1	15.936	-98.114	1	0.15	285.7
199603271234	Guerrero, Mexico	5.5	16.492	-98.064	4	0.9	101.8-279.3
199607152123	Guerrero, Mexico	6.6	17.514	-101.019	13	32.61	27.8-206.6
199609090434	Kyushu, Japan	5.7	30.517	130.771	5	39.9	35.3-48.4
199610191444	Hyuga-Nada #1, Japan	6.7	31.911	131.574	154	23.41	27.7-442.9

Event ID	Event name	Mag	Latitude	Longitude	No. recs	Max PGA (%g)	R_{rup} range (km)
199612022217	Hyuga-Nada #2, Japan	6.7	31.828	131.323	121	21.23	11.5-457.5
199612210128	Honshu, Japan	5.5	36.121	139.769	47	53.47	60.1-186.7
199612242216	Tadmuriyah, Syria	5.5	34.301	38.585	10	2.65	53-294.7
199701112028	Michoacan, Mexico	7.1	18.193	-102.795	14	40.43	37.8-371.8
199703160551	Honshu, Japan	5.6	34.895	137.483	206	53.51	39.3-274.8
199705080253	India-Burma Border	5.9	24.923	92.27	11	16.24	39.2-124.4
199705220750	Michoacan, Mexico	6.5	18.652	-101.642	12	4.79	97.5-281.1
199710131339	Kalamata, Greece	6.4	36.374	22.161	5	12.04	56.2-109.5
199711052110	Itea, Greece	5.6	38.394	22.304	4	5.84	35-76.4
199711181307	Strofades, Greece	6.6	37.481	20.779	10	13.16	42.2-151.4
199712161148	Guerrero, Mexico	5.9	16.145	-98.877	3	0.97	93.6-140.7
199802030302	Oaxaca, Mexico	6.3	15.9	-96.245	2	0.29	303.4-333.4
199807110521	Guerrero, Mexico	5.4	17.419	-101.373	6	4.89	28.6-207.5
199807120811	Guerrero, Mexico	5.5	16.94	-100.3	9	0.94	28.9-151.9
199903252331	Honshu, Japan	5.2	36.489	140.483	96	34.97	56.5-227.4
199906152042	Puebla, Mexico	6.9	18.381	-97.445	15	3.58	177.1-413
199907030143	Satsop, Washington	5.8	47.075	-123.355	4	10.29	47.8-53.9
199909301631	Oaxaca, Mexico	7.4	16.055	-96.905	10	5.3	154.3-415.7
199912290519	Guerrero, Mexico	5.9	18.169	-101.509	9	6.93	59-201.8
200007201839	Honshu, Japan	6.0	36.552	140.947	215	26.56	41.3-444.1
200008091141	Michoacan, Mexico	6.5	18.151	-102.557	5	15.37	36.8-203.9
200010301642	Southern Honshu, Japan	5.5	34.288	136.271	181	39.21	35.9-279.3
200011011035	Charles Sound, New Zealand	6.1	-45.13	167.125	1	2.15	124.9
200011151505	Altinsac, Turkey	5.5	38.43	42.97	1	1.33	45.9

Event ID	Event name	Mag	Latitude	Longitude	No. recs	Max PGA (%g)	R_{rup} range (km)
200101131733	San Miguel, El Salvador	7.7	13.076	-88.702	15	88.18	87.9-145.9
200102281854	Nisqually, Washington	6.8	47.112	-122.603	66	27.39	56.1-431.3
200103240627	Geiyo, Japan	6.8	34.108	132.54	316	84.57	40.1-435.6
200104031457	Honshu, Japan	5.3	34.933	138.084	165	24.32	30-223
200104251440	Shikoku, Japan	5.7	32.847	132.071	138	25.26	43.9-288.1
200107102142	Pasinler, Turkey	5.4	39.822	41.616	1	2.17	49.7
200109160200	Kallirro, Greece	5.4	37.238	21.929	1	0.14	104.7
200110150349	New Zealand	5.5	-39.692	176.632	4	2.76	47.8-199
200110311233	Koyyeri, Turkey	5.2	37.175	36.127	1	0.66	65
200112071927	Fiordland, New Zealand	5.8	-44.2	168.84	10	2.1	96.5-322.6
200201211434	Haciveliler, Turkey	4.8	38.633	27.887	2	0.69	66.5-92.8
200201220453	Off coast of Karpathos, Greece	6.2	35.62	26.64	1	0.17	195.7
200204251741	Tbilisi, Georgia	4.8	41.767	44.857	1	10.82	36.1
200206140242	Honshu, Japan	4.9	36.244	139.834	5	3.28	64.2-87.6
200209251814	Guerrero, Mexico	5.3	16.92	-99.949	4	4.65	30.8-111.3
200211030337	Honshu, Japan	6.4	38.954	141.948	193	39.27	46.4-494.4
200212241703	Sahneh, Iran	5.2	34.542	47.476	5	9.13	33-372.9
200301220206	Tecoman, Mexico	7.5	18.9	-104.063	6	2.84	131.2-324.5
200305260924	Miyagi-Oki, Japan	7.0	38.868	141.508	364	113.43	74.1-497.7
200308211212	Fiordland, New Zealand	7.2	-45.205	167.144	32	11.51	77.4-477.7
200309251950	Tokachi-Oki, Japan	8.3	41.864	143.878	273	98.96	43.5-498.1
200309252108	Tokachi-Oki, Japan (Aftershock)	7.3	41.8	143.558	246	60.34	48.6-494.6
200310080906	Tokachi-Oki, Japan (Aftershock)	6.7	42.652	144.531	79	9.99	50.4-468.2
200311141843	Honshu, Japan	5.7	36.469	141.068	173	12.12	58.7-402.3

Event ID	Event name	Mag	Latitude	Longitude	No. recs	Max PGA (%g)	R_{rup} range (km)
200401012331	Guerrero, Mexico	6.0	17.426	-101.319	13	6.77	21.5-194.1
200402170746	Hokkaido, Japan	5.5	43.193	145.822	39	25.55	46.4-427.1
200404032302	Honshu, Japan	5.9	36.41	141.029	173	11.52	58.1-409.3
200404111806	Hokkaido, Japan	6.1	42.9	144.861	74	29.26	40.6-477.1
200409051007	Kii Peninsula, Japan (Foreshock)	7.2	33.055	136.641	406	20.57	83.7-498.5
200409051457	Kii Peninsula, Japan	7.4	33.18	137.106	419	39.14	83.1-498.7
200409062329	Kii Peninsula, Japan (Aftershock)	6.6	33.201	137.233	297	11.31	123.8-480.2
200410061440	Honshu, Japan	5.7	35.935	139.938	34	17.89	66.8-111.7
200411222026	West of Invercargill, New Zealand	7.1	-46.7	164.82	12	8	213.7-493.5
200411281832	Hokkaido, Japan	7.0	43.003	145.13	173	56.08	39.9-498.9
200412061415	Hokkaido, Japan (Aftershock)	6.7	42.885	145.23	172	34.95	41.8-493.2
200412211534	Hokkaido, Japan (Aftershock)	5.6	42.949	145.422	58	11.47	48.1-491.8
200501181409	Hokkaido, Japan (Aftershock)	6.2	42.952	144.878	125	14.49	45.3-497.9
200502151946	Ibaraki Prefecture, Japan	5.4	36.004	139.721	177	32.58	48-344.8
200504102222	Honshu, Japan	5.9	35.6	140.4	9	23.22	48.5-72.4
200507230734	Honshu, Japan	5.9	35.52	139.97	51	19.59	69.8-152.3
200508160246	Miyagi-Oki, Japan	7.2	38.279	142.036	363	52.39	68.1-499
200510160705	Ibaraki Prefecture, Japan	5.0	36.021	139.794	22	19.7	50.1-93.2
200510191144	Honshu, Japan	6.3	36.39	140.87	224	23.61	43.8-463
200603270250	Kyushu, Japan	5.5	32.602	132.157	7	16.94	45.5-78.4
200606112001	Kyushu, Japan	6.4	33.13	131.15	65	18.8	141.6-319.3
200610151707	Kiholo Bay, Hawaii	6.7	19.878	-155.935	23	105.1	39.5-264.5
200610151714	Kiholo Bay, Hawaii (Aftershock)	6.0	20.129	-155.983	18	26.12	29.1-130.8
200704201937	Ryukyu Islands, Japan	5.7	27.471	128.379	3	11.02	48.9-73.7
200708152340	Pisco, Peru	8.0	-13.358	-76.522	13	49.79	36.1-186.8

Appendix 3 – Stable Continent Instrumental Data

Individual earthquakes that comprise the stable continental region instrumental ground-motion database.

Event ID	Event name	Mag	Latitude	Longitude	No. recs	Max PGA (%g)	R_{rup} range (km)
198811252346	Saguenay, Canada	5.8	48.061	-71.277	2	9.16	190.4-319.2
199001170638	Meckering, Australia	4.2	-31.654	117.067	1	0.50	72.1
199408061103	Ellalong, Australia	4.7	-32.917	151.292	22	0.74	43-922.7
199607150013	Epagny, France	4.3	45.99	6.033	3	0.80	24-203.9
199609250453	Thomson Reservoir, Australia	4.5	-37.863	146.422	26	10.24	12.3-581
200008291205	Boolarra, Australia	4.2	-38.402	146.245	25	2.14	21-636.9
200101260316	Bhuj, India	7.6	23.402	70.287	14	65	47.9-268.9
200302222041	Saint Die, France	5.0	48.317	6.626	13	1.56	110.7-460.4
200804180937	Mt. Carmel, Illinois	5.2	38.45	-87.89	11	6.52	205.1-334.6
200804181514	Mt. Carmel, Illinois (Aftershock)	4.6	38.483	-87.8914	2	0.72	204.5-208.2

Appendix 4 – Active Crustal Macroseismic Data

Individual earthquakes that comprise the active crustal macroseismic intensity database. Many of the events where DYFI? data were collected are not indicated in the present list. Most maximum intensity values given to one decimal point are from the online DYFI? system. Note that not all macroseismic data gathered are Modified Mercalli Intensities (MMI). However, in this study we assume equivalence between the various intensity scales used around the world.

Event ID	Event name	Mag	Latitude	Longitude	No. recs	Max MMI	R_{rup} range (km)
196002292340	Agadir, Morocco	6.3	30.45	-9.62	33	9	7.4-263.7
196209011920	Buyin-Zara, Iran	6.6	35.63	49.87	184	9	0.1-54.1
196307260417	Skopje, Yugoslavia	6.1	42.008	21.455	15	9	6-130.1
196606280426	Parkfield, California	6.1	35.875	-120.487	175	7	1-319.9
196608191222	Varto, Turkey	6.8	39.161	41.58	390	8.5	0.1-74.6
196707300000	Caracas, Venezuela	6.6	10.555	-67.31	40	8	18.5-318.2
196804090229	Borrego Mountain, California	6.6	33.157	-116.194	262	8	0.9-394
196805231724	Inangahua, New Zealand	7.2	-41.76	171.96	138	10	9.1-398.8
196808311047	Dasht-e Bayaz, Iran	7.2	34.045	58.96	90	9	0.1-61.6
197009121430	Lytle Creek, California	5.4	34.27	-117.54	221	7	9.5-210.3
197102091400	San Fernando, California	6.6	34.4	-118.391	581	11	4.7-399.2
197212230629	Managua, Nicaragua	6.2	12.146	-86.269	56	8	0.5-107.1
197412281211	Pattan, Pakistan	6.2	35.023	72.9	45	8	14.6-47.6
197502041136	Haicheng, China	7.0	40.667	122.646	22	9	1.3-39.5
197508012020	Oroville, California	5.8	39.503	-121.392	320	8	12.2-333.1
197509060920	Lice, Turkey	6.7	38.515	40.768	11	8	5.8-56.3
197602040901	Guatemala	7.6	15.296	-89.145	54	8	6.3-150.1
197604090708	Ecuador	6.6	0.85	-79.564	45	8	18.3-298.9
197605062000	Friuli, Italy	6.5	46.262	13.3	704	9.5	10-307.3
197607271942	Tangshan, China	7.6	39.59	118.185	81	9	1.1-256.3
197609150315	Friuli, Italy	6.0	46.314	13.206	35	8.5	5.6-256.9

Event ID	Event name	Mag	Latitude	Longitude	No. recs	Max MMI	R_{rup} range (km)
197610060912	Ecuador	5.7	-0.726	-78.732	69	8	5.4-207.6
197703212118	Bandar Abbas, Iran	6.7	27.608	56.358	94	8	35.6-80
197711230926	Caucete, Argentina	7.5	-31.729	-67.755	131	9	13.7-356.1
197712192334	Bob-Tangol, Iran	5.9	30.915	56.414	30	7.5	0.3-15.4
197809161535	Tabas, Iran	7.3	33.242	57.382	178	9	1.6-56.5
197904150619	Montenegro, Serbia	6.9	42.001	19.154	124	9	7-265.7
197908061705	Coyote Lake, California	5.7	37.069	-121.6	269	7	7.9-352.2
197910152316	Imperial Valley, California	6.5	32.814	-115.648	219	9	5-382.7
197911140221	Korizan, Iran	6.5	33.959	59.723	23	6	2.8-102.9
197911271710	Khuli-Buniabad, Iran	7.0	34.059	59.757	24	8	1.1-57.1
198001241900	Livermore, California	5.8	37.712	-121.728	281	7	15.2-297.3
198001270233	Livermore, California	5.8	37.737	-121.74	105	7	16.5-282.5
198005251633	Mammoth Lakes, California	6.2	37.525	-118.835	260	7	19.1-395
198005271450	Mammoth Lakes, California	5.9	37.417	-118.797	336	6	19.5-397
198010101225	El Asnam, Algeria	7.1	36.143	1.404	47	9	1.6-290.3
198011231834	Irpinia, Italy	6.9	40.788	15.31	1036	10	0.3-391
198102141727	Baiano, Italy	4.9	40.995	14.614	85	7.5	5.7-107.9
198102242053	Corinth, Greece	6.6	38.159	22.976	277	9	16.8-188.3
198102250235	Corinth, Greece (Aftershock)	6.3	38.097	23.17	178	9	6.9-173.3
198104261209	Westmoreland, California	5.9	33.125	-115.644	101	7	14-371.7
198212130912	Dhamar, Yemen	6.2	14.675	44.223	8	8	0.6-14.1
198305022342	Coalinga, California	6.3	36.218	-120.305	437	8	10.3-398.7
198307220239	Coalinga, California	5.7	36.195	-120.338	205	6	9.3-367.8
198310281406	Borah Peak, Idaho	6.9	44.078	-113.8	207	7	6.8-394.1
198404242115	Morgan Hill, California	6.2	37.303	-121.707	425	8	4.7-383.3
198607080920	North Palm Springs, California	6.0	33.969	-116.779	293	7	12.1-362.9
198703020142	Edgecumbe, New Zealand	6.5	-38.015	176.921	238	9	0.1-287.8
198710011442	Whittier Narrows, California	5.9	34.061	-118.135	424	8	12-353

Event ID	Event name	Mag	Latitude	Longitude	No. recs	Max MMI	R_{rup} range (km)
198711240154	Elmore Ranch, California	6.0	33.257	-115.756	129	6	13.2-386.7
198711241315	Superstition Hills, California	6.5	33.07	-115.952	214	7	14-390
198812070741	Spitak, Armenia	6.7	40.919	44.118	294	9	0.2-327.4
198910180004	Loma Prieta, California	6.9	37.11	-121.764	578	8	1.5-386.7
199007160726	Luzon, Philippines	7.7	15.721	121.18	8	8	2.2-108.4
199012130024	Sicily, Italy	5.8	37.286	15.402	256	7.5	20.6-206.7
199204130120	Roermond, Netherlands	5.4	51.15	5.93	2730	7	15.3-399.4
199206281157	Landers, California	7.3	34.19	-116.52	325	9	0.1-396.1
199208190204	Suusamyr, Kyrgyzstan	7.2	42.111	73.588	41	9	3.5-103.4
199210121309	Cairo, Egypt	5.8	29.729	31.158	12	8	22.5-72.8
199210181511	Altrato, Colombia	7.1	7.093	-76.764	23	9	2.6-214.8
199307220457	Colombia	6.0	6.38	-71.206	12	8	23.2-374.8
199401171230	Northridge, California	6.7	34.164	-118.563	980	9	5.2-399.6
199408180113	Mascara, Algeria	5.9	35.48	-0.092	22	7	12.7-66.1
199501162046	Kobe, Japan	6.9	34.58	135.025	32	9	0.5-247.1
199505130847	Kozani-Grevena, Greece	6.6	40.151	21.713	548	8	16.5-308.4
199505271303	Neftegorsk, Russia	7.0	52.604	142.823	63	8	1.1-225.9
199602031114	Lijiang, China	6.6	27.271	100.262	19	9	1.9-107.4
199709260940	Umbria-Marche, Italy	6.0	43.078	12.781	877	9	1.2-246.2
199804121055	Bovec, Slovenia	5.6	46.271	13.653	28	8.5	7.8-39
199805220448	Aiquile, Bolivia	6.6	-17.783	-65.401	12	8	0.1-69.9
199806271355	Adana-Ceyhan, Turkey	6.3	36.903	35.325	9	8	15.3-30.3
199807090519	Faial Island, Portugal	6.1	38.621	-28.566	31	8	10.4-48.9
199901251819	Armenia, Colombia	6.1	4.44	-75.659	13	9	23.4-318.8
199903281905	Chamoli, India	6.5	30.48	79.4	90	8	9-32.1
199908170001	Kocaeli, Turkey	7.6	40.773	30.003	15	9	1.8-349.5
199909071156	Athens, Greece	6.0	38.119	23.598	31	9	0.4-26
200203251456	Nahrin, Afghanistan	6.1	36.05	69.21	57	7	10.9-25.6

Event ID	Event name	Mag	Latitude	Longitude	No. recs	Max MMI	R_{rup} range (km)
200210311033	Molise, Italy	5.7	41.738	14.852	50	7	5.7-47.9
200305211844	Boumerdes, Algeria	6.8	36.88	3.694	159	9	3.2-354.2
200312260156	Bam, Iran	6.6	28.95	58.268	24	10	0.4-184.3
200402240227	Al Hoceima, Morocco	6.4	35.184	-3.985	24	9	0.1-36.4
200409281715	Parkfield, California	6.0	35.761	-120.307	438	6.3	4.9-321.4
200502220225	Dahuiyeh, Iran	6.4	30.691	56.794	3	5.8	56.6-256.2
200510080350	Kashmir, Pakistan	7.6	34.465	73.584	77	9.1	2.8-395.2
200602222219	Machaze, Mozambique	7.0	-21.259	33.48	10	4.9	132.1-381.4
200603310117	Chalan Chulan, Iran	6.1	33.5	48.78	11	8	20.1-59.4
200605262253	Yogyakarta, Indonesia	6.3	-7.955	110.43	17	8.8	9-253.4
200703250041	Noto Peninsula, Japan	6.7	37.22	136.69	18	6.2	64.2-335.5
200710310304	Milpitas, California	5.6	37.432	-121.776	433	6.2	9.9-247.6
200802090712	Baja California, Mexico	5.1	32.419	-115.292	72	5.6	34.1-261.7
200807291842	Chino Hills, California	5.4	33.953	-117.761	690	6.4	15.1-372.8

Appendix 5 – Subduction Zone Macroseismic Data

Individual earthquakes that comprise the subduction-zone macroseismic intensity database. Many of the events where DYFI? data were collected are not indicated in the present list. Most maximum intensity values given to one decimal point are from the online DYFI? system. Note that not all macroseismic data gathered are Modified Mercalli Intensities (MMI). However, in this study we assume equivalence between the various intensity scales used around the world.

Event ID	Event name	Mag	Latitude	Longitude	No. recs	Max MMI	R_{rup} range (km)
196005221911	Concepcion, Chile	9.5	-38.235	-73.047	21	11	12.5-92.9
196403280336	Prince William Sound, Alaska	9.2	61.017	-147.648	106	8	3.6-393.1
196504291528	Puget Sound, Washington	6.5	47.317	-122.333	597	8	65.8-399.2
196702091524	Huila, Colombia	7.2	2.89	-74.801	85	9	45.7-387.6
196707291024	Bucaramanga, Colombia	5.9	6.788	-73.073	51	8	162.3-397.8
197005312023	Peru	7.9	-9.248	-78.841	80	9	66-399.6
197012100434	Peru-Ecuador Border	7.6	-3.989	-80.724	34	9	26.9-326.6
197107090303	Valparaiso, Chile	6.6	-32.536	-71.154	20	9	72.7-379
197410031421	Lima, Peru	8.1	-12.254	-77.524	113	8	33.6-307.2
197608161611	Moro Gulf, Philippines	8.0	6.292	124.089	16	7	56.3-278.9
197703041921	Vrancea, Romania	7.5	45.776	26.702	746	8	80-390.9
197902161008	Peru	7.1	-16.537	-72.553	142	7	56-399.4
197903141107	Petatlan, Mexico	7.5	17.759	-101.222	31	8	17-391.3
197911232340	El Cairo, Colombia	7.2	4.793	-76.19	52	9	108.1-390.6
197912120759	Tumaco, Colombia	8.1	1.603	-79.363	36	9	36-310.3
198303311312	Popayan, Colombia	5.6	2.439	-76.659	7	7	30.3-40.6
198503032247	Valparaiso, Chile	7.9	-33.132	-71.708	27	7.5	36.9-232.1
199003251322	Nicoya Gulf, Costa Rica	7.3	9.941	-84.775	7	8	13.8-71
199005301040	Vrancea, Romania	7.0	45.861	26.64	7	7	89.3-220.4
199111192228	Western Colombia	7.2	4.552	-77.356	8	5	151.7-275.2
199204251806	Petrolia, California	7.2	40.337	-124.088	123	8	10.5-394.4

Event ID	Event name	Mag	Latitude	Longitude	No. recs	Max MMI	R_{rup} range (km)
199212120529	Flores Island, Indonesia	7.7	-8.498	121.832	7	9	39.9-347
199406021817	East Java, Indonesia	7.8	-10.409	112.934	13	5	147.1-191.5
199611121659	Nazca Ridge, Peru	7.7	-14.959	-75.562	3	5	81-302.3
200102281854	Nisqually, Washington	6.8	47.112	-122.603	518	8.1	50-399.5
200106232033	Arequipa, Peru	8.4	-16.385	-73.505	25	8	28.5-378.5
200301220206	Tecoman, Mexico	7.5	18.9	-104.063	72	7	28.9-315.7
200410061440	Honshu, Japan	5.7	35.935	139.938	3	5.4	74.3-102.4
200411150906	Buenaventura, Colombia	7.2	4.691	-77.509	6	7	53.5-326.4
200411222026	West of Invercargill, New Zealand	7.1	-46.7	164.82	1	4.1	274.4-274.4
200412260058	Sumatra-Andaman Islands, Indonesia	9.0	3.287	95.972	4	9.1	19.4-324.9
200503281609	Nias, Sumatra	8.6	2.069	97.097	10	9.1	40-350.4
200504102222	Honshu, Japan	5.9	35.6	140.4	7	3.7	74.9-125.7
200507230734	Honshu, Japan	5.9	35.52	139.97	11	5.7	73.4-93.4
200601081134	Kythira, Greece	6.7	36.3	23.34	241	7.5	70.6-394.7
200606112001	Kyushu, Japan	6.4	33.13	131.15	6	5.6	150.4-325.8
200610151707	Kiholo Bay, Hawaii	6.7	19.878	-155.935	71	8.3	41.4-300.7
200704201937	Ryukyu Islands, Japan	5.7	27.471	128.379	6	3.7	139.9-161.1
200708152340	Pisco, Peru	8	-13.358	-76.522	45	8.9	30.9-381.1
200711141540	Tocopilla, Chile	7.7	-22.247	-69.89	14	7	30-235.3

Appendix 6 – Stable Continent Macroseismic Data

Individual earthquakes that comprise the stable continental region macroseismic intensity database. Many of the events where DYFI? data were collected are not indicated in the present list. Most maximum intensity values given to one decimal point are from the online DYFI? system. Note that not all macroseismic data gathered are Modified Mercalli Intensities (MMI). However, in this study we assume equivalence between the various intensity scales used around the world.

Event ID	Event name	Mag	Latitude	Longitude	No. recs	Max MMI	R_{rup} range (km)
196712102251	Koyna, India	6.3	17.39	73.774	11	8	4.8-64
196810140258	Meckering, Australia	6.5	-31.523	116.978	124	8	2.2-397.5
197003101715	Calingiri, Australia	5.5	-31.093	116.513	146	6	3.8-300.7
197303091909	Picton, Australia	5.5	-34.023	150.11	245	6.5	29.1-376.6
197404032305	Mt. Carmel, Illinois	4.7	38.592	-88.094	1314	6	11.4-399.4
197603250041	Lepanto, Arkansas	5.0	35.637	-90.327	701	6	15.4-398.9
197809030508	Swabian Jura, Germany	5.2	48.261	8.978	569	7.5	15.4-109.6
197906020947	Cadoux, Australia	6.1	-30.822	117.104	166	9	0.3-392.4
198007271852	Sharpsburg, Kentuky	5.0	38.205	-83.943	1138	7	16.6-396.2
198201091253	Miramichi, Canada	5.5	46.988	-66.618	226	6	86.9-398.9
198201210033	Faulkner County, Arkansas	4.7	35.17	-92.208	105	6	2.4-257.7
198206280957	Bad Marienberg, Germany	4.8	50.733	7.804	295	5.5	10.1-202.4
198310071018	Goodnow, New York	4.9	43.953	-74.342	2353	6	10.2-398.9
198311080049	Liege, Belgium	4.9	50.63	5.5	545	7	4.3-232.6
198801220035	Tennant Creek #1, Australia	6.2	-19.866	133.795	35	7	38.6-394.5
198801221204	Tennant Creek #3, Australia	6.6	-19.896	133.854	7	6	71.3-331.2
198811252346	Saguenay, Canada	5.8	48.061	-71.277	879	8	31.1-399.4
198905280255	Mt Olga, Australia	5.8	-25.139	130.755	14	7	30.8-275.9
198912272326	Newcastle, Australia	5.4	-32.952	151.61	118	8	10.6-348.8
199001170638	Meckering, Australia	4.2	-31.654	117.067	68	6	3.6-249.2
199309292225	Latur-Killari, India	6.2	18.06	76.478	45	8	14.2-37.3

Event ID	Event name	Mag	Latitude	Longitude	No. recs	Max MMI	R_{rup} range (km)
199408061103	Ellalong, Australia	4.7	-32.917	151.292	208	7.5	1.9-327.1
199609250453	Thomson Reservoir, Australia	4.5	-37.863	146.422	83	6	12.7-207.7
199703050615	Burra, Australia	4.8	-33.768	138.931	203	6	20-292.1
199708100920	Collier Bay, Australia	6.2	-16.159	124.333	37	7	71.6-399.8
200008291205	Boolarra, Australia	4.2	-38.402	146.245	357	5	15.2-198.7
200101260316	Bhuj, India	7.6	23.402	70.287	98	9	15.2-263.7
200204201050	Au Sable Forks, New York	5.1	44.487	-73.718	1541	6.1	97.2-399.9
200302222041	Saint Die, France	5.0	48.317	6.626	1098	6	9.7-166
200804180937	Mt. Carmel, Illinois	5.2	38.45	-87.89	673	6.3	12.3-399.4
200804181514	Mt. Carmel, Illinois (Aftershock)	4.6	38.483	-87.891	39	4.4	53.4-245.5
200804210538	Mt. Carmel, Illinois (Aftershock)	4.0	38.483	-87.857	257	4.6	12.2-383.7

Appendix 7 – Active Crustal GMPE Magnitude Dependence for PGA

The transition of PGA residuals with magnitude for candidate GMPEs for active crustal regions. Each plot shows the transition of the median residuals in 0.5 magnitude windows. The magnitude window is indicated on the top-left plot in each case.

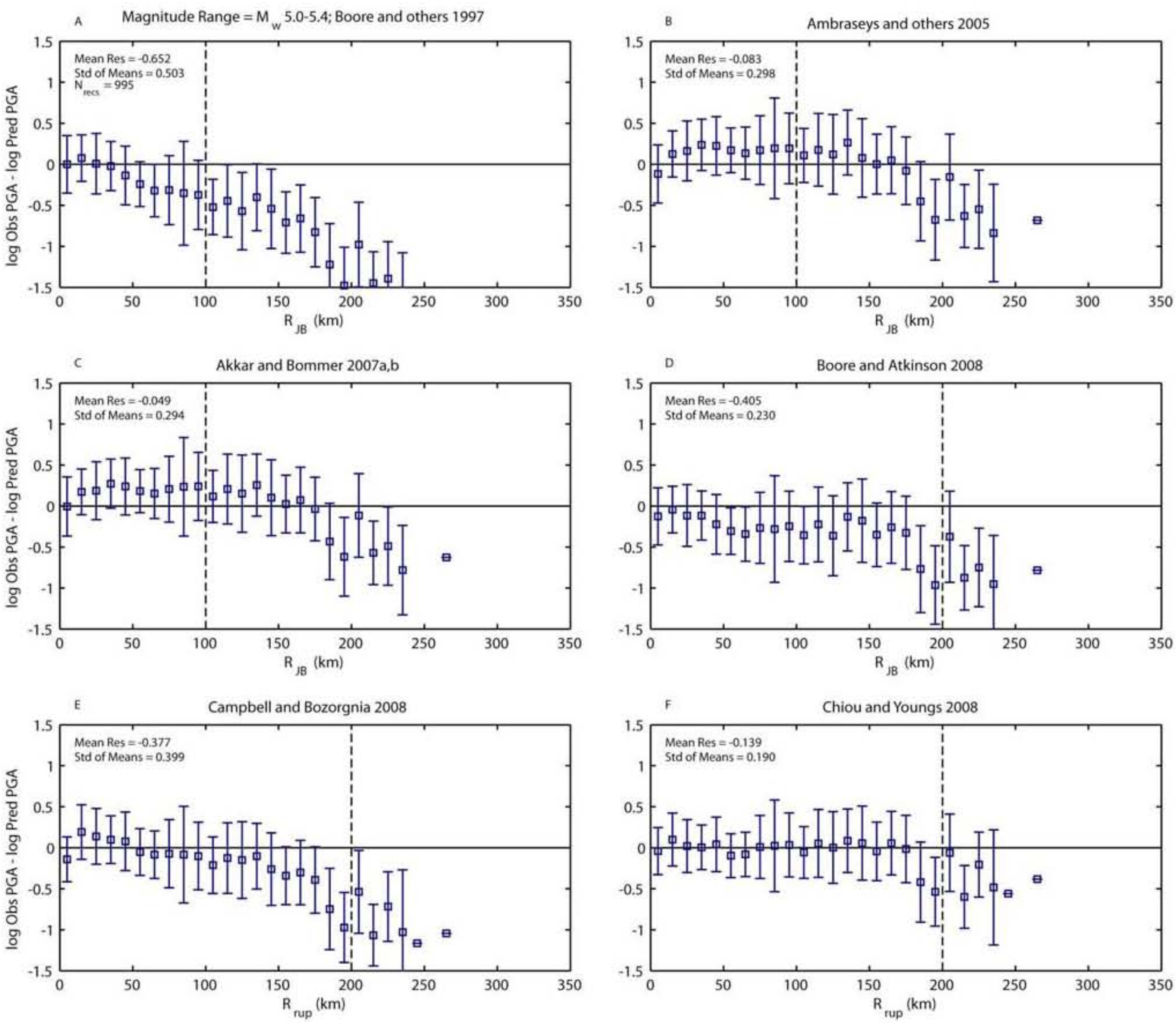

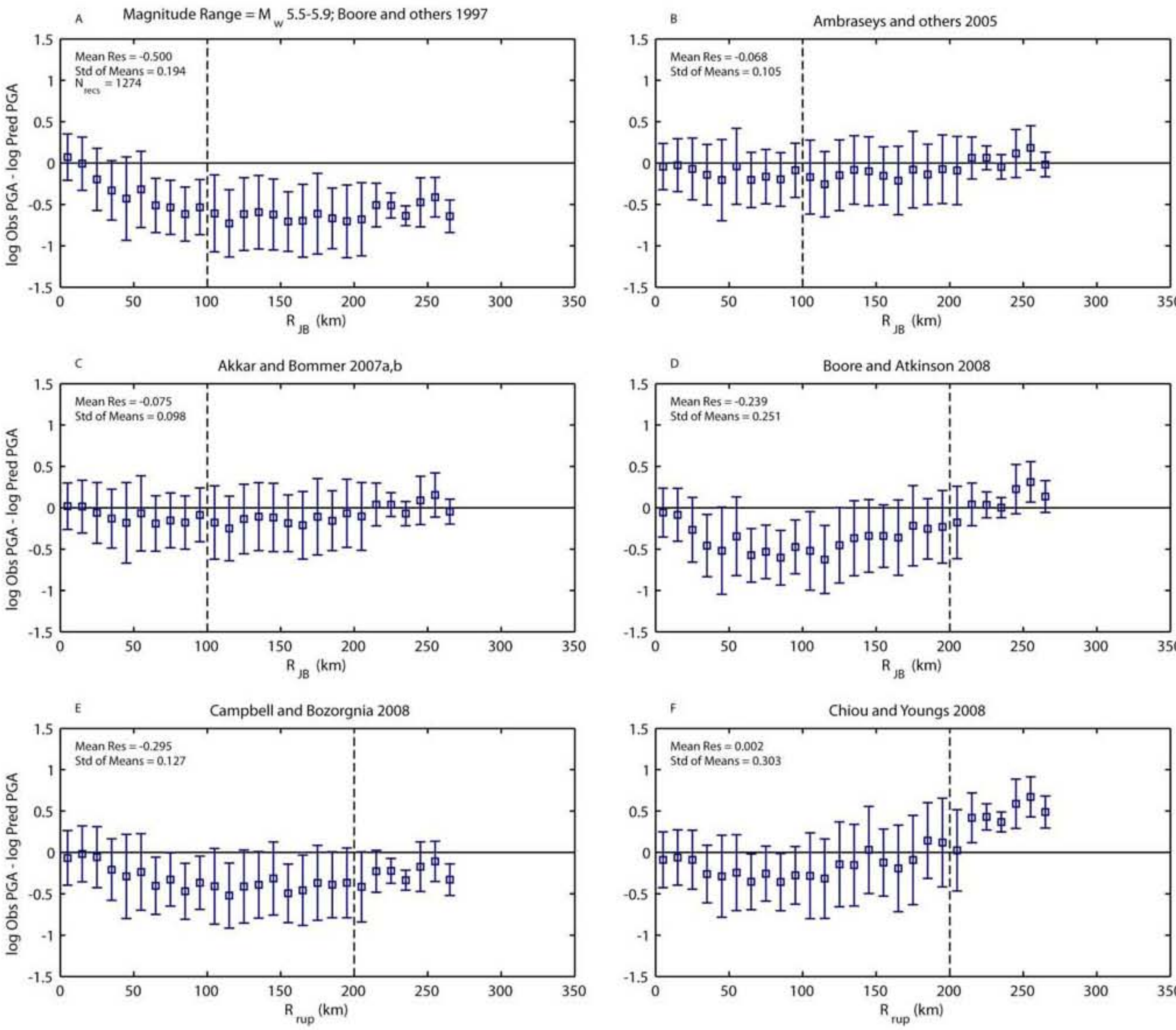
A
Magnitude Range = M w 5.5-5.9; Boore and others 1997
Mean Res = -0.500
Std of Means = 0.194
N recs = 1274
B
Ambraseys and others 2005
Mean Res = -0.068
Std of Means = 0.105
C
Akkar and Bommer 2007a,b
Mean Res = -0.075
Std of Means = 0.098
D
Boore and Atkinson 2008
Mean Res = -0.239
Std of Means = 0.251
E
Campbell and Bozorgnia 2008
Mean Res = -0.295
Std of Means = 0.127
F
Chiou and Youngs 2008
Mean Res = 0.002
Std of Means = 0.303
log Obs PGA - log Pred PGA
R JB (km)
R rup (km)

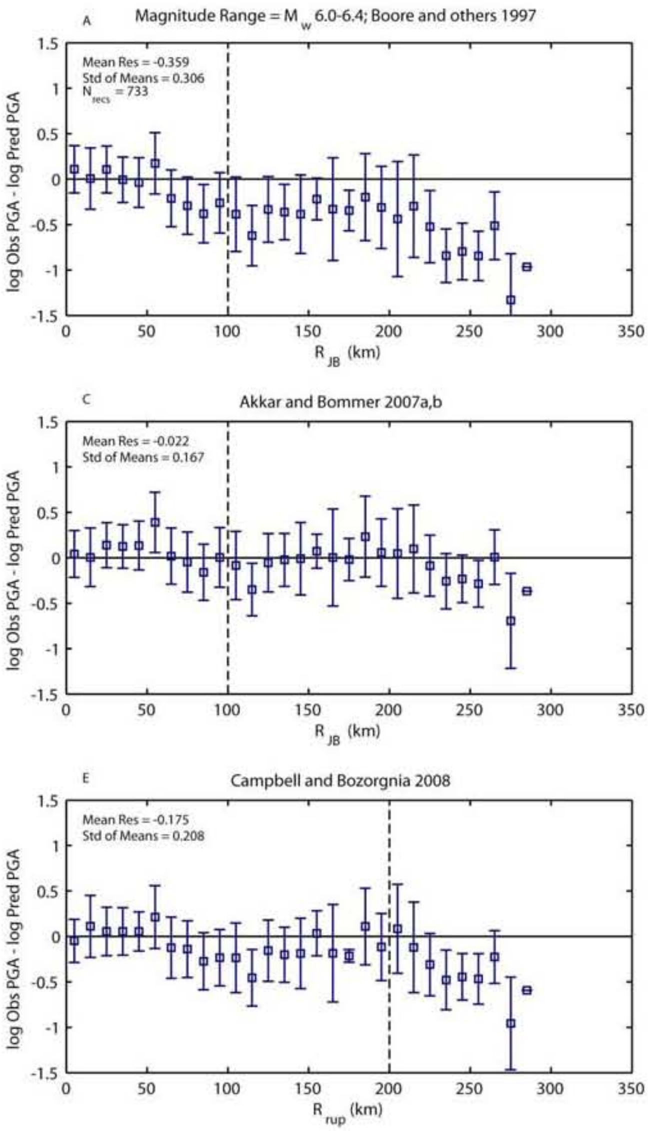
A
Magnitude Range = M_w 6.0-6.4; Boore and others 1997
Mean Res = -0.359
Std of Means = 0.306
N_{recs} = 733
B
Ambraseys and others 2005
Mean Res = 0.017
Std of Means = 0.157
C
Akkar and Bommer 2007a,b
Mean Res = -0.022
Std of Means = 0.167
D
Boore and Atkinson 2008
Mean Res = -0.009
Std of Means = 0.194
E
Campbell and Bozorgnia 2008
Mean Res = -0.175
Std of Means = 0.208
F
Chiou and Youngs 2008
Mean Res = 0.015
Std of Means = 0.158
log Obs PGA - log Pred PGA
R_{JB} (km)
R_{rup} (km)

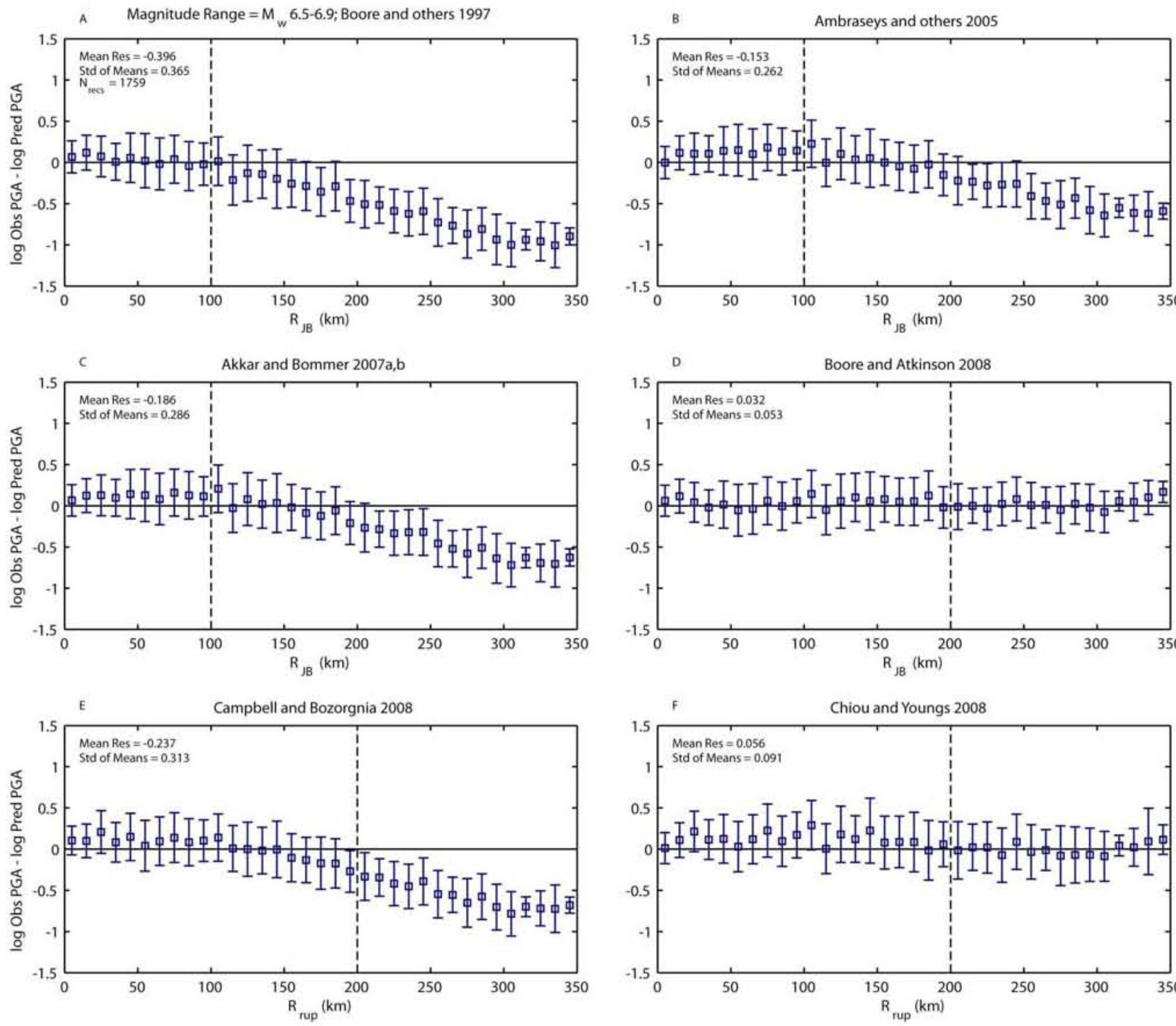

A
Magnitude Range = M w 6.5-6.9; Boore and others 1997
Mean Res = -0.396
Std of Means = 0.365
N recs = 1759
log Obs PGA - log Pred PGA
R JB (km)
B
Ambraseys and others 2005
Mean Res = -0.153
Std of Means = 0.262
R JB (km)
C
Akkar and Bommer 2007a,b
Mean Res = -0.186
Std of Means = 0.286
log Obs PGA - log Pred PGA
R JB (km)
D
Boore and Atkinson 2008
Mean Res = 0.032
Std of Means = 0.053
R JB (km)
E
Campbell and Bozorgnia 2008
Mean Res = -0.237
Std of Means = 0.313
log Obs PGA - log Pred PGA
R rup (km)
F
Chiou and Youngs 2008
Mean Res = 0.056
Std of Means = 0.091
R rup (km)

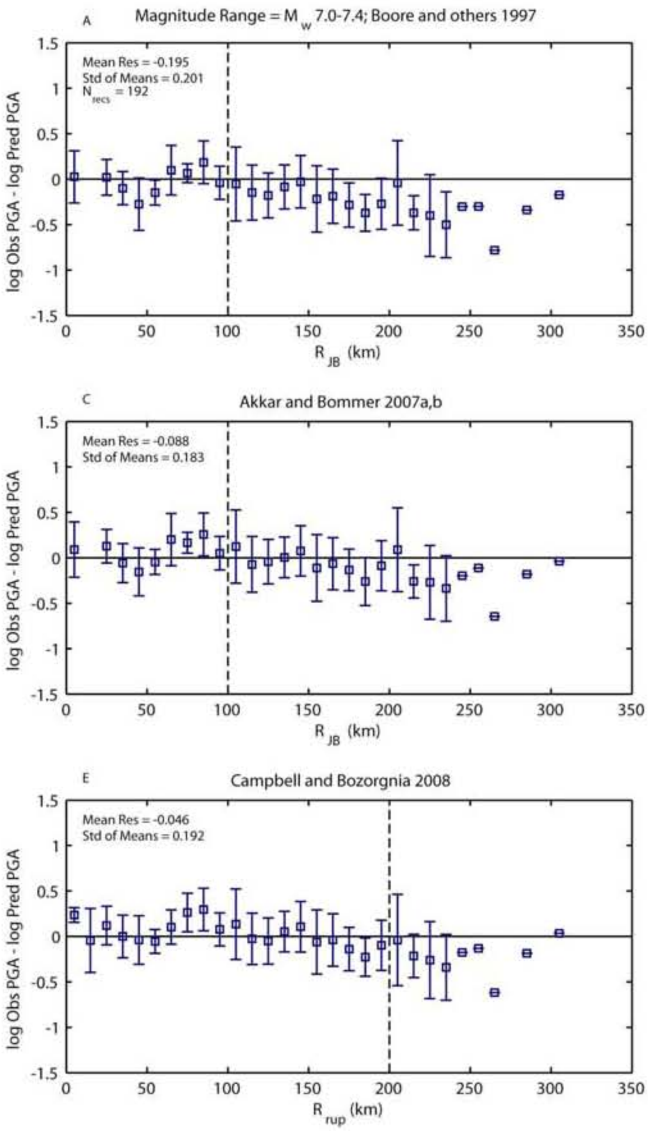

A
Magnitude Range = M w 7.0-7.4; Boore and others 1997
Mean Res = -0.195
Std of Means = 0.201
N recs = 192
B
Ambraseys and others 2005
Mean Res = -0.119
Std of Means = 0.170
C
Akkar and Bommer 2007a,b
Mean Res = -0.088
Std of Means = 0.183
D
Boore and Atkinson 2008
Mean Res = 0.101
Std of Means = 0.213
E
Campbell and Bozorgnia 2008
Mean Res = -0.046
Std of Means = 0.192
F
Chiou and Youngs 2008
Mean Res = 0.078
Std of Means = 0.195
log Obs PGA - log Pred PGA
R JB (km)
R rup (km)

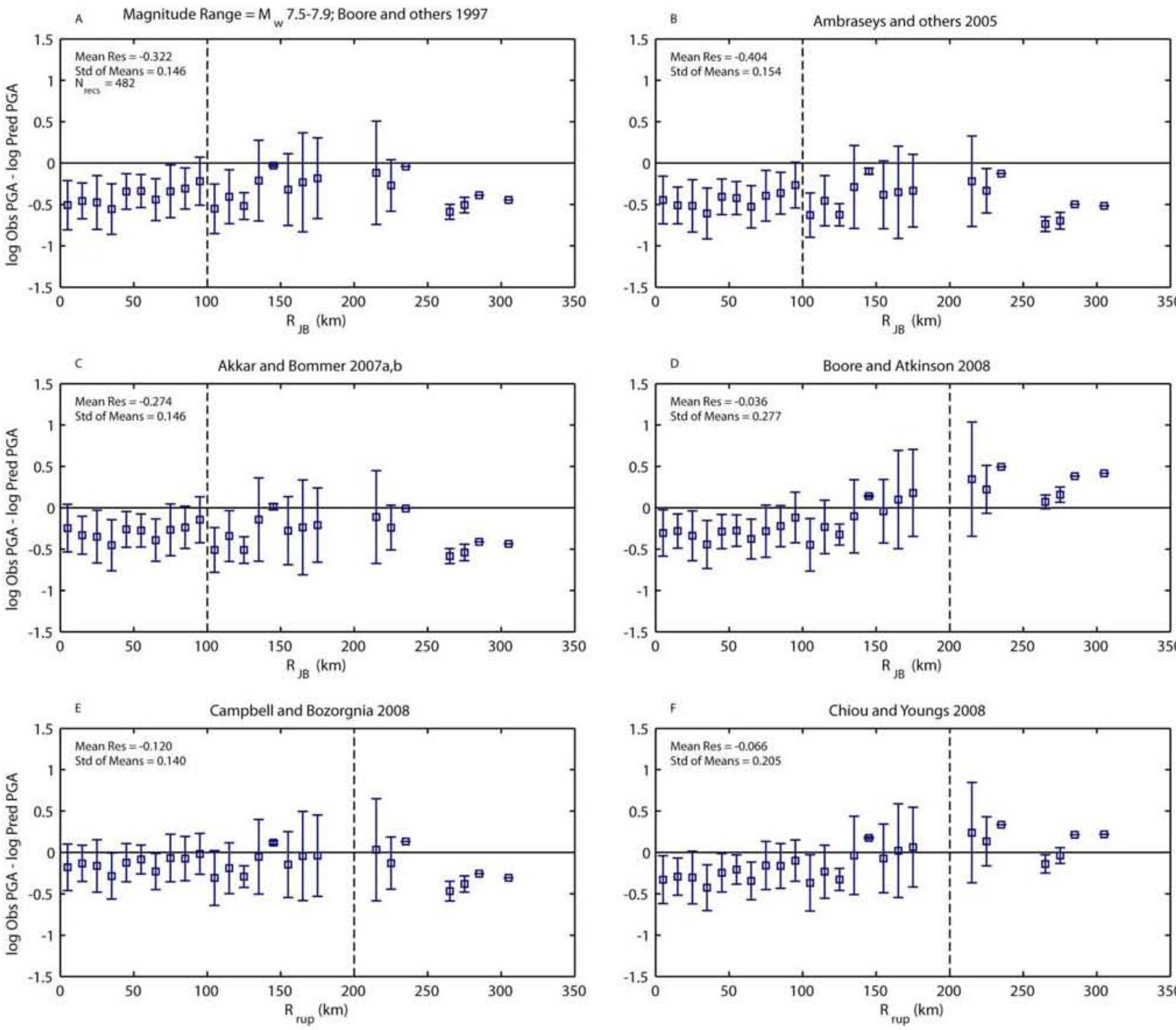
A
Magnitude Range = M w 7.5-7.9; Boore and others 1997
Mean Res = -0.322
Std of Means = 0.146
N recs = 482
log Obs PGA - log Pred PGA
R JB (km)
B
Ambraseys and others 2005
Mean Res = -0.404
Std of Means = 0.154
R JB (km)
C
Akkar and Bommer 2007a,b
Mean Res = -0.274
Std of Means = 0.146
log Obs PGA - log Pred PGA
R JB (km)
D
Boore and Atkinson 2008
Mean Res = -0.036
Std of Means = 0.277
R JB (km)
E
Campbell and Bozorgnia 2008
Mean Res = -0.120
Std of Means = 0.140
log Obs PGA - log Pred PGA
R rup (km)
F
Chiou and Youngs 2008
Mean Res = -0.066
Std of Means = 0.205
R rup (km)

Appendix 8 – Active Crustal GMPE Magnitude Dependence for PGV

The transition of PGV residuals with magnitude for candidate GMPEs for active crustal regions. Each plot shows the transition of the median residuals in 0.5 magnitude windows. The magnitude window is indicated on the top-left plot in each case.

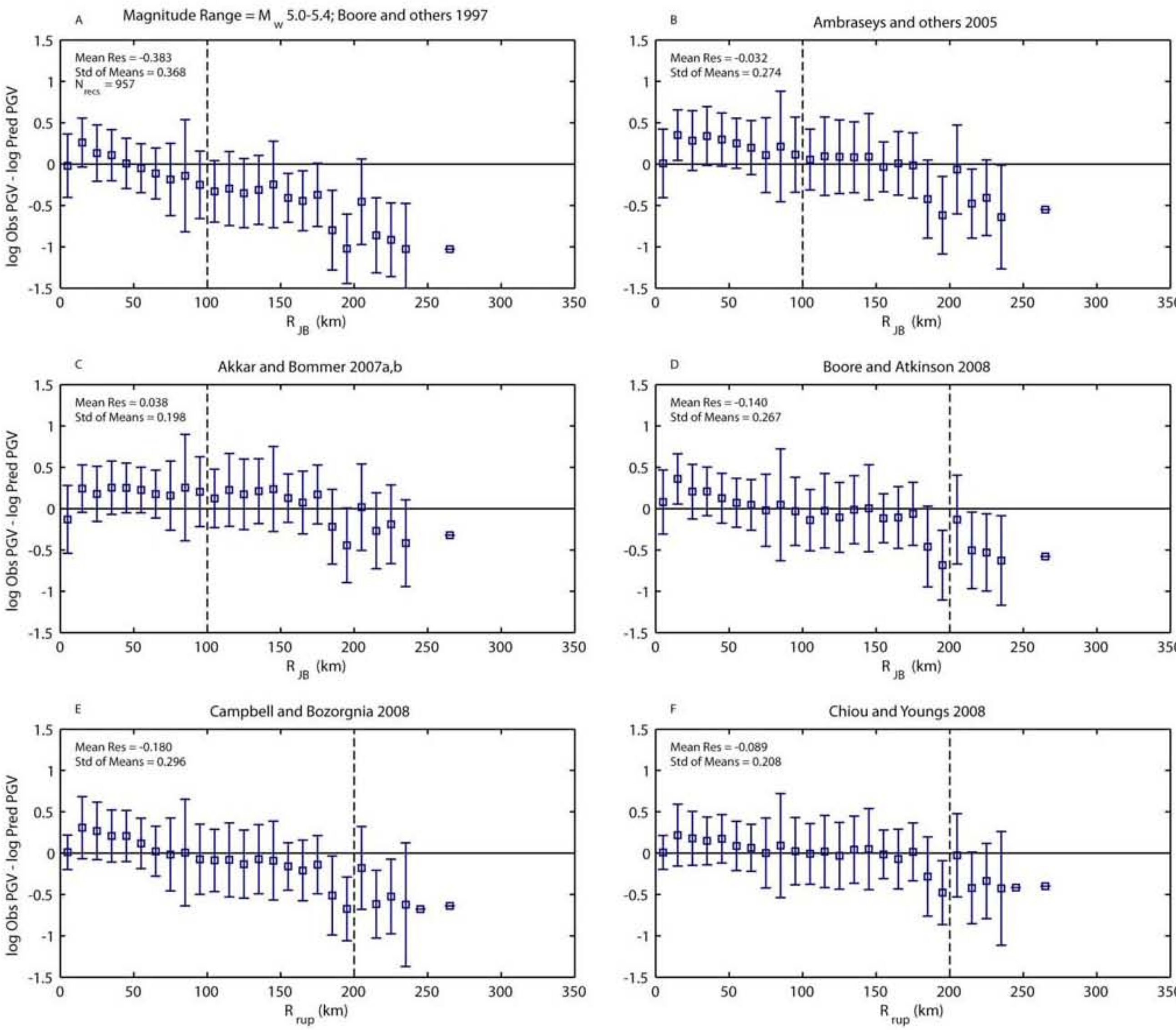

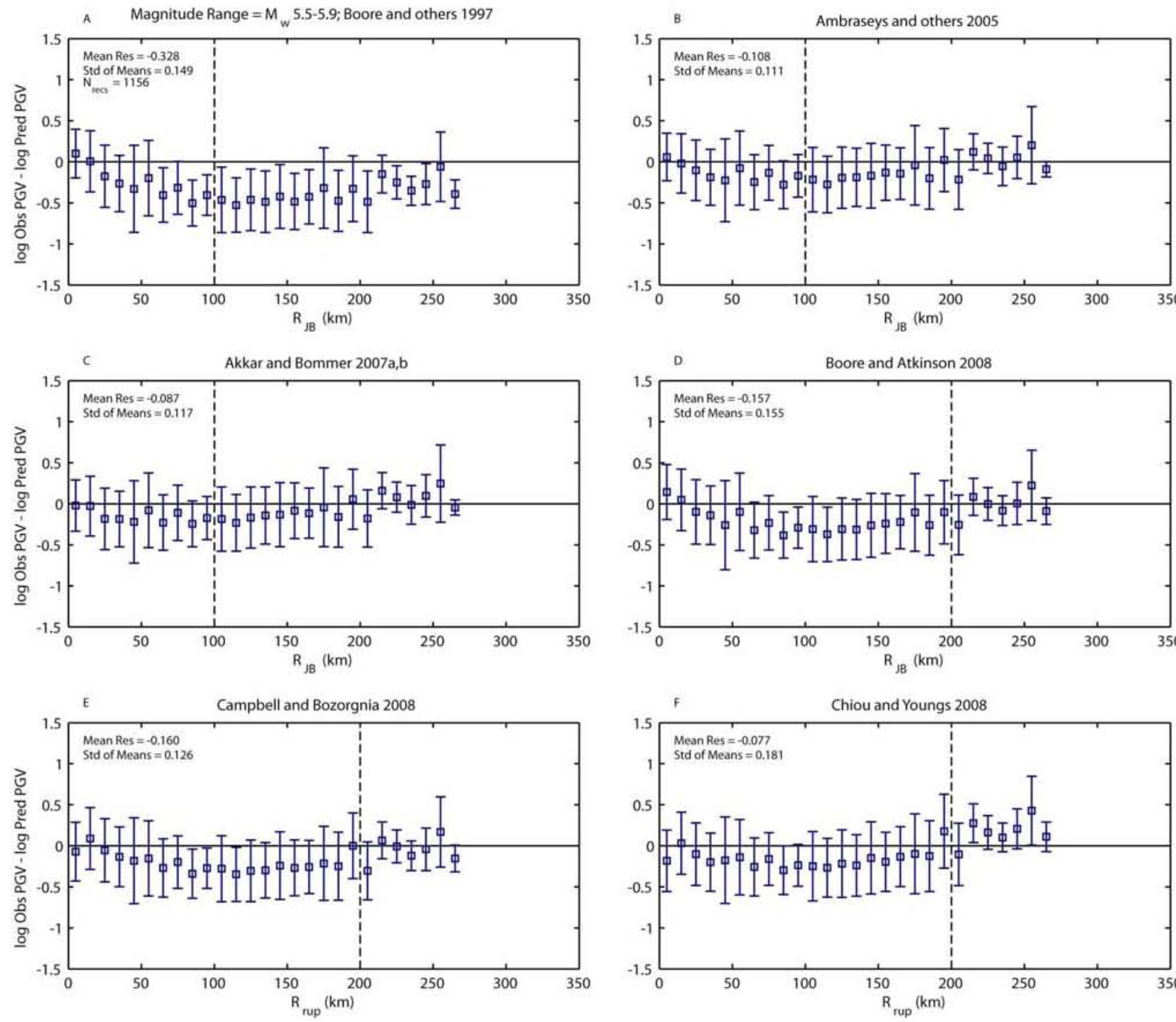

A
Magnitude Range = M_w 5.5-5.9; Boore and others 1997
Mean Res = -0.328
Std of Means = 0.149
N_{recs} = 1156
B
Ambraseys and others 2005
Mean Res = -0.108
Std of Means = 0.111
C
Akkar and Bommer 2007a,b
Mean Res = -0.087
Std of Means = 0.117
D
Boore and Atkinson 2008
Mean Res = -0.157
Std of Means = 0.155
E
Campbell and Bozorgnia 2008
Mean Res = -0.160
Std of Means = 0.126
F
Chiou and Youngs 2008
Mean Res = -0.077
Std of Means = 0.181
log Obs PGV - log Pred PGV
R_{JB} (km)
R_{rup} (km)

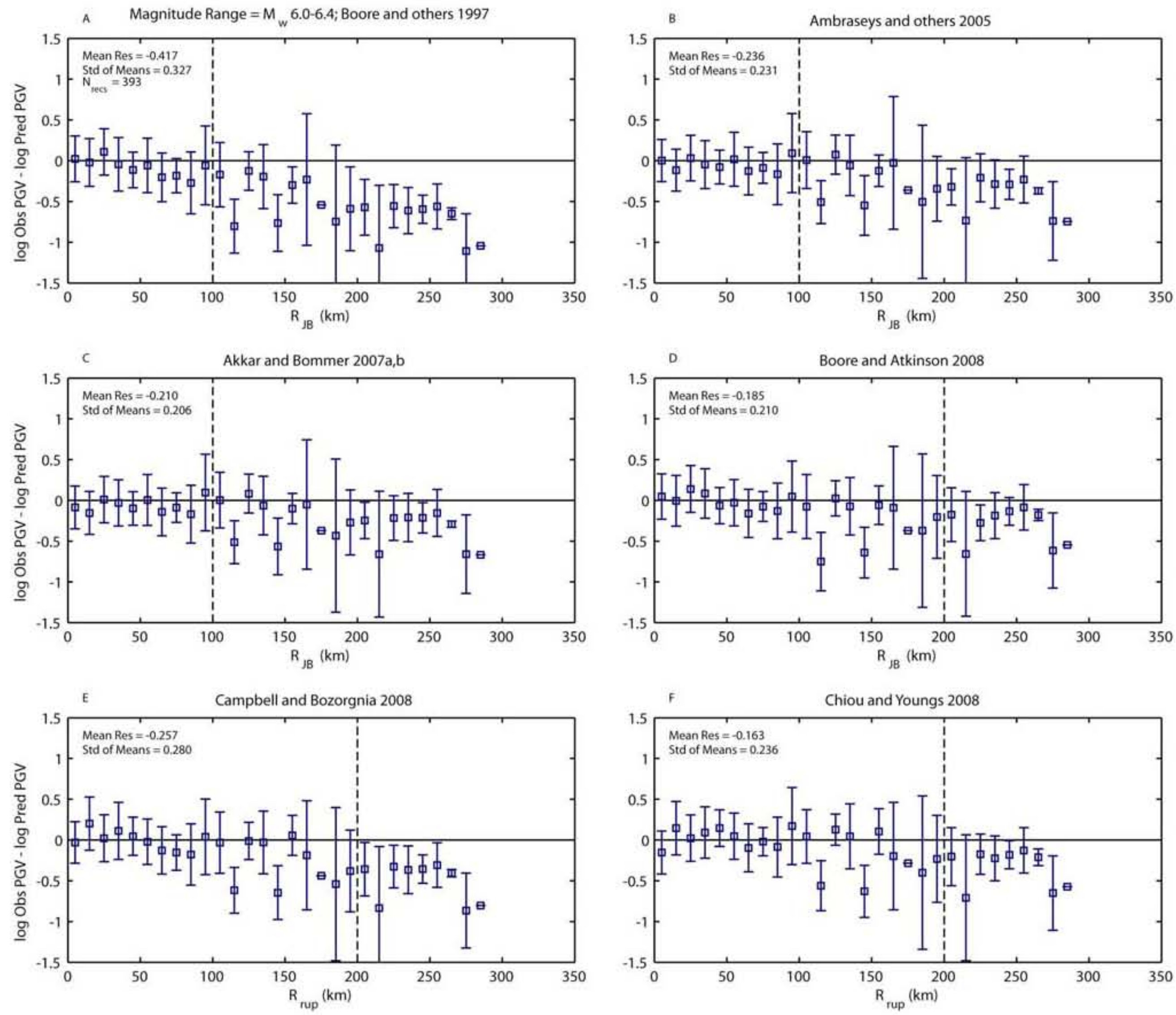
A
Magnitude Range = M w 6.0-6.4; Boore and others 1997
Mean Res = -0.417
Std of Means = 0.327
N recs = 393
B
Ambraseys and others 2005
Mean Res = -0.236
Std of Means = 0.231
C
Akkar and Bommer 2007a,b
Mean Res = -0.210
Std of Means = 0.206
D
Boore and Atkinson 2008
Mean Res = -0.185
Std of Means = 0.210
E
Campbell and Bozorgnia 2008
Mean Res = -0.257
Std of Means = 0.280
F
Chiou and Youngs 2008
Mean Res = -0.163
Std of Means = 0.236
log Obs PGV - log Pred PGV
R JB (km)
R rup (km)

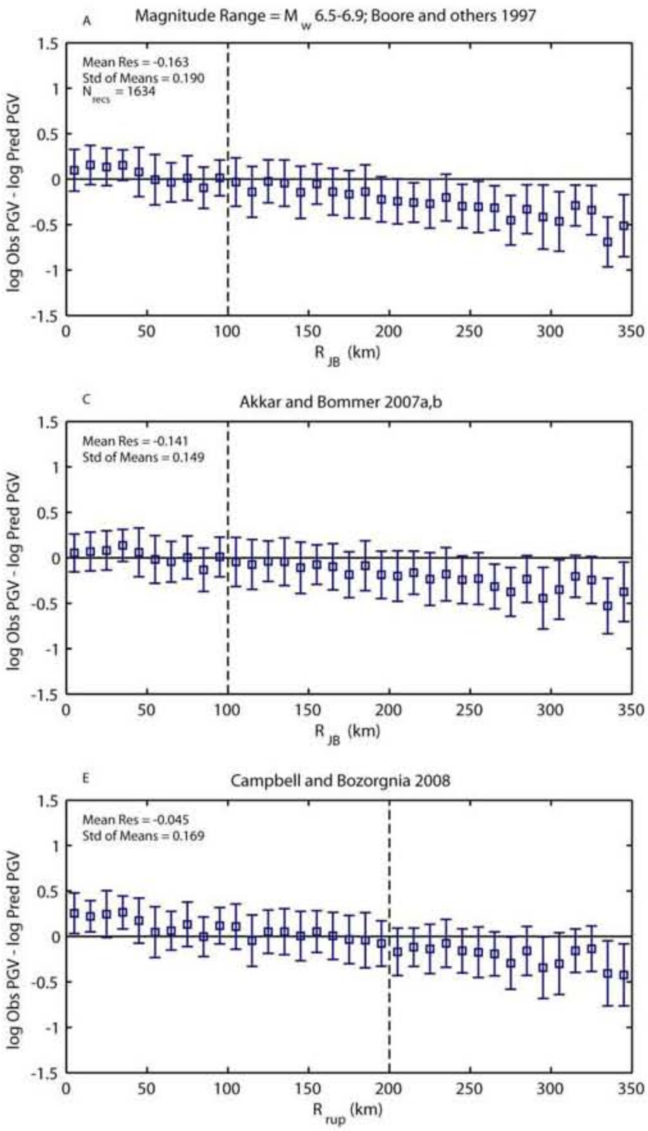
A
Magnitude Range = M_w 6.5-6.9; Boore and others 1997
Mean Res = -0.163
Std of Means = 0.190
N_{recs} = 1634
log Obs PGV - log Pred PGV
R_{JB} (km)
B
Ambraseys and others 2005
Mean Res = -0.068
Std of Means = 0.112
R_{JB} (km)
C
Akkar and Bommer 2007a,b
Mean Res = -0.141
Std of Means = 0.149
log Obs PGV - log Pred PGV
R_{JB} (km)
D
Boore and Atkinson 2008
Mean Res = -0.027
Std of Means = 0.102
R_{JB} (km)
E
Campbell and Bozorgnia 2008
Mean Res = -0.045
Std of Means = 0.169
log Obs PGV - log Pred PGV
R_{rup} (km)
F
Chiou and Youngs 2008
Mean Res = 0.063
Std of Means = 0.109
R_{rup} (km)

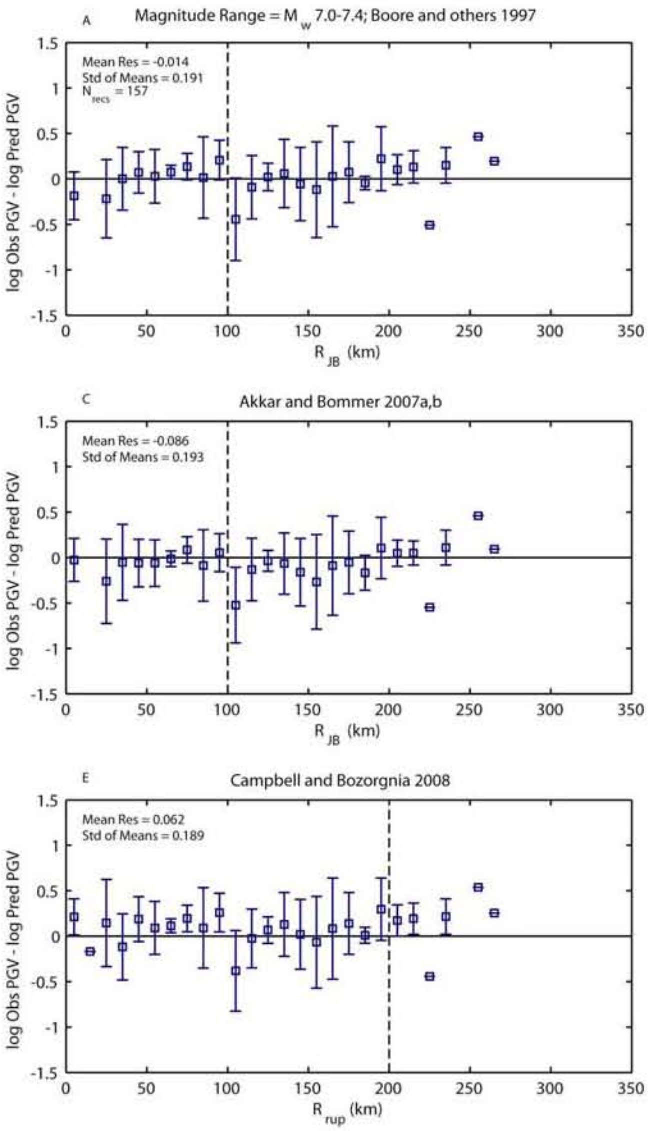

A
Magnitude Range = M w 7.0-7.4; Boore and others 1997
Mean Res = -0.014
Std of Means = 0.191
N recs = 157
B
Ambraseys and others 2005
Mean Res = -0.088
Std of Means = 0.220
C
Akkar and Bommer 2007a,b
Mean Res = -0.086
Std of Means = 0.193
D
Boore and Atkinson 2008
Mean Res = 0.040
Std of Means = 0.211
E
Campbell and Bozorgnia 2008
Mean Res = 0.062
Std of Means = 0.189
F
Chiou and Youngs 2008
Mean Res = 0.188
Std of Means = 0.209
log Obs PGV - log Pred PGV
R JB (km)
R rup (km)

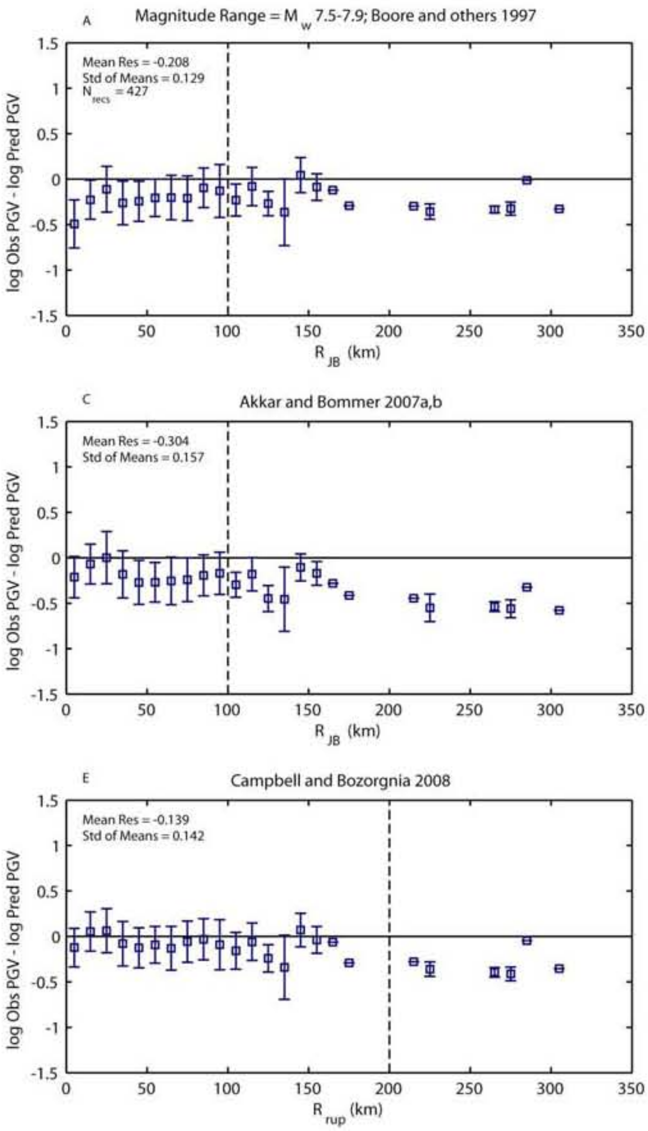

A
Magnitude Range = M w 7.5-7.9; Boore and others 1997
Mean Res = -0.208
Std of Means = 0.129
N recs = 427
B
Ambraseys and others 2005
Mean Res = -0.406
Std of Means = 0.123
C
Akkar and Bommer 2007a,b
Mean Res = -0.304
Std of Means = 0.157
D
Boore and Atkinson 2008
Mean Res = -0.118
Std of Means = 0.110
E
Campbell and Bozorgnia 2008
Mean Res = -0.139
Std of Means = 0.142
F
Chiou and Youngs 2008
Mean Res = 0.011
Std of Means = 0.113
log Obs PGV - log Pred PGV
R JB (km)
R rup (km)

Appendix 9 – Magnitude Dependence of the Abrahamson and Silva (2008) GMPE

The transition of PGA and PGV residuals with magnitude for the Abrahamson and Silva (2008) GMPE for active crustal regions. Each plot shows the transition of the median residuals in 0.5 magnitude windows. The magnitude window is indicated for each plot.

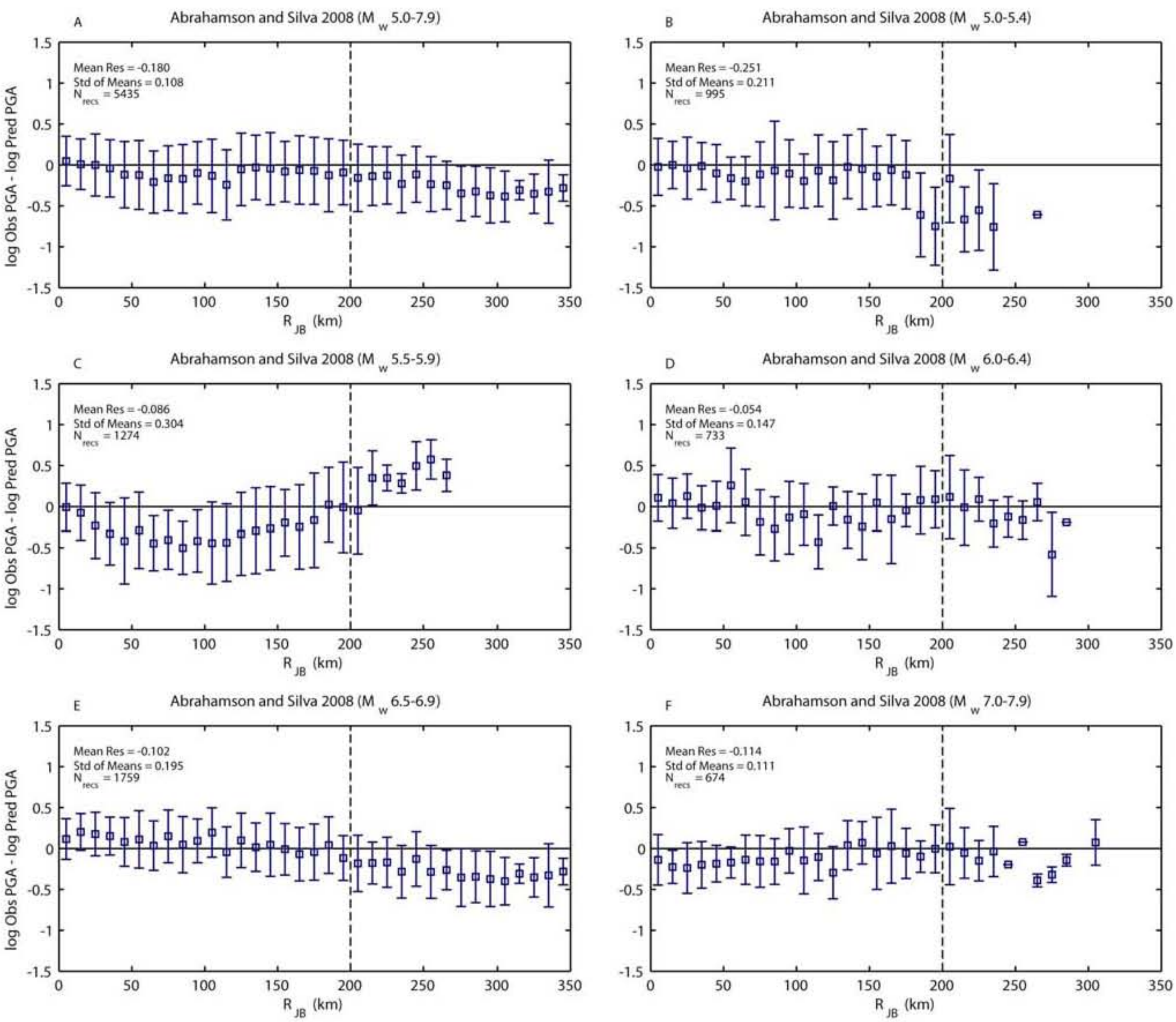

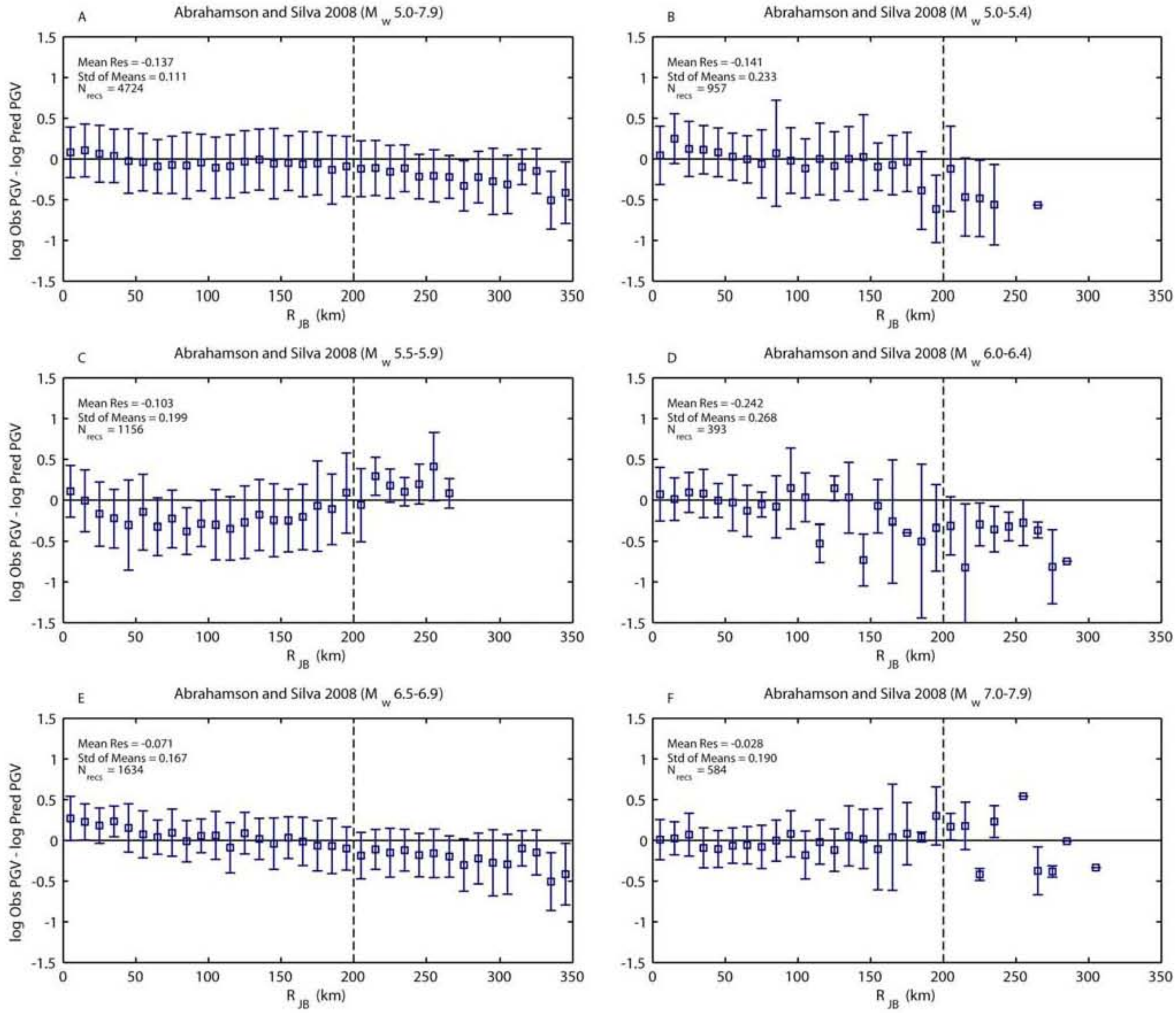
A
Abrahamson and Silva 2008 (M w 5.0-7.9)
Mean Res = -0.137
Std of Means = 0.111
N recs = 4724
B
Abrahamson and Silva 2008 (M w 5.0-5.4)
Mean Res = -0.141
Std of Means = 0.233
N recs = 957
C
Abrahamson and Silva 2008 (M w 5.5-5.9)
Mean Res = -0.103
Std of Means = 0.199
N recs = 1156
D
Abrahamson and Silva 2008 (M w 6.0-6.4)
Mean Res = -0.242
Std of Means = 0.268
N recs = 393
E
Abrahamson and Silva 2008 (M w 6.5-6.9)
Mean Res = -0.071
Std of Means = 0.167
N recs = 1634
F
Abrahamson and Silva 2008 (M w 7.0-7.9)
Mean Res = -0.028
Std of Means = 0.190
N recs = 584
log Obs PGV - log Pred PGV
R JB (km)

Appendix 10 – Magnitude Dependence of the Idriss (2008) GMPE

The transition of PGA and PGV residuals with magnitude for the Idriss (2008) GMPE for active crustal regions. PGV is evaluated from 1.0 second spectral acceleration using the approach of Newmark and Hall (1982). Each plot shows the transition of the median residuals in 0.5 magnitude windows. The magnitude window is indicated for each plot.

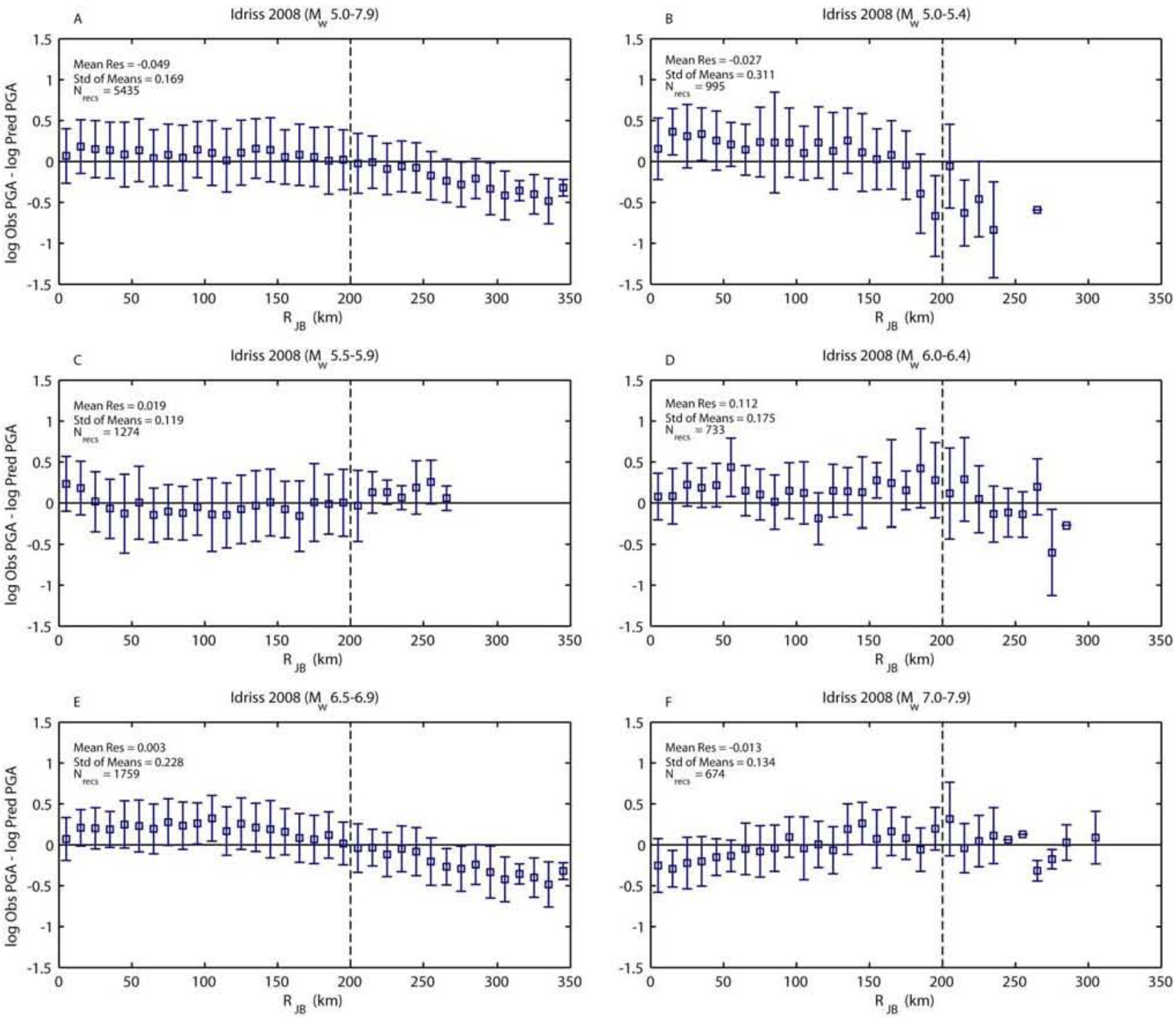

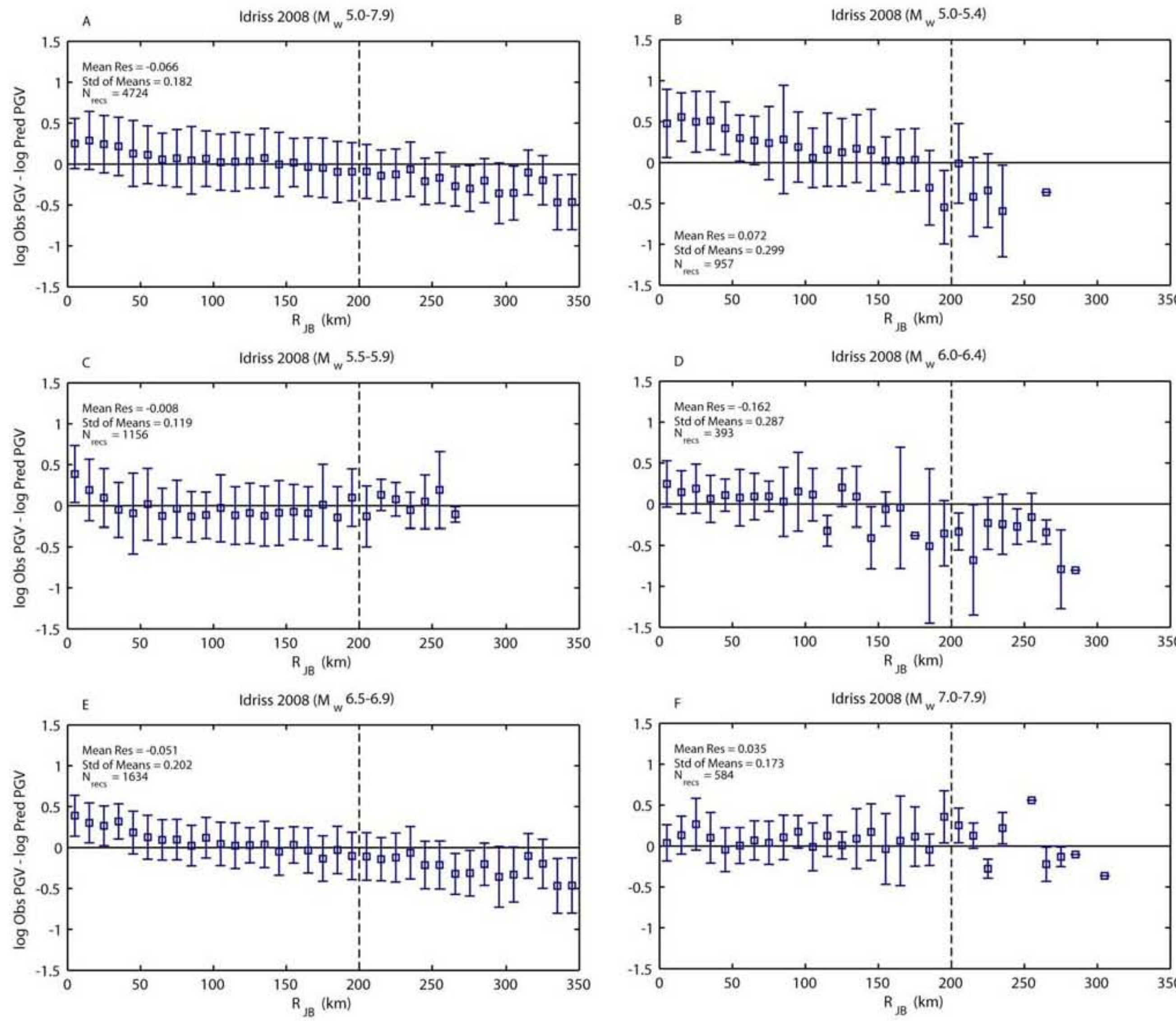
A
Idriss 2008 (M w 5.0-7.9)
Mean Res = -0.066
Std of Means = 0.182
N recs = 4724
B
Idriss 2008 (M w 5.0-5.4)
Mean Res = 0.072
Std of Means = 0.299
N recs = 957
C
Idriss 2008 (M w 5.5-5.9)
Mean Res = -0.008
Std of Means = 0.119
N recs = 1156
D
Idriss 2008 (M w 6.0-6.4)
Mean Res = -0.162
Std of Means = 0.287
N recs = 393
E
Idriss 2008 (M w 6.5-6.9)
Mean Res = -0.051
Std of Means = 0.202
N recs = 1634
F
Idriss 2008 (M w 7.0-7.9)
Mean Res = 0.035
Std of Means = 0.173
N recs = 584
log Obs PGV - log Pred PGV
R JB (km)

Appendix 11 – Magnitude Dependence of the Cua and Heaton GMPE

The transition of PGA and PGV residuals with magnitude for the Cua and Heaton (G. Cua, written commun., 2008). GMPE for active crustal regions. Each plot shows the transition of the median residuals in 0.5 magnitude windows. The magnitude window is indicated for each plot.

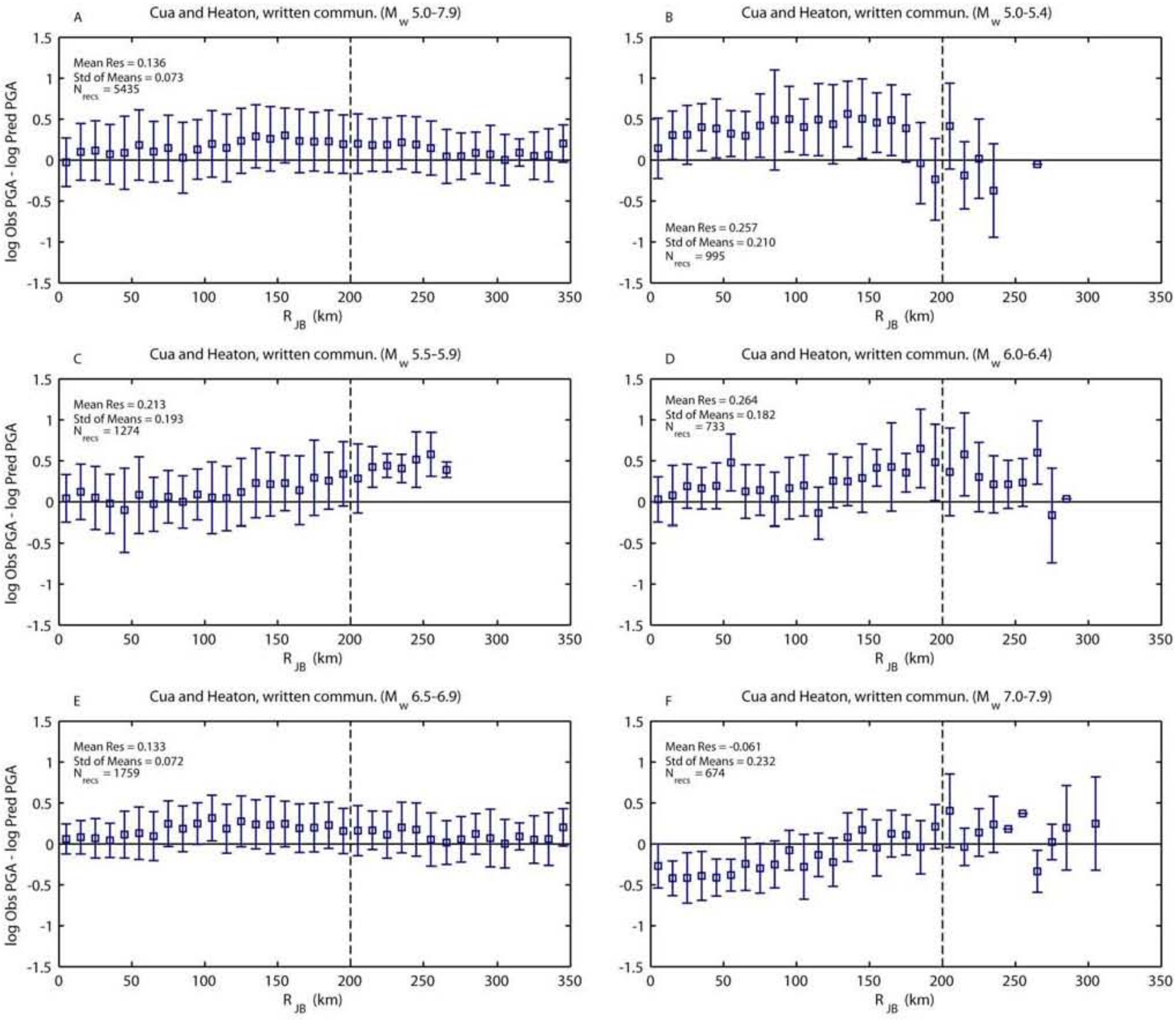

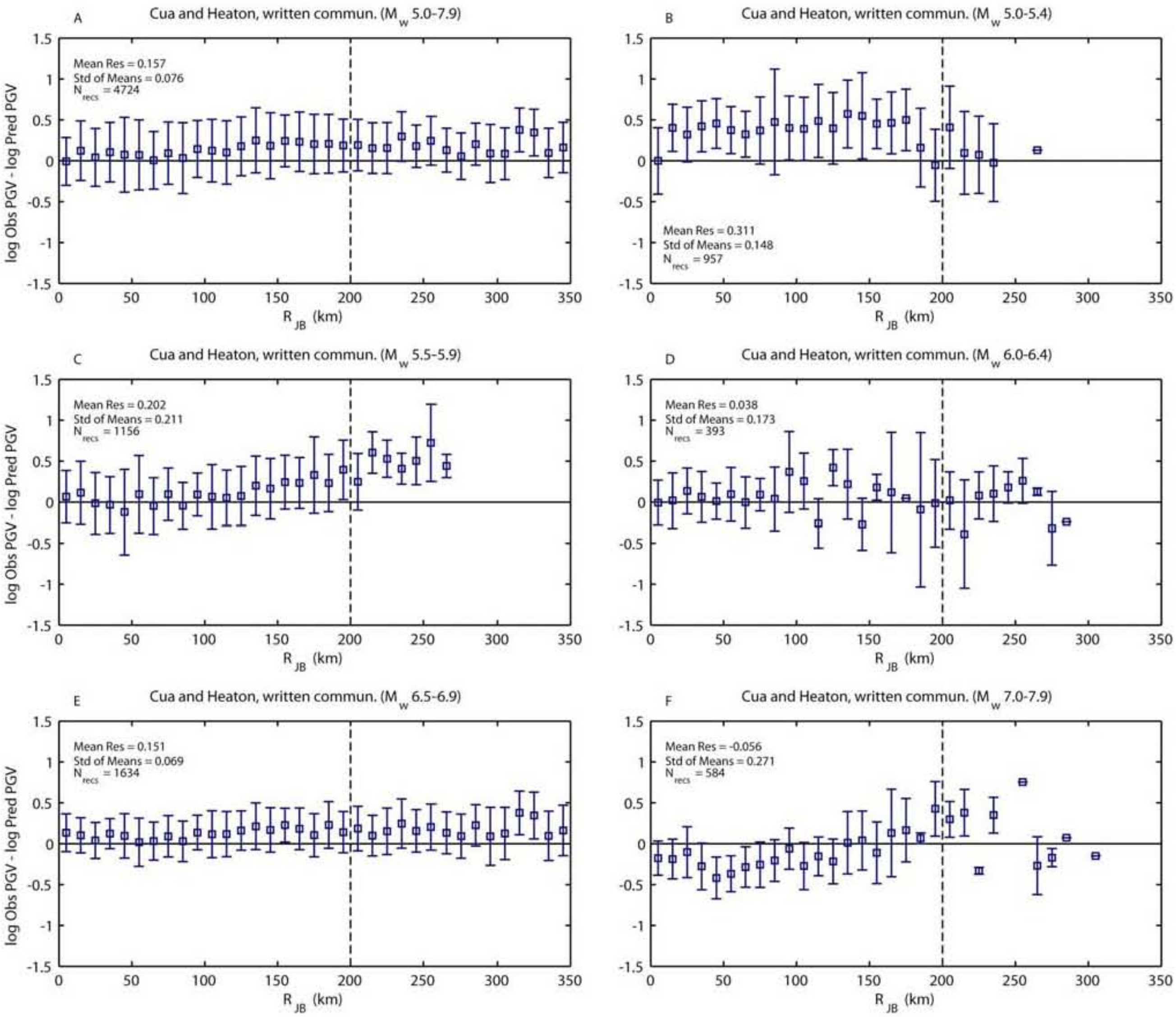
A
Cua and Heaton, written commun. (M w 5.0-7.9)
Mean Res = 0.157
Std of Means = 0.076
N recs = 4724
B
Cua and Heaton, written commun. (M w 5.0-5.4)
Mean Res = 0.311
Std of Means = 0.148
N recs = 957
C
Cua and Heaton, written commun. (M w 5.5-5.9)
Mean Res = 0.202
Std of Means = 0.211
N recs = 1156
D
Cua and Heaton, written commun. (M w 6.0-6.4)
Mean Res = 0.038
Std of Means = 0.173
N recs = 393
E
Cua and Heaton, written commun. (M w 6.5-6.9)
Mean Res = 0.151
Std of Means = 0.069
N recs = 1634
F
Cua and Heaton, written commun. (M w 7.0-7.9)
Mean Res = -0.056
Std of Means = 0.271
N recs = 584
log Obs PGV - log Pred PGV
R JB (km)

Appendix 12 – Subduction Zone GMPE Magnitude Dependence for PGA

The transition of PGA residuals with magnitude for candidate GMPEs for subduction zones. Each plot shows the transition of the median residuals in 0.5 magnitude windows. The magnitude window is indicated on the top-left plot in each case.

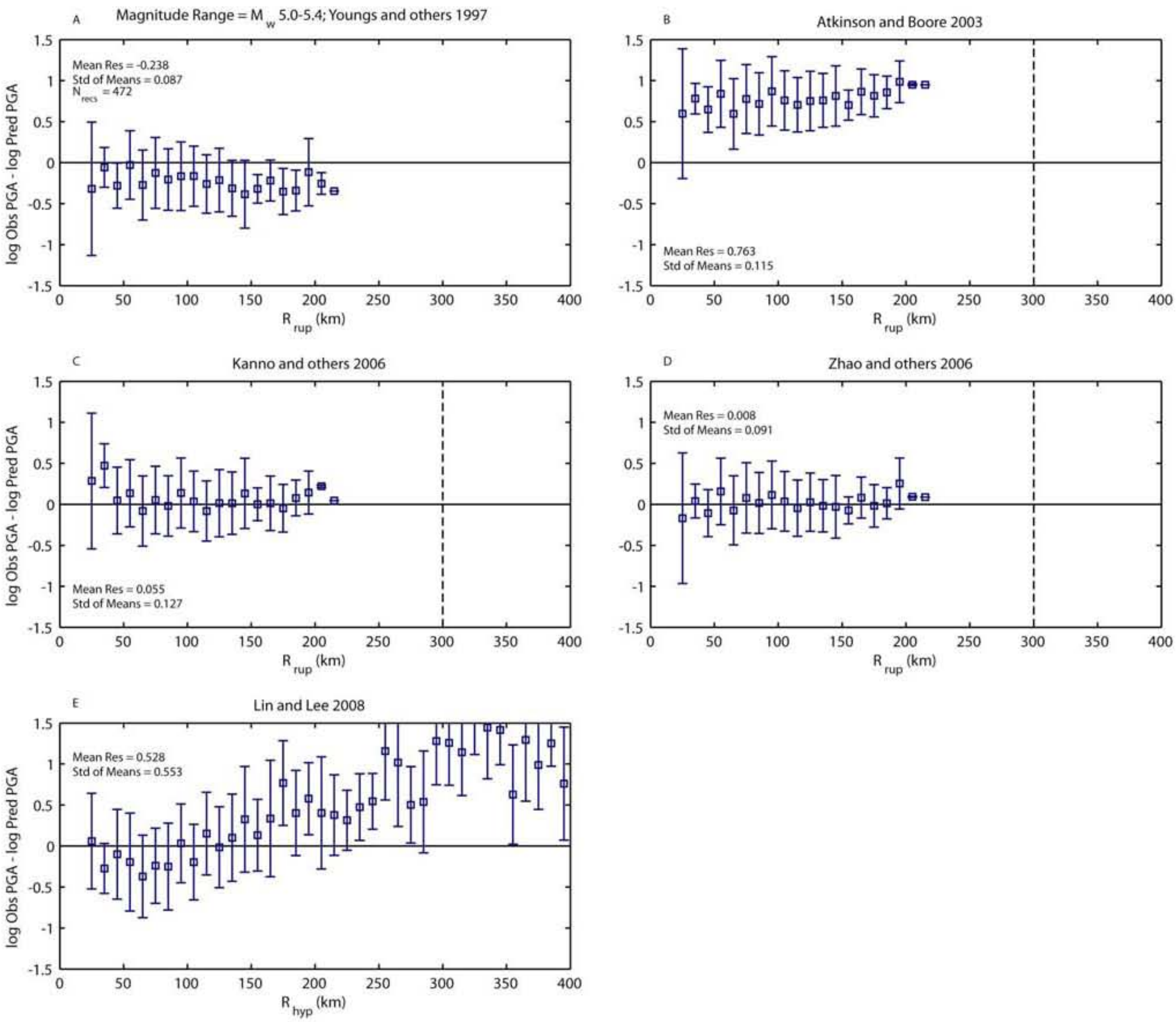

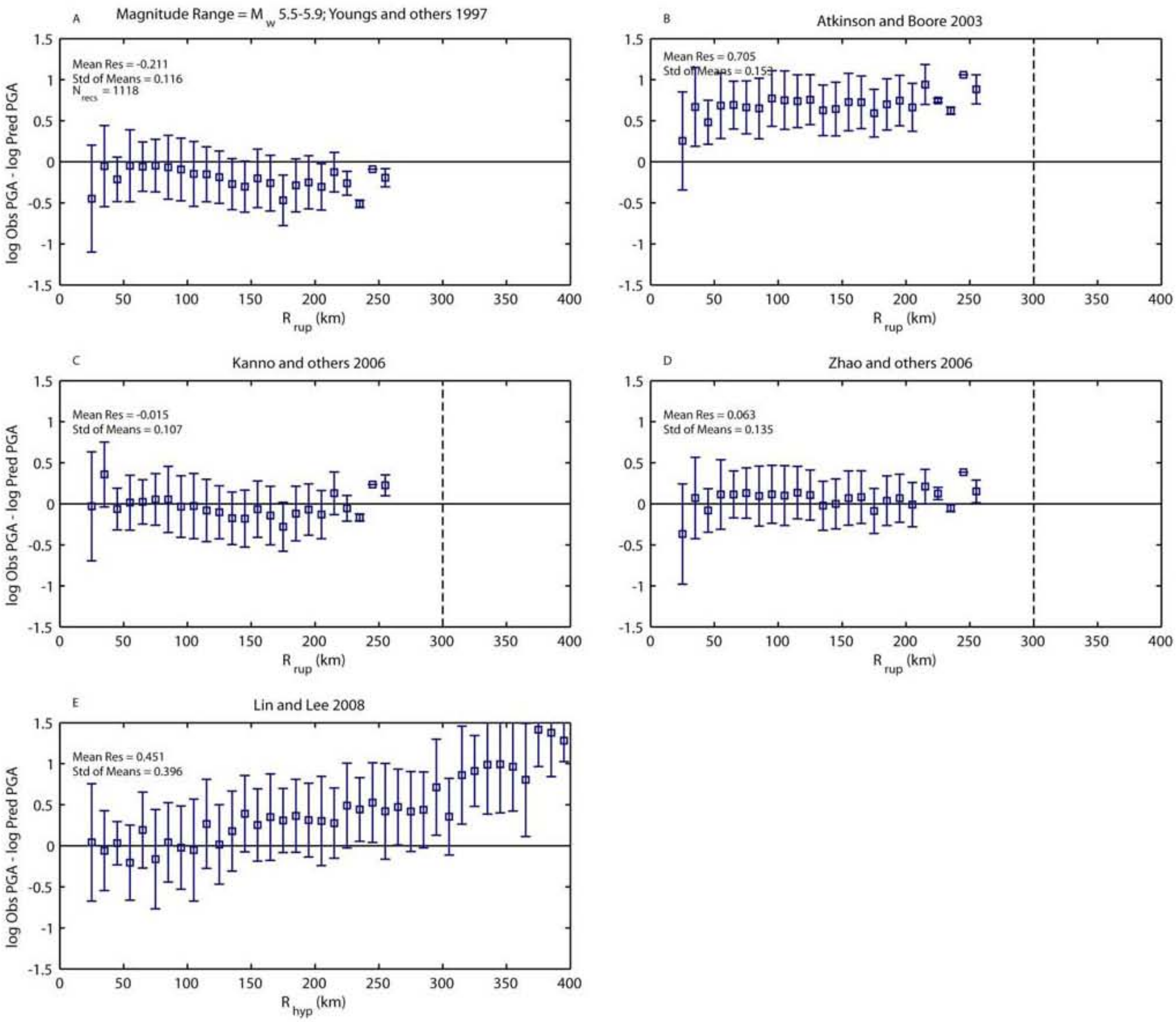
A
Magnitude Range = M w 5.5-5.9; Youngs and others 1997
Mean Res = -0.211
Std of Means = 0.116
N recs = 1118
log Obs PGA - log Pred PGA
R rup (km)
B
Atkinson and Boore 2003
Mean Res = 0.705
Std of Means = 0.153
R rup (km)
C
Kanno and others 2006
Mean Res = -0.015
Std of Means = 0.107
log Obs PGA - log Pred PGA
R rup (km)
D
Zhao and others 2006
Mean Res = 0.063
Std of Means = 0.135
R rup (km)
E
Lin and Lee 2008
Mean Res = 0.451
Std of Means = 0.396
log Obs PGA - log Pred PGA
R hyp (km)

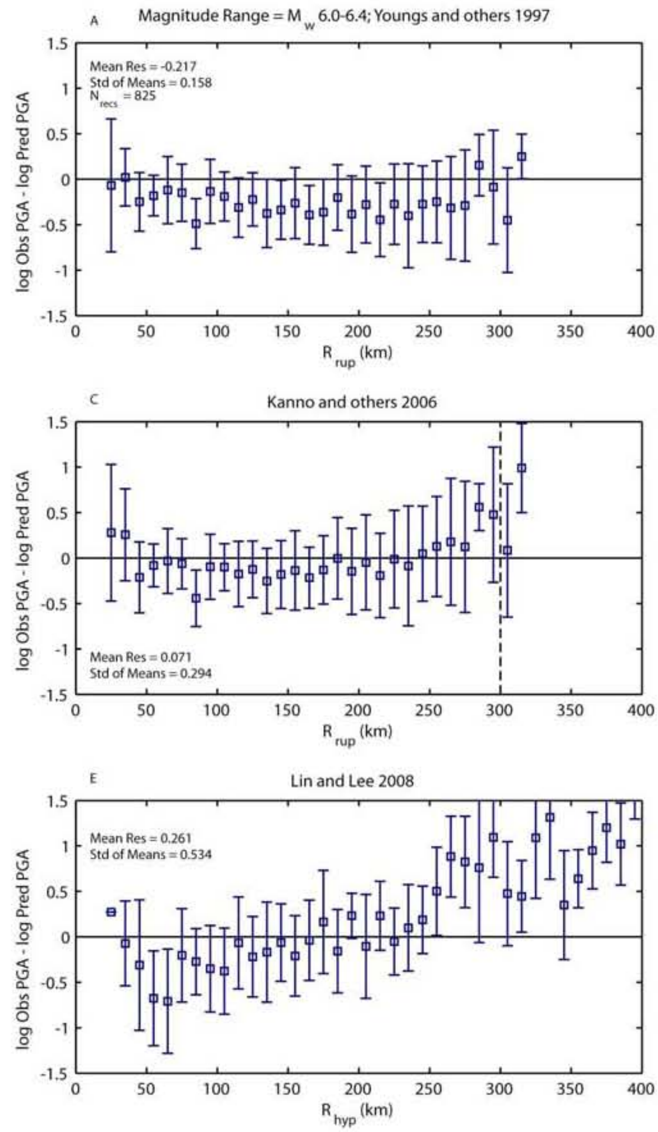
A
Magnitude Range = M_w 6.0-6.4; Youngs and others 1997
Mean Res = -0.217
Std of Means = 0.158
N_{recs} = 825
log Obs PGA - log Pred PGA
R_{rup} (km)
B
Atkinson and Boore 2003
Mean Res = 0.575
Std of Means = 0.221
R_{rup} (km)
C
Kanno and others 2006
Mean Res = 0.071
Std of Means = 0.294
log Obs PGA - log Pred PGA
R_{rup} (km)
D
Zhao and others 2006
Mean Res = 0.090
Std of Means = 0.247
R_{rup} (km)
E
Lin and Lee 2008
Mean Res = 0.261
Std of Means = 0.534
log Obs PGA - log Pred PGA
R_{hyp} (km)

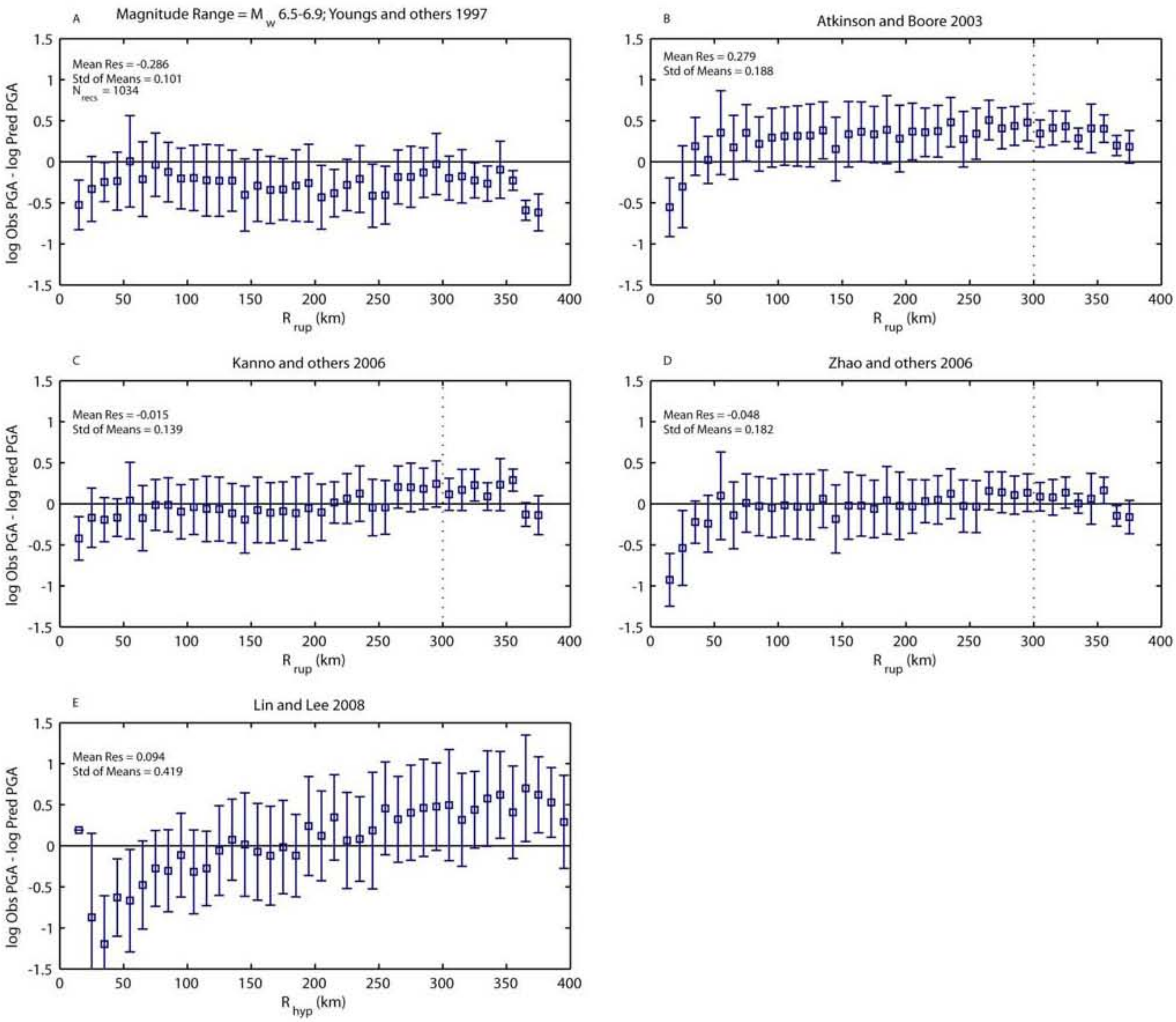
A
Magnitude Range = M w 6.5-6.9; Youngs and others 1997
Mean Res = -0.286
Std of Means = 0.101
N recs = 1034
log Obs PGA - log Pred PGA
R rup (km)
B
Atkinson and Boore 2003
Mean Res = 0.279
Std of Means = 0.188
R rup (km)
C
Kanno and others 2006
Mean Res = -0.015
Std of Means = 0.139
log Obs PGA - log Pred PGA
R rup (km)
D
Zhao and others 2006
Mean Res = -0.048
Std of Means = 0.182
R rup (km)
E
Lin and Lee 2008
Mean Res = 0.094
Std of Means = 0.419
log Obs PGA - log Pred PGA
R hyp (km)

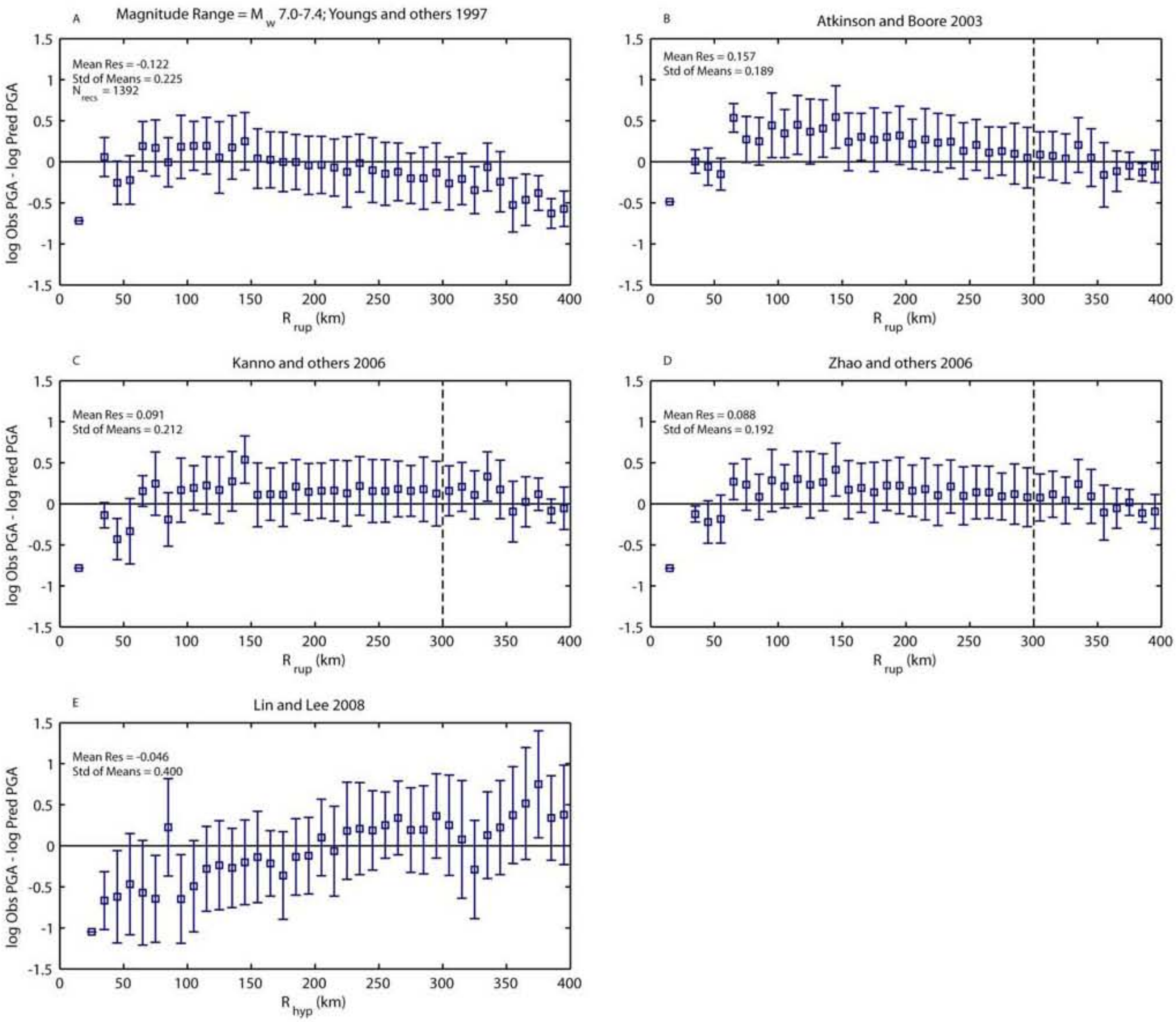
A
Magnitude Range = M_w 7.0-7.4; Youngs and others 1997
Mean Res = -0.122
Std of Means = 0.225
N_{recs} = 1392
log Obs PGA - log Pred PGA
R_{rup} (km)
B
Atkinson and Boore 2003
Mean Res = 0.157
Std of Means = 0.189
C
Kanno and others 2006
Mean Res = 0.091
Std of Means = 0.212
D
Zhao and others 2006
Mean Res = 0.088
Std of Means = 0.192
E
Lin and Lee 2008
Mean Res = -0.046
Std of Means = 0.400
R_{hyp} (km)

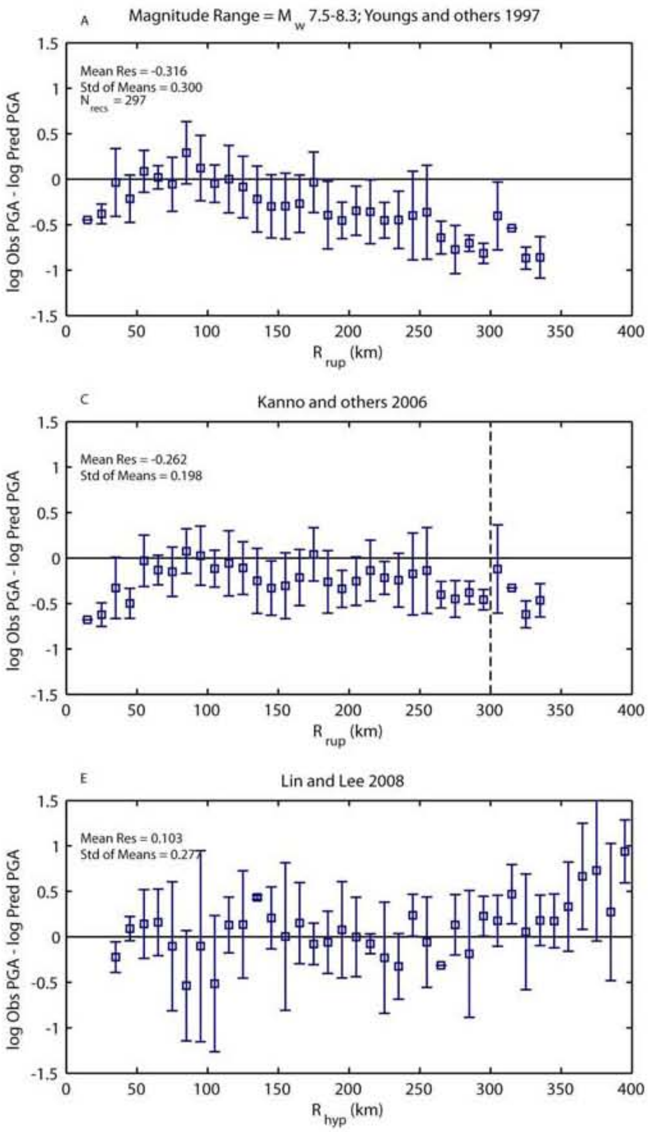
A
Magnitude Range = M w 7.5-8.3; Youngs and others 1997
Mean Res = -0.316
Std of Means = 0.300
N recs = 297
log Obs PGA - log Pred PGA
R rup (km)
B
Atkinson and Boore 2003
Mean Res = -0.248
Std of Means = 0.276
R rup (km)
C
Kanno and others 2006
Mean Res = -0.262
Std of Means = 0.198
log Obs PGA - log Pred PGA
R rup (km)
D
Zhao and others 2006
Mean Res = -0.219
Std of Means = 0.212
R rup (km)
E
Lin and Lee 2008
Mean Res = 0.103
Std of Means = 0.277
log Obs PGA - log Pred PGA
R hyp (km)

Appendix 13 – Subduction Zone GMPE Magnitude Dependence for PGV

The transition of PGV residuals with magnitude for candidate GMPEs for subduction zones. Each plot shows the transition of the median residuals in 0.5 magnitude windows. The magnitude window is indicated on the top-left plot in each case. For all GMPEs except Kanno and others (2006), we evaluate PGV from 1.0 second spectral acceleration using the approach of Newmark and Hall (1982).

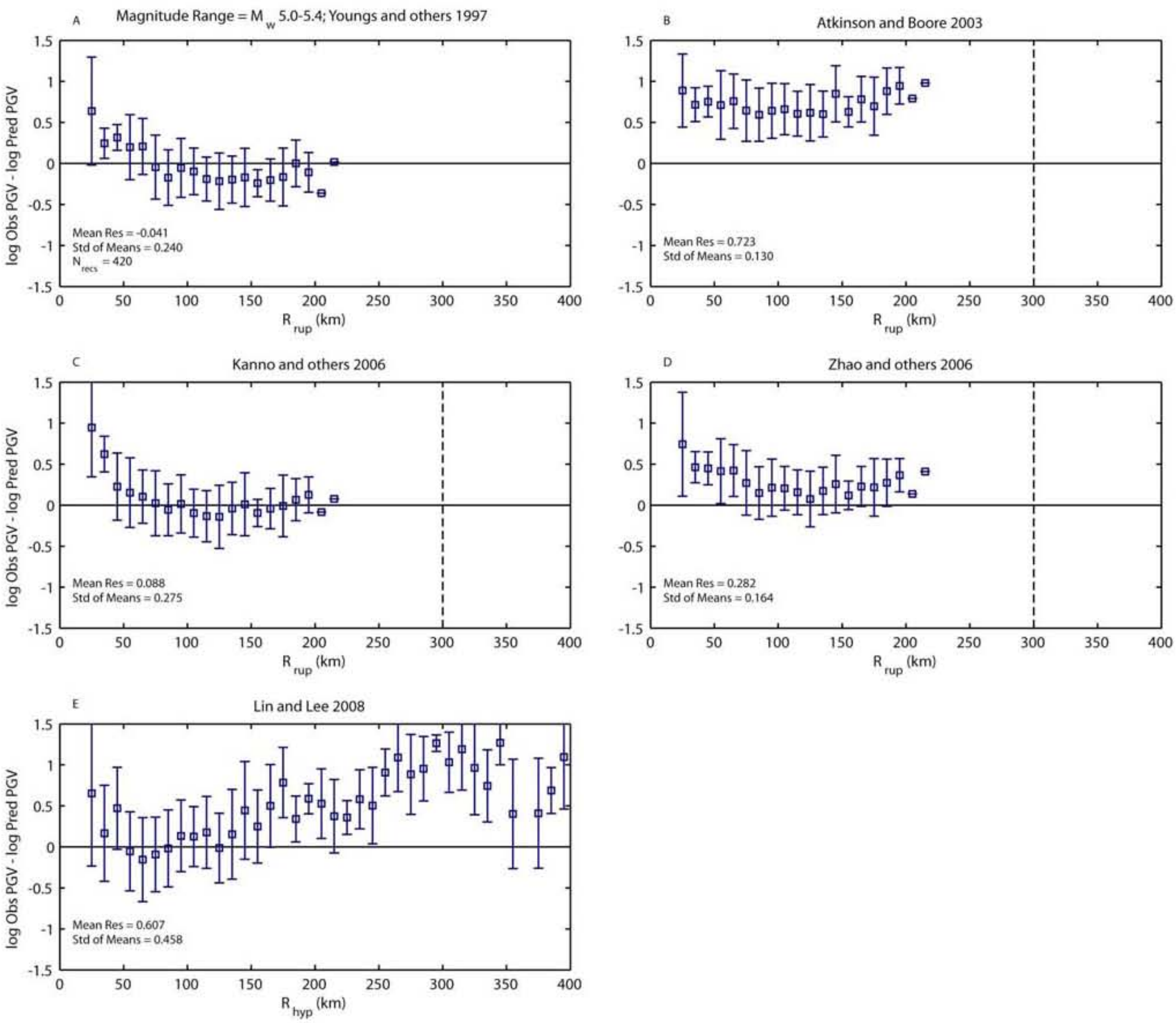

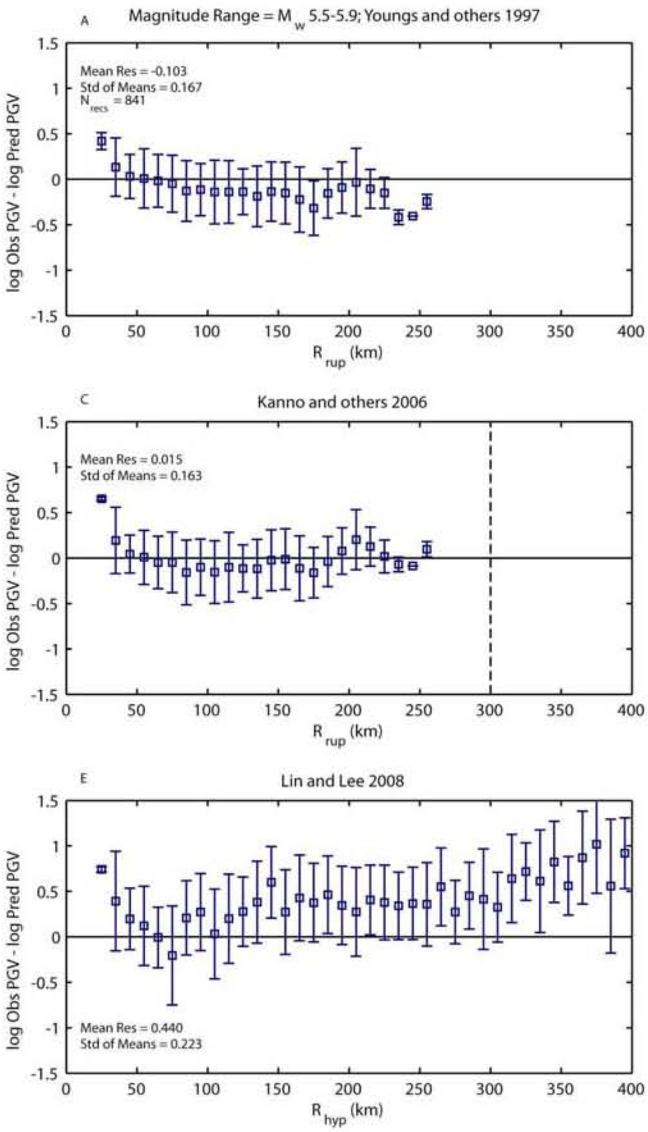
A
Magnitude Range = M_w 5.5-5.9; Youngs and others 1997
Mean Res = -0.103
Std of Means = 0.167
N_{recs} = 841
B
Atkinson and Boore 2003
Mean Res = 0.609
Std of Means = 0.117
C
Kanno and others 2006
Mean Res = 0.015
Std of Means = 0.163
D
Zhao and others 2006
Mean Res = 0.268
Std of Means = 0.072
E
Lin and Lee 2008
Mean Res = 0.440
Std of Means = 0.223
log Obs PGV - log Pred PGV
R_{rup} (km)
R_{hyp} (km)

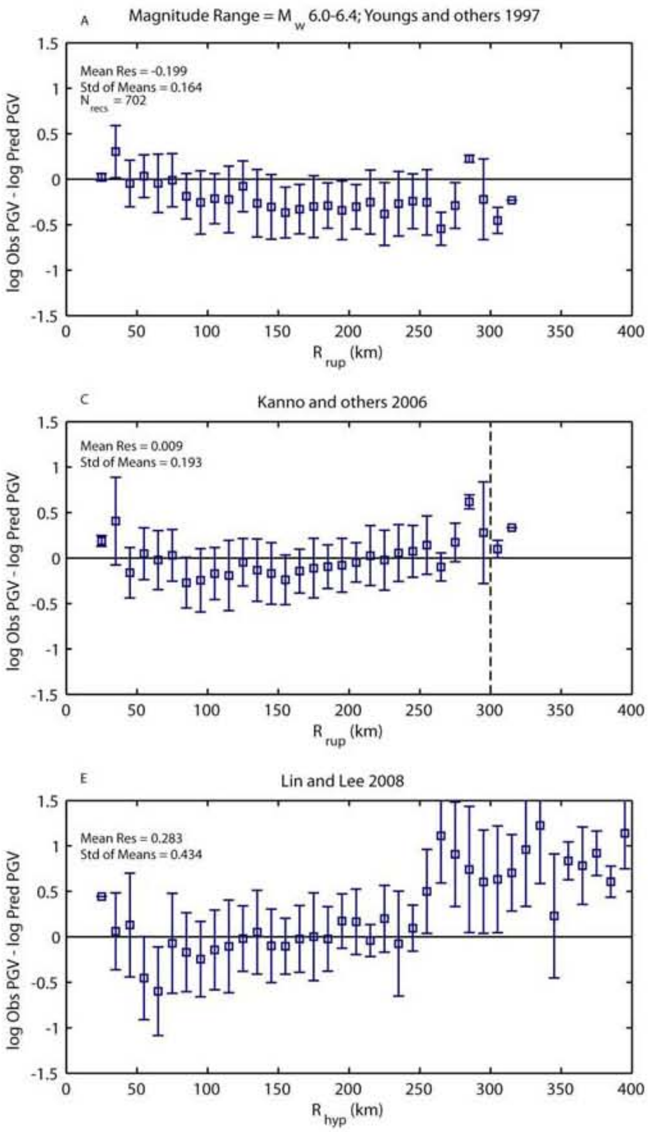
A
Magnitude Range = M w 6.0-6.4; Youngs and others 1997
Mean Res = -0.199
Std of Means = 0.164
N recs = 702
B
Atkinson and Boore 2003
Mean Res = 0.402
Std of Means = 0.226
C
Kanno and others 2006
Mean Res = 0.009
Std of Means = 0.193
D
Zhao and others 2006
Mean Res = 0.202
Std of Means = 0.129
E
Lin and Lee 2008
Mean Res = 0.283
Std of Means = 0.434
log Obs PGV - log Pred PGV
R rup (km)
R hyp (km)

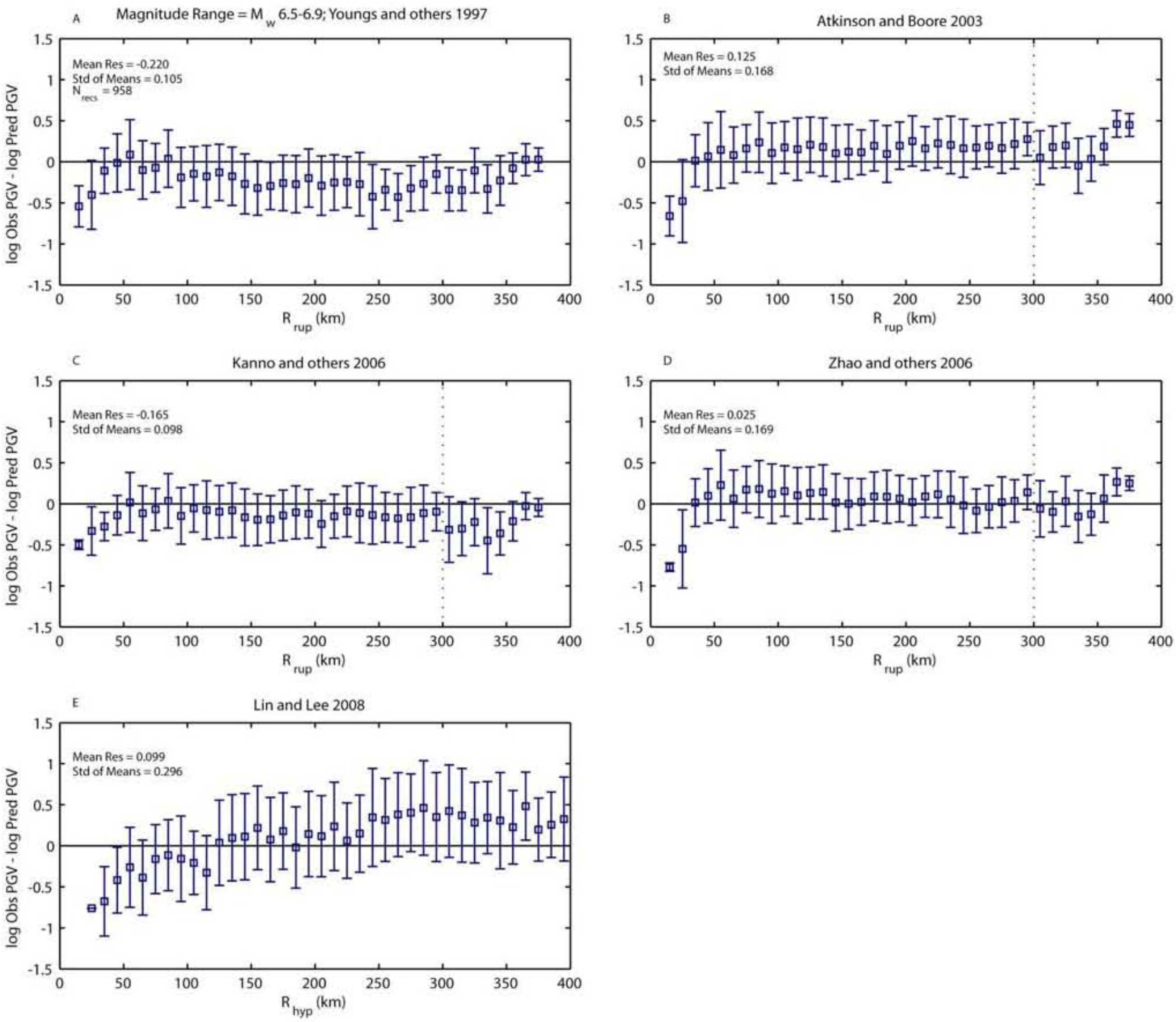
A
Magnitude Range = M w 6.5-6.9; Youngs and others 1997
Mean Res = -0.220
Std of Means = 0.105
N recs = 958
B
Atkinson and Boore 2003
Mean Res = 0.125
Std of Means = 0.168
C
Kanno and others 2006
Mean Res = -0.165
Std of Means = 0.098
D
Zhao and others 2006
Mean Res = 0.025
Std of Means = 0.169
E
Lin and Lee 2008
Mean Res = 0.099
Std of Means = 0.296
log Obs PGV - log Pred PGV
R rup (km)
R hyp (km)

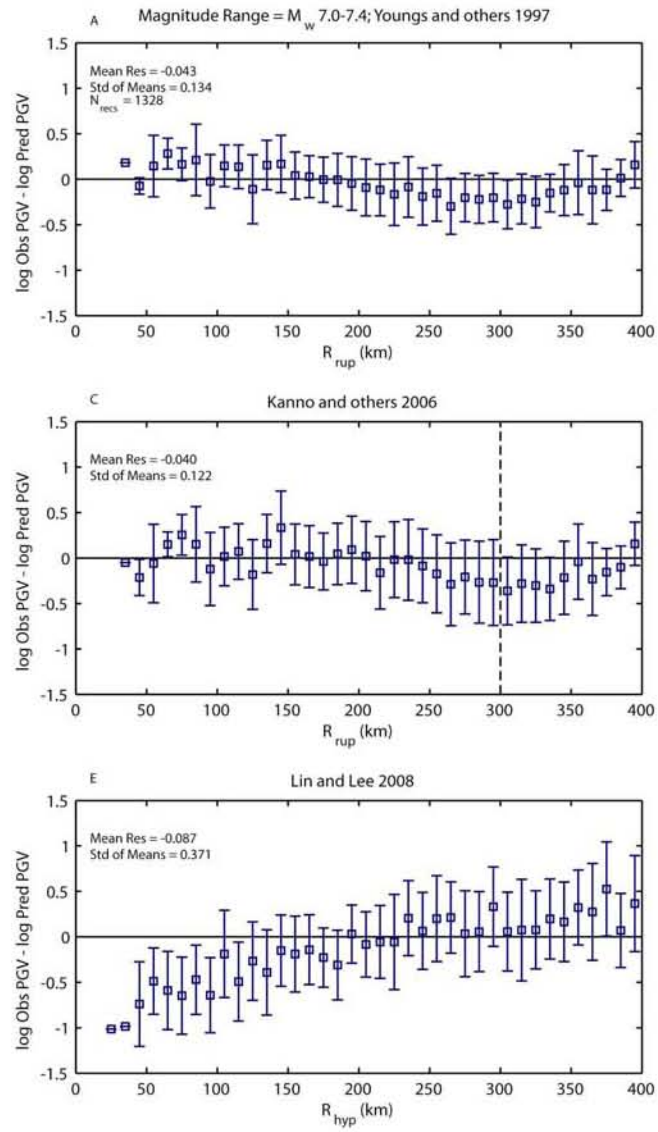
A
Magnitude Range = M w 7.0-7.4; Youngs and others 1997
Mean Res = -0.043
Std of Means = 0.134
N recs = 1328
log Obs PGV - log Pred PGV
R rup (km)
B
Atkinson and Boore 2003
Mean Res = 0.102
Std of Means = 0.128
R rup (km)
C
Kanno and others 2006
Mean Res = -0.040
Std of Means = 0.122
log Obs PGV - log Pred PGV
R rup (km)
D
Zhao and others 2006
Mean Res = 0.151
Std of Means = 0.123
R rup (km)
E
Lin and Lee 2008
Mean Res = -0.087
Std of Means = 0.371
log Obs PGV - log Pred PGV
R hyp (km)

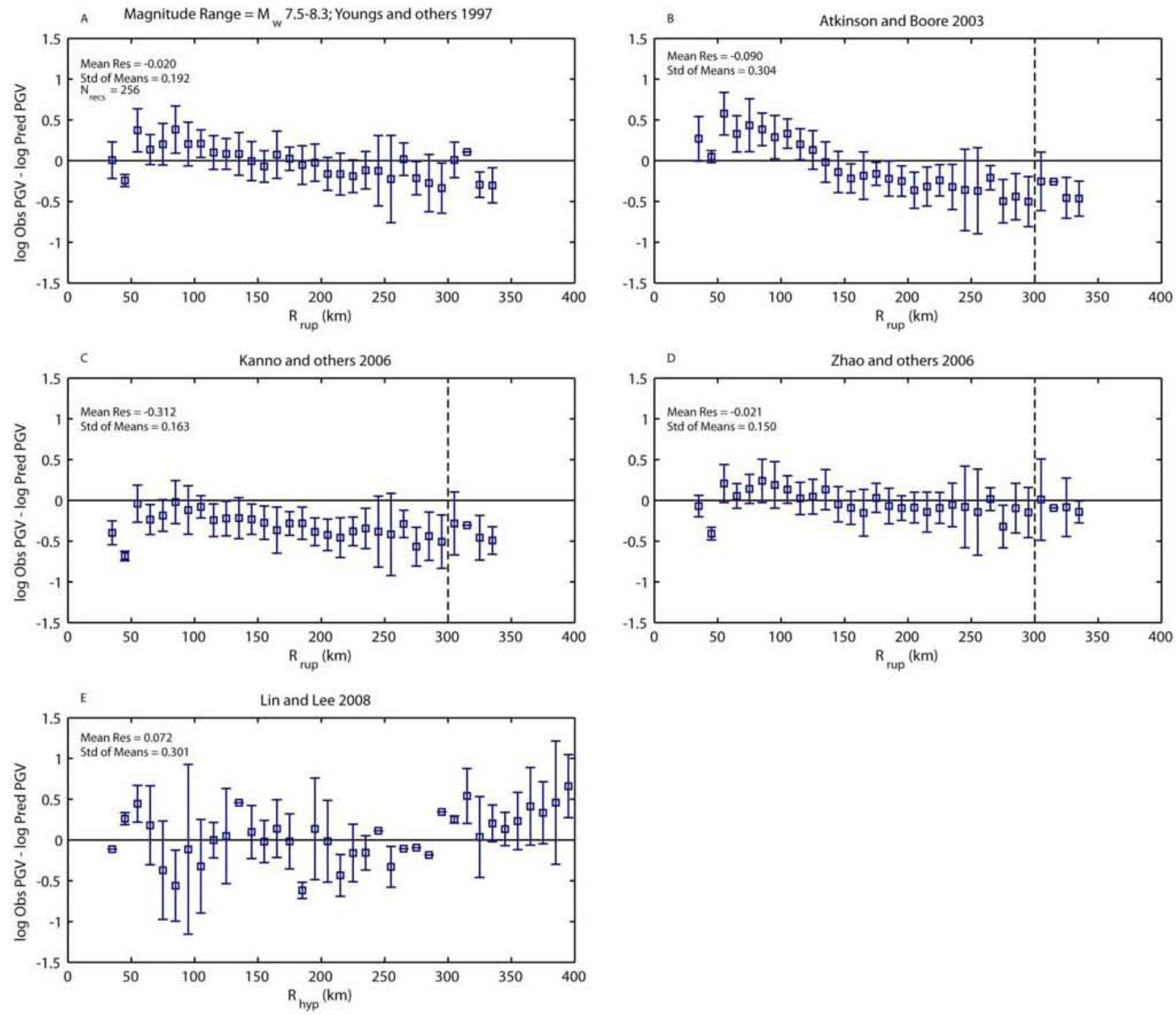

A
Magnitude Range = M w 7.5-8.3; Youngs and others 1997
Mean Res = -0.020
Std of Means = 0.192
N recs = 256
log Obs PGV - log Pred PGV
R rup (km)
B
Atkinson and Boore 2003
Mean Res = -0.090
Std of Means = 0.304
R rup (km)
C
Kanno and others 2006
Mean Res = -0.312
Std of Means = 0.163
log Obs PGV - log Pred PGV
R rup (km)
D
Zhao and others 2006
Mean Res = -0.021
Std of Means = 0.150
R rup (km)
E
Lin and Lee 2008
Mean Res = 0.072
Std of Means = 0.301
log Obs PGV - log Pred PGV
R hyp (km)